DEVELOPMENT OF DIRECT ELECTRON TRANSFER

(DET)-BASED ENZYMATIC BIOFUEL CELLS

by

Shuai Xu

A dissertation submitted to the faculty of
The University of Utah
in partial fulfillment of the requirements for the degree of

Doctor of Philosophy

Department of Chemistry

The University of Utah

August 2014

The University of Utah Graduate School

STATEMENT OF DISSERTATION APPROVAL

The dissertation of **Shuai Xu**

has been approved by the following supervisory committee members:

Shelley D. Minteer	, Chair	**March 11, 2014** Date Approved
Henry S. White	, Member	**March 11, 2014** Date Approved
John C. Conboy	, Member	**March 11, 2014** Date Approved
Jennifer M. Heemstra	, Member	**March 11, 2014** Date Approved
Anil V. Virkar	, Member	**April 11, 2014** Date Approved

and by **Cynthia J. Burrows** , Chair/Dean of

the Department/College/School of **Chemistry**

and by David B. Kieda, Dean of The Graduate School.

ABSTRACT

Research on biofuel cells is the interdisciplinary combination of fuel cells and biotechnology. Like conversional fuel cells, biofuel cells convert chemical energy into electrical energy by catalyzing redox reactions at the cathode and anode and manage the flow of electrons and charge-compensating positive ions to form a complete electric circuit. Unlike conventional fuel cells, biofuel cells utilize living organisms, organelles, enzymes, or DNA as catalysts to facilitate the charge transfer. Most of the current biofuel cell technology utilizes mediated enzymatic system at the anode. It is of interest to employ enzymes that can act as "electron transducers" and directly convert the chemical signal to an electrical one through internal charge transfer without any electron shuttling mediator which could result in poor electrochemistry, limited lifetimes, and complicated fabrication methods. The goal is to utilize direct electron transfer (DET) capable pyrroloquinoline quinone (PQQ)-dependent enzymes to fabricate mediatorless bioanode, which will add versatility and simplicity to biofuel cell technology.

There are two approaches to optimize DET biofuel cell performance: (1) to use enzymes in a series to perform multiple-step oxidation of fuel to release the maximum amount of chemical energy stored in each fuel molecule, which allows for enhanced fuel utilization and higher energy density of the fuel cell and (2) to modify enzyme

immobilization techniques in order to increase the electron transfer efficiency of each enzyme molecule.

In this thesis, a novel bioanode design to perform complete oxidation of glucose will be described. A six-enzyme cascade is immobilized on a carbon fiber paper electrode to stepwise oxidize glucose to carbon dioxide. A further study of the impact of DET enzyme orientation on direct bioelectrocatalysis is carried out by isotropic immobilization of DET enzymes on flat surface gold electrode. A modern method to facilitate electron transfer is also studied by utilizing conducting polyaniline film to covalently bond the PQQ-dependent enzymes to the high surface area polymer matrix.

This dissertation is dedicated to my family and many friends.
A special feeling of gratitude to my loving parents, Li and Shengmin Xu, whose words of encouragement ring in my ears.
Also, this dissertation is dedicated to all those who believe in the richness of learning.

TABLE OF CONTENTS

ACKNOWLEDGEMENTS

I would like to express the deepest appreciation to my advisor and committee chair Professor Shelley D. Minteer, who has shown the attitude and the substance of a genius: she continually and persuasively conveyed a spirit of adventure in regard to research and scholarship and an excitement in regard to teaching. Without her supervision and constant help, this dissertation would not have been possible.

I would like to thank my committee members, Professor Henry S. White, Professor Jennifer Heemstra, Professor John C. Conboy, and Professor Anil V. Virkar for all of their help and guidance. I also would like to thank the members of the Minteer Research Group past and present, all of the graduate students, faculty, and support staff who all make the University of Utah Chemistry Department a great place to work and learn. Finally I want to acknowledge my family. They are always there for me even though we are thousands of miles away. I can't believe I did it!

CHAPTER 1

INTRODUCTION

1.1 Traditional Fuel Cells and Biological Fuel Cells

Fuel cells, a promising renewable energy technology, have been given particular research attention in the past few decades.[1–3] They have shown high energy conversion efficiency and ability to sustain consistent power production over time by consumption of renewable fuel, in contrast to a battery's reliance on the input of electrical energy to recharge and solar cell's dependence on the presence of sunlight. Traditional fuel cells convert chemical energy of small molecular weight fuels such as hydrogen gas,[4, 5] methane,[6, 7] and methanol[8, 9] to electrical energy with precious metal catalysts. Barriers in the development of this type of technology are (1) operational temperature of traditional fuel cells is usually high (60 to 1100˚C), which requires power input for the fuel cells to function, (2) the precious metal catalysts often suffer from reduction in performance due to passivation or poisoning of the catalyst caused by fuel impurities, and (3) only a few simple structured molecules such as hydrogen, methane, and methanol can be used as fuel for proton exchange membrane (PEM) fuel cells.

Biological fuel cells work on the same general principles as all fuel cells. They consist of an anode and a cathode where the oxidation and reduction reaction takes

place. The biocatalyst(s) catalyzes the oxidation reaction of the fuel and liberates electrons. The freed electrons travel through an external circuit to create the electric current and arrive at the cathode to reduce another substrate, which is often oxygen. A schematic representation of an enzyme-based biofuel cell is shown in Figure 1.1.

Biological fuel cells are an alternative to precious-metal-based fuel cell technologies. Biological fuel cells operate with the same concept as traditional fuel cells.[10] However, instead of expensive metal catalysts, biofuel cells utilize biological catalysts such as microorganisms,[11] enzymes,[12] DNA,[13] or organelles.[14] Biological biofuel cells have been demonstrated to operate at more moderate temperatures (20–37 ˚C) and in a more neutral pH range (6.0–8.0), which is a great advantage over traditional fuel cells. Biological catalysts can be utilized at both the cathode and anode to perform reduction/oxidation catalysis, which results in the accepting/release of electrons thereby generating an electrical current. Microorganism-based biological fuel cells (microbial fuel cells), which have the longest history, use whole cells that contain many oxido-reductase enzymes to perform complex metabolic pathways to oxidize fuel substrates. The advantages of microbial fuel cells are (1) the living organisms contain many enzymes that are capable of complete oxidation of a wide variety of fuels and (2) microorganisms are stable on electrodes due to their ability to regenerate the enzymes and co-enzymes needed for biocatalysis giving rise to lifetimes of over 5 years.[15, 16] However, this type of devices has shown very low power densities due to the transport and internal resistance due to the membrane and cell wall structure of the microorganisms. The volumetric catalytic activity is also low due to the large amount of unutilized space in the cell cytoplasm. Enzymes have been considered as great

alternative biocatalysts to microorganisms. The sizes of enzymes are on the nanometer scale, so the volumetric catalytic activity of enzymes is much higher in comparison to microorganisms.[17, 18]

1.2 Enzyme as Bioelectrocatalyst

1.2.1 Enzymatic Bioelectrocatalysis

In general, catalysts accelerate the rate of a reaction by lowering the transition state energy level relative to the ground state, which leads to a decrease of activation energy. Enzymes are proteins that are produced by living organisms and facilitate specific biological reactions while keeping their physical structure and chemical component intact. There is a certain temperature and pH value at which an enzyme's catalytic activity is at its greatest.[19] The optimal temperature and pH for the majority of enzymes is 20–37˚C and near neutral conditions (pH ~7.0).

Enzymes begin biocatalysis by binding the substrate to a small cavity in the enzyme (active site) and forming an enzyme substrate complex. Only a dozen or so amino acid residues can make up the active site. Only two or three of those amino acid residues can be involved directly in substrate binding, but in some enzymes cofactors are also present in the active site.[20–22] Most enzymes that catalyze redox reactions contain a prosthetic group, which often includes one or more metal ions and requires an additional organic molecule or transition metal complex known as a coenzyme or cofactor to assist in the electron transfer.

We express the enzyme catalyzed reaction as below

$$E + S \underset{k_{-1}}{\overset{k_1}{\rightleftharpoons}} ES \xrightarrow{k_2} P + E$$

where E represents the enzyme of interest, S represents the substrate, and P represents the product. The stability of the enzyme substrate complex (ES) is related to

the affinity of the substrate to the enzyme active site, which is measured by the substrate's dissociation constant for the ES, K_s. If we assume $K_{-1} << K_2$, the first step achieves equilibrium

$$k_s = \frac{k_{-1}}{k_1} = \frac{[E][S]}{[ES]}$$

The general expression for the rate of the reaction is

$$v_0 = \frac{d[P]}{d[t]} = k_2[\mathrm{ES}]$$

And the overall rate of production of ES is

$$\frac{d[ES]}{dt} = k_1[\mathrm{E}][\mathrm{S}] - k_{-1}[\mathrm{ES}] - k_2[\mathrm{ES}]$$

At steady state, the rate of enzyme substrate complex concentration change equals to 0

$$\frac{d[ES]}{dt} = 0$$

[E], [ES] are difficult to quantify, but we know the total enzyme concentration

$$[E]_T = [E] + [ES]$$

Combining the last three equations gives

$$[ES](k_{-1} + k_2 + k_1[S])$$

We rewrite the dissociation constant Ks and refer to it as K_m (Michaelis Menten constant). K_m represents the substrate concentration at which the reaction rate is half of the maximum rate, $K_M = \frac{k_{-1}+k_2}{k_1}$, then

$$v_0 = \left(\frac{d[P]}{dt}\right) = k_2[ES] = \frac{k_2[E]_T[S]}{K_M + [S]}$$

We refer to the term k_2 as the k_{cat} (catalytic rate constant). The K_{cat} or turnover

number represents the maximum number of substrate molecules (in μmoles) converted to product molecules per active site per unit of time (in seconds). Oxido-reductase enzymes can experience turnover numbers on the order of 10^3 s^{-1} or higher. The Michaelis Menten mechanism is one of the simplest models of enzyme kinetics. It is usually used to describe single substrate and single product reaction. Most dehydrogenases have more complex kinetics. Enzymatic reactions involving two substrates and yielding two products account for ~60% of known biochemical reactions.[23]

1.2.2 Enzyme Catalyzed Reaction Electron Transfer Mechanisms

When discussing the transport of the electron removed from the substrate at the active site of the enzyme to the electrode surface thus generating catalytic current, there are two types of electron transfer mechanisms: mediated electron transfer (MET) and direct electron transfer (DET), as shown in Figure 1.2. Most enzymes studied in biofuel cell systems are not capable of transferring electrons to the electrode surface by themselves due to long electron transfer distances. In this case, an electron transfer shuttle or mediator is needed to assist the electron transfer process. In this approach, a redox active molecule participates in the catalytic reaction by reacting with the enzyme or its cofactor to become oxidized or reduced and then shuttles the electron to the electrode surface and completes the electron transfer process.[24, 25] The redox chemistry for the chosen mediator must be reversible and require low overpotential. There are many methods to incorporate mediators into biofuel cell systems. They can be simply added to the fuel solution, co-immobilized with enzymes, or polymerized on the

electrode surface prior to the enzyme immobilization process. The MET method has been attempted at both cathodic and anodic interfaces and has been achieved through solution phase mediators and mediators immobilized in various ways with or near the enzymes themselves. These mediated systems do have drawbacks in that the species utilized to assist electron transfer are often not biocompatible or have short lifetimes themselves.

A mediator would not be needed if electrons can be transferred to the electrode surface via the active site of the enzyme. This type of electron transfer is called direct electron transfer (DET). Several enzymes have been reported that are capable of DET.[26–31] These enzymes generally contain redox active metal centers that can be stable at several different oxidation states so the enzyme can perform the catalytic transfer of electrons. This type of enzyme is capable of acting as a "molecular transducer" that catalyzes the redox reaction of the fuel and transfers the electrical signal through the transfer of charge to a stable redox species, which is in turn capable of transferring electrons to another molecule or electrode surface. Many PQQ-dependent enzymes, for example, contain at least one heme group, which contains a metal iron center that is capable of existing in several redox states and accepts electrons that are generated through the catalytic reaction at the active site of the enzyme.[20, 32] Enzymes that are capable of DET eliminate the need for mediator molecules that can be nonselective and decrease the open circuit potential, which limits the optimal performance of the cell. With the advantages of DET enzymes described above, the main focus of this study has set to develop, characterize, and optimize the "mediatorless" bioanode with DET enzymes.

1.2.3 DET Enzyme Resources

The first studies of DET enzymes involved utilizing cathodic enzymes to reduce oxygen to water and perform a four-electron transfer.[33, 34] Most known DET capable anodic enzymes are PQQ-dependent enzymes that can be isolated from several gram-negative acetic acid bacteria such as *Acetobacter, Gluconobacter*, *Pseudomonas*, and *Commamonas*.[35–38] PQQ-dependent enzymes isolated from those bacteria have significant differences with respect to structure and specificity. Acetic acid bacteria have been demonstrated to be able to incompletely oxidize a great variety of carbohydrates, alcohols, and related compounds.[38] The genus *Gluconobacter* belongs to the group of acetic acid bacteria.

In nature, the acetic acid bacteria are well adapted to sugar or alcohol solutions. Therefore, flowers and fruits are the natural habitats of *Gluconobacter*.[38] It can also be found in alcoholic beverages such as wine, beer, and soft drinks.[39, 40] The genus *Gluconobacter* also exhibits extraordinary uniqueness in their growth behavior and response to extreme culture conditions. Acetic acid bacteria are especially known for their rapid and incomplete oxidation of a wide range of sugars and alcohols and the near-quantitative excretion of the oxidation products into the medium.[41–43]

A series of membrane bound dehydrogenases involved in the oxidation of substrates has been identified and characterized in the past two decades.[44–46] Enzymes that showed potential to be utilized in electrochemical applications include glucose, fructose, alcohol, aldehyde, sorbitol, aldehyde, and glycerol dehydrogenases.

1.3 Enzyme-Based Biological Fuel Cells

1.3.1 Introduction of Enzymatic Biofuel Cells

Enzymes are very efficient redox reaction catalysts. Many oxido-reductase enzymes have shown the capability to increase the rate of reaction by as much as 10^{14} times compared to the rate without catalyst present.[19] The fast development of protein purification technologies combined with advances in genetically enhanced enzyme expression has resulted in simple and inexpensive large scale production of these catalysts. This makes enzymes considerably less expensive than precious metal catalysts. All the above advantages qualify enzymes to be great potential bioelectrocatalysts to be utilized in energy producing devices.

However, enzyme-based biological fuel cells have many limitations that plague the performance of these systems. (1) Enzymes only catalyze specific reactions. Most oxido-reductase enzymes can only catalyze one step, a two electron oxidation reaction, which results in incomplete oxidation of fuels. (2) Without the protection of the cell wall and membranes, enzymes are directly exposed to the fuel cell operation environment; thus the lifetime of this type of biocatalysts in devices is decreased, and this decrease can lead to a short device lifetime. (3) The performance of enzyme-based biological fuel cells can be reduced due to the slow kinetics of direct electron transfer or problems associated with the stability or thermodynamics of the redox mediator that is required in most enzyme-based systems. In order to overcome these limitations of enzymatic biofuel cells, solutions have been proposed to optimize the electrochemical performance of the device as well as to increase the biofuel cell lifetime. Solutions include (1) utilization of promiscuous enzymes to form an enzyme cascade to perform

multistep oxidation of the fuel; (2) elimination of factors/components in the biofuel cell that can potentially decrease the lifetime of the electrochemical device; and (3) developing new enzyme immobilization techniques to improve the electric contact between the enzyme and the electrode surface, which lead to a higher power density.

1.3.2 Promiscuous Enzymes

One of the most known attributes of enzymes is specificity to a single substrate. However, not all enzymes are only active toward one substrate. Enzymes that are capable of catalyzing reactions with different substrates or different transition states are called "promiscuous enzymes."[47] By utilizing such enzymes in biofuel cell systems, it can be possible to decrease the number of enzymes needed in a biological pathway or use a higher energy density fuel with the enzyme. For example, PQQ-dependent alcohol dehydrogenase catalyzes reversible reactions with primary and secondary alcohols.[48] So when designing an oxidation pathway for glucose, PQQ-dependent alcohol dehydrogenase can be used when intermediates with a hydroxyl group need to be oxidized.

1.3.3 Enzyme Cascade

Enzymes catalyze one step oxidation/reduction reactions, which involve two electron transfers. Most complex fuels utilized in biofuel cell systems require more than two electrons to be completely oxidized. Since most enzymes are not promiscuous, a multiple enzyme system (enzyme cascade) is needed to perform sequential oxidations of a fuel to form a small molecule final product. The first enzyme cascade was shown by

Palmore et al.[49] They utilized a three enzyme cascade including alcohol dehydrogenase, aldehyde dehydrogenase, and formate dehydrogenase to completely oxidize methanol to carbon dioxide. Alcohol dehydrogenase oxidizes methanol to formaldehyde followed by oxidation to formate catalyzed by aldehyde dehydrogenase. Formate is then oxidized to carbon dioxide with formate dehydrogenase. Each of the three enzymes catalyzed a single two electron oxidation step to form the substrate for the next enzyme in the cascade. The utilization of an enzyme cascade makes deep oxidation of substrates possible and can potentially lead to high power density. In 2008 Sokic-Lazic *et al.* reported a bioanode that use enzyme cascade to mimic the citric acid cycle and achieved complete oxidation of ethanol at a bioanode.[50] By mimicking the complete citric acid cycle on a carbon electrode, power density was increased 8.71-fold compared to a single enzyme (alcohol dehydrogenase)-based ethanol/air biofuel cell.

1.4 Enzyme Immobilization

1.4.1 Enzymatic Biofuel Cell Limitations

The electrical connection from enzymes to electrode surfaces basically determines how efficient the biofuel cell devices can be. Two major limitations have been challenging the enzymatic biofuel cell development: (1) maintaining the original three-dimensional structure and performance of those sensitive biomacromolecules over time and (2) efficient electrical transfer from the enzyme to electrode surface to form catalytic current. For the first limitation, the integrity of the protein structure of both the active site and the macromolecule is essential to the catalytic performance of the enzyme. Enzyme activities are dependent on the temperature, pH, and chemical

composition of the operation environment. Early studies of enzymatic biofuel cells utilized free enzyme solutions or suspensions to produce catalytic current. This method resulted in lifetimes of the devices of only a few hours to less than 5 days in pH and temperature controlled solutions due to the enzyme denaturation during the operation time. Allowing enzymes to diffuse freely in solution also has a negative impact on electron transfer from the enzyme to electrode surface. Although enzymes have high catalytic activity (turnover rate between 10,000 s^{-1} to 500,000s^{-1}) and can supply ample amounts of electrons, they cannot be efficiently transferred to the electrode surface to form catalytic current, causing the overall device performance to fall far short of theoretical calculations.

1.4.2 Modified Nafion® Polymer for Enzyme Immobilization

In the past 2 decades, research efforts have focused on the controlled immobilization of enzymes on electrode surfaces to reduce the impact of the limitations mentioned previously.[51–54] Enzymes are extremely efficient catalysts when immobilized at the electrode surface. Modifying the electrode surface with a thin polymer film has often been the chosen method due to function and simplicity. Designing polymer films for enzyme immobilization should follow a couple of rules: (1) the polymer film should provide a mechanically and chemically stable layer that can entrap the enzyme while providing a buffered environment to keep the structural integrity of enzymes and maintain the performance of the biocatalysts and (2) the polymer film should not form a capacitive region at the electrode surface.

A breakthrough in enzyme immobilization was introduced by the Minteer

research group.[18] They modified Nafion polymer to accommodate the physical and chemical requirements of an enzyme while retaining the electrical conductivity of Nafion. The modified Nafion polymer showed the ability to provide suitable micellar pores to maintain enzymes' three-dimensional structure while providing a buffered environment. The stability and lifetime of dehydrogenases have increased, and bioanodes fabricated using this technique have been operated for approximately 60 days.

The modification of Nafion consists of two steps. The first step involves casting a suspension of Nafion with tetrabutylammonium bromide (TBAB) dissolved in the suspension. Nafion is a perfluorinated ion exchange polymer which shows excellent conductivity. However, as an acidic polymer membrane, unmodified Nafion cannot provide a neutral environment for immobilized enzymes, which decreases the lifetime and activity of the enzymes. By introducing TBAB to this polymer system, Nafion polymer acidity has been neutralized, which leads to an increase of the mass transport of small analytes through the polymer film and decreases the selectivity of the membrane against anions. The second step of modification involves recasting these initial membranes after removing the excess bromide salts from the cast solution. Salt-extracted membranes retain the presence of the quaternary ammonium cations at the sulfonic acid exchange sites but eliminate complications from excess salt that can cause voids in the equilibrated membrane. The modified films are then resuspended in lower aliphatic alcohols. This modified Nafion polymer film has been demonstrated to extend enzyme lifetime by a factor of over 10.[18]

1.4.3 DET Enzyme Immobilization

Unlike MET enzymes, the efficiency of direct electron transfer enzymes is heavily dependent on the proximity and orientation of those enzymes toward the electrode surface for electron tunneling to occur.[55] In PQQ-dependent enzymes, for example, the distance between the closest heme group in the enzyme and the electrode surface determines the electron transfer rate and hence the catalytic current density. There are generally two methods to increase the electrical connection between DET enzymes and electrode surfaces: (1) uniformly immobilize the enzyme on the electrode surface to expose the active site of enzyme to substrate while holding the last redox center in the enzyme within the electron tunneling distance from the electrode surface or (2) increase the electrode surface area and roughness to decrease the distance between the redox active site and the electrode surface. In this research, the modified Nafion polymer method was utilized to demonstrate that a six-enzyme cascade can completely oxidize glucose. Then, the impact of enzyme orientations on DET properties was studied by isotropic alignment of enzymes on flat electrode surface using self-assembled monolayer (SAM) linker, and the last project was to utilize a polyaniline conducting polymer to covalently bond to the enzyme macromolecules to decrease the average distance between the enzymes and electrode surface.

1.5 Biological Fuels

As discussed previously, in the long history of traditional fuel cell system development, research has been focused on increasing the system efficiency and decreasing the cost of building those systems.[9] Biological fuel cells, especially

enzymatic biofuel cells, have opened a window to a much larger selection of fuels. Oxido-reductase enzymes in living cells have activity toward a variety of substrates in metabolic pathways, such as the Krebs cycle,[56] glycolysis,[57] and the fatty acid[58] degradation pathway. These enzymes allow for the metabolic substrates to be considered as possible fuel choices. In recent years, biological fuel cells utilizing fructose[59], glycerol,[60, 61] pyruvate,[62, 63] lactate,[64] and many other substrates as fuel have been reported, and the diversity of fuels for enzymatic biofuel cells have been vastly enriched.

The first thing to consider when choosing a fuel for a biofuel cell system is the energy density of the fuel. The theoretical energy density gives a first approximation of the maximum energy density of a biofuel cell given that the substrate can be completely oxidized. However, for most reported enzymatic biofuel cell systems, fuels are not completely oxidized but rather partially oxidized.[65, 66] Most reported enzymatic biofuel cell systems only utilize one enzyme to perform partial oxidation of each fuel, so most of the chemical energy stored in the fuel is not converted to electrical energy. For example, glucose biofuel cells have been vastly studied; most of the glucose biofuel cells utilize only one anodic enzyme (glucose oxidase or glucose dehydrogenase) to oxidize glucose to gluconolactone and release two electrons per molecule.[67, 68] Although glucose has a high energy density itself, those biofuel cell systems have a low energy density because of incomplete oxidation. Therefore, not just the energy density of the fuel that will be utilized in a biofuel cell but also the degree of oxidation should be considered when choosing a fuel. One of my goals is to achieve high energy density by utilizing a multiple-enzyme system to perform a series of sequential oxidation of fuel.

Details of this research will be discussed in Chapter 2.

Further considerations include abundance and cost of the fuel, toxicity of the fuel and byproduct(s) along the pathway, and physical and chemical properties of the fuel and its byproduct(s), as well as the ability of the fuel to interfere with the electrode chemistry. My research has focused on using glucose as the fuel because it is not only abundant in nature and in the bloodstream but also demonstrates low volatility, is nontoxic, and is inexpensive. Those qualities coupled with its relatively high energy density qualify glucose as a promising fuel.

1.6 Conclusions

Many oxido-reductases that are capable of DET have been identified and isolated from different microorganisms.[69, 70] A few of them have shown promiscuous activity toward a wide range of substrates with a certain functional group.[32, 71] For example, PQQ-dependent alcohol dehydrogenase has shown activity on a variety of primary and secondary alcohols (ethanol, glycerol, etc.). This unique property of PQQ-dependent enzymes has provided an opportunity to broaden substrate variety as well as simplify enzyme cascade design. This study set out to explore the application of DET enzymes on bioanode of enzymatic biofuel cells and sought to answer three questions:

1. Can DET enzymes form a minimal enzyme cascade to perform multiple step oxidations of carbohydrates such as glucose to release the maximum energy density of the fuel?

2. What are the most important factors that affect the direct electron transfer from enzyme to electrode, and how do they impact the direct bioelectrocatalysis rate?

3. How can the electrochemical communication between the enzyme and electrode surface be improved to increase the power density of the bioanode?

Answers to these three questions are crucial to DET enzymatic biofuel cell development as incomplete usage of fuel energy density and low power density have been challenging this field research for decades.[72]

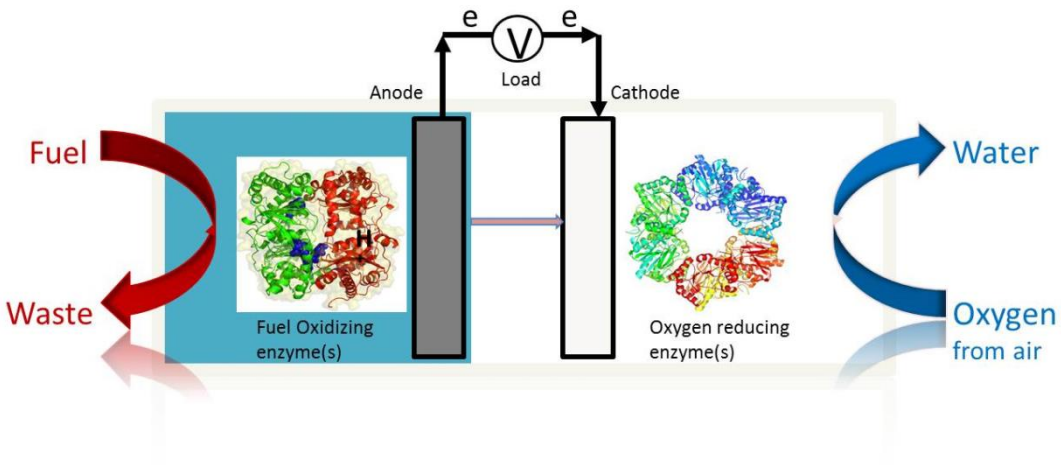

Figure 1.1. Schematic representative of enzyme-based biological fuel cells.

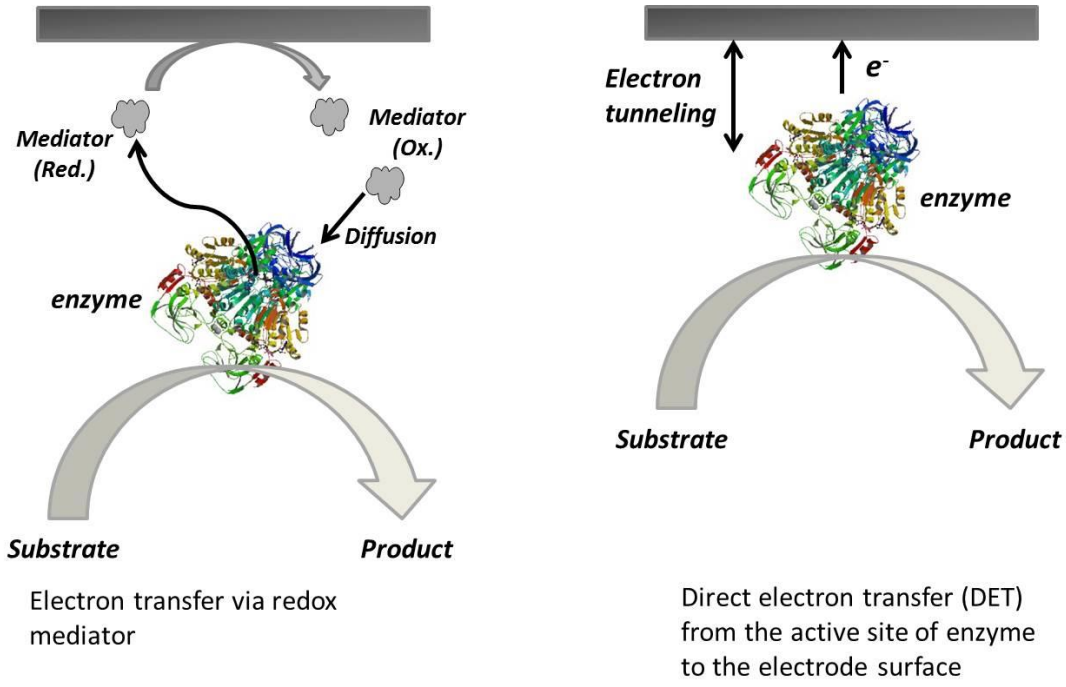

Figure 1.2. Schematic illustration of mediated electron transfer (MET) mechanism (left) and direct electron transfer (DET) mechanism (right).

1.7 References

1. Grubb, W. T.; Niedrach, L. W. *J. Electrochem. Soc.* **1960,** *107*, 131–135.

2. Williams, K. R. *An Introduction to Fuel Cells*. Elsevier Publishing Company: New York, 1966; Vol. 113.

3. Linden, D. *Handbook of Batteries and Fuel Cells*. McGraw-Hill Inc.: New York, 1984.

4. Trimm, D. L.; Önsan, Z. I. *Catal. Rev.* **2001,** *43*, 31–84.

5. Cheng, X.; Shi, Z.; Glass, N.; Zhang, L.; Zhang, J.; Song, D.; Liu, Z.-S.; Wang, H.; Shen, J. *J. Power Sources* **2007,** *165*, 739–756.

6. Murray, E. P.; Tsai, T.; Barnett, S. *Nature* **1999,** *400*, 649–651.

7. Park, S.; Vohs, J. M.; Gorte, R. J. *Nature* **2000,** *404*, 265–267.

8. Liu, H.; Song, C.; Zhang, L.; Zhang, J.; Wang, H.; Wilkinson, D. P. *J. Power Sources* **2006,** *155*, 95–110.

9. Hogarth, M.; Hards, G. *Platin. Met. Rev.* **1996,** *40*, 150–1591.

10. Aston, W. J.; Turner, A. P. F. *Biotechnol. Genet. Eng.* **1984,** *1*, 89–120.

11. Bennetto, H. P.; Stirling, J. L.; Tanaka, K.; Vega, C. A. *Biotechnol. Bioeng.* **1983,** *25*, 559–568.

12. Atanassov, P.; Colon, F.; Rajendran, V., *Abstracts of Papers, 228th ACS National Meeting, Philadelphia, PA, United States, August 22–26,* **2004**, COLL-207.

13. Rusling, J. F.; Hvastkovs, E. G.; Hull, D. O.; Schenkman, J. B. *Chem. Commun.* **2008,** 2, 141–154.

14. Arechederra, R. L.; Minteer, S. D. *Electrochim. Acta* **2008,** *53*, 6698–6703.

15. Vielstich, W.; Gasteiger, H. A.; Lamm, A. *Handbook of Fuel Cells - Fundamentals, Technology and Applications*, Eds. John Wiley & Sons, Ltd: Jerusalem, 2003; Vol. 1.

16. Davis, F.; Higson, S. P. J. *Biosens. Bioelectron.* **2007,** *22*, 1224–1235.

17. Moore, C. M.; Minteer, S. D.; Martin, R. S. *Lab Chip* **2004,** *5*, 218–225.

18. Akers, N. L.; Moore, C. M.; Minteer, S. D. *Electrochim. Acta* **2005,** *50*, 2521–2525.

19. Silverman, R. B. *The Organic Chemistry of Enzyme Catalyzed Reactions*. Academic Press: San Diego, 2000.

20. Duine, J. A. *Eur. J. Biochem.* **1991,** *200*, 271–284.

21. Klinman, J. P.; Dooley, D. M.; Duine, J. A.; Knowles, P. F.; Mondovi, B.; Villafranca, J. *J. FEBS Lett.* **1991,** *282*, 1–4.

22. Bardea, A.; Katz, E.; Bueckmann, A. F.; Willner, I. *J. Am. Chem. Soc.* **1997,** *119*, 9114–9119.

23. Schienbein, M.; Gruler, H. *Phys. Rev. E* **1997,** *56*, 7116–7127.

24. Foulds, N. C.; Lowe, C. R. *Anal. Chem.***1988,** *60*, 2473–2478.

25. Ryabov, A. D.; Amon, A.; Gorbatova, R. K.; Ryabova, E. S.; Gnedenko, B. B. *J. Phys. Chem.* **1995,** *99*, 14072–14077.

26. Berezin , I. V.; Bogdanovskaya, V. A.; Varfolomeev, S. D.; Tarasevich, M. R.; Yaropolov, A. I. *Dokl. Akad. Nauk. USSR* **1978,** *240*, 615–618.

27. Ghindilis, A. L. *Biochem. Soc. Trans.* **2000,** *28*, 84–89.

28. Johnson, D. L.; Thompson, J. L.; Brinkmann, S. M.; Schuller, K. A.; Martin, L. L. *Biochem.***2003,** *42*, 10229–10237.

29. Shleev, S.; El Kasmi, A.; Ruzgas, T.; Gorton, L. *Electrochem. Commun.* **2004,** *6*, 934–939.

30. Tsujimura, S.; Nakagawa, T.; Kano, K.; Ikeda, T. *Electrochemistry* **2004,** *72*, 437–439.

31. Treu, B. L.; Minteer, S. D. *Bioelectrochemistry* **2008,** *74*, 73–77.

32. Ikeda, H.; Kobayashi, D.; Matsushita, F.; Sagara, T.; Niki, D. *J. Electroanal. Chem.* **1993,** *361*, 221–228.

33. Martinek, K.; Pshezhetskii, A. V.; Merker, S.; Pepanyan, G. S.; Klyachko, N. L.; Levashov, A. V. *Biokhimiya* **1988,** *53*, 1013–1016.

34. Varfolomeev, S. D.; Kurochkin, I. N.; Yaropolov, A. I. *Biosens. Bioelectron.* **1996,** *11*, 863–871.

35. Adachi, O.; Tayama, K.; Shinagawa, E. *Agric. Biol. Chem.* **1978,** *42*, 2045.

36. Groen, B.; Frank, J.; Duine, J. A. *Biochem. J.* **1984,** *223*, 921–924.

37. Groen, B. W.; Van Kleef, M. A.; Duine, J. A. *Biochem. J.***1986,** *234*, 611–615.

38. Deppenmeier, U.; Hoffmeister, M.; Prust, C. *Appl. Microbiol. Biotechnol.* **2002,** *60*, 233–242.

39. Gupta, A.; Singh, V. K.; Qazi, G. N.; Kumar, A. *J. Mol. Microbiol. Biotechnol.* **2001,** *3*, 445–456.

40. Battey, A. S.; Schaffner, D. W. *J. Appl. Microbiol.* **2001,** *91*, 237–247.

41. Yamada, Y.; Hoshino, K.-I.; Ishikawa, T. *Biosci., Biotechnol., Biochem.* **1997,** *61*, 1244–1251.

42. Yamada, Y.; Hosono, R.; Lisdyanti, P.; Widyastuti, Y.; Saono, S.; Uchimura, T.; Komagata, K. *J. Gen. Appl. Microbiol.***1999,** *45*, 23–28.

43. Franke, I. H.; Fegan, M.; Hayward, C.; Leonard, G.; Stackebrandt, E.; Sly, L. I. *Int. J. Syst. Bacteriol.* **1999,** *49*, 1681–1693.

44. Matsushita, K.; Toyama, H.; Adachi, O. *Adv. Microb. Physiol.* **1994,** *36*, 247–301.

45. Sugisawa, T.; Hoshino, T. *Biosci., Biotechnol., Biochem.* **2002,** *66*, 57–64.

46. Matsushita, K.; Yamashita, T.; Aoki, N.; Toyama, H.; Adachi, O. *Biochemistry* **1999,** *38*, 6111–6118.

47. Khersonsky, O.; Roodveldt, C.; Tawfik, D. S. *Curr. Opin. Chem. Biol.* **2006,** *10*, 498–508.

48. Matsushita, K.; Yakushi, T.; Takaki, Y.; Toyama, H.; Adachi, O. *J. Bacteriol.***1995,** *177*, 6552–6559.

49. Palmore, G.; Bertschy, H.; Bergens, S. H.; Whitesides, G. M. *J. Electroanal. Chem.* **1998,** *443*, 155–161.

50. Sokic-Lazic, D.; Minteer, S. D. *Biosens. Bioelectron.* **2008,** *24*, 945–950.

51. Luo, J.; Dong, M.; Lin, F.; Liu, M.; Tang, H.; Li, H.; Zhang, Y.; Yao, S. *Analyst* **2011,** *136*, 4500–4506.

52. Lojou, E. *Electrochim. Acta* **2011,** *56*, 10385–10397.

53. Feng, W.; Ji, P. *Biotechnol. Adv.* **2011,** *29*, 889–895.

54. Kim, H.; Lee, I.; Kwon, Y.; Kim, B. C.; Ha, S.; Lee, J.-H.; Kim, J. *Biosens. Bioelectron.* **2011,** *26*, 3908–3913.

55. Gray, H. B.; Winkler, J. R. *Annu. Rev. Biochem.* **1996,** *65*, 537–561.

56. Krebs, H. A.; Salvin, E.; Johnson, W. A. *Biochem. J.* **1938,** *32*, 113–117.

57. Mair, T.; Muller, S. C. *J. Biol. Chem.* **1996,** *271*, 627–630.

58. Novak, J. T.; Carlson, D. A., *J. Water Pollut. Control Fed.* **1970**, 1932–1943.

59. Chetty, L.; Kim, J.; Zhao, N. H.; Scott, D.; Liaw, B. Y. *Prepr. Symp. - Am. Chem. Soc., Div. Fuel Chem.* **2010,** *55*, 139–141.

60. Arechederra, R. L.; Minteer, S. D. *Fuel Cells* **2009,** *9*, 63–69.

61. Arechederra, R. L.; Treu, B. L.; Minteer, S. D. *J. Power Sources* **2007,** *173*, 156–161.

62. Treu, B. L., Sokic-Lazic, D. and S. D. Minteer, *ECS Trans.* **2010,** *25*, 1–11.

63. Moehlenbrock, M. J.; Toby, T. K.; Waheed, A.; Minteer, S. D. *J. Am. Chem. Soc.* **2010,** *132*, 6288–6289.

64. Sokic-Lazic, D.; De Andrade, A. R.; Minteer, S. D. *Electrochim. Acta* **2011,** *56*, 10772–10775.

65. Zebda, A.; Gondran, C.; Le Goff, A.; Holzinger, M.; Cinquin, P.; Cosnier, S., *Nat. Commun.* **2011,** *2*, 370–371.

66. Neto, S. A.; Forti, J. C.; De Andrade, A. R. *Electrocatalysis* **2010,** *1*, 87–94.

67. Saleh, F. S. M., L.; Ohsaka, T. *Sens. Actuators, B* **2011,** *152*, 6–8.

68. Tanne, C.; Goebel, G.; Lisdat, F. *Biosens. Bioelectron.* **2010,** *26*, 530–535.

69. Wang, Y.; Du, J.; Li, Y.; Shan, D.; Zhou, X.; Xue, Z.; Lu, X. *Colloids Surf., B* **2012,** *90*, 62–67.

70. Treu, B. L.; Arechederra, R. L.; Minteer, S. D. *J. Nanosci.Nanotech.* **2009,** *9*, 2374–2380.

71. Arechederra, R. L.; Minteer, S. D. *Electrochemi. Acta* **2009,** 54, 7268–7272.

72. Moehlenbrock, M. J.; Minteer, S. D. *Chem. Soc. Rev.* **2008,** *37*, 1188–1196.

CHAPTER 2

ENZYME CASCADE FOR COMPLETE OXIDATION OF GLUCOSE

2.1 Background

2.1.1 Energy Density, Power Density, and Enzyme Cascade

Energy density (Wh/L) and power density (W/cm^2) of biofuel cells are the two crucial criteria of enzymatic biofuel cell technology. Energy density describes the total chemical energy stored in fuels that can be transformed to electrical energy; power density measures the amount of power generated per unit electrode surface area. In other words, more efficient use of fuel (i.e., multiple step oxidation/reduction) will lead to higher energy density, and a faster electron transfer rate will lead to higher power density for a biofuel cell device.

Enzyme-based biobatteries and biofuel cells have remained a popular focus for research due to the high turnover rates associated with enzymes that could lead to a high bio-electrocatalysis rate,[1, 2] which in turn could lead to high power density. However, enzymatic biofuel cells have been plagued by low energy density due to incomplete oxidation of biofuels. For instance, the glucose enzymatic biofuel cells in literature utilize glucose dehydrogenase or glucose oxidase to oxidize glucose to gluconolactone and generate two electrons,[3–7] but there are six carbons that can be oxidized in one

glucose molecule, and 24 electrons are available to be liberated. So $11/12^{th}$ of the energy density of glucose is left in the waste stream of the biofuel cell (assuming the energy released with each electron release is the same). To maintain the high power densities of biofuel cells while increasing the energy density, the Palmore research group has introduced the use of enzyme cascades in 1998 in which research they used a three enzyme cascade employing alcohol dehydrogenase, formaldehyde dehydrogenase, and formate dehydrogenase to completely oxidize methanol to carbon dioxide.[8] Previous work has demonstrated that enzyme cascades can mimic metabolic enzyme pathways like the citric acid cycle to completely oxidize substrates such as ethanol and increase the power density by 9-fold compared to a single-enzyme-based ethanol biofuel cell.[9] Harnessing all 12 electrons from ethanol oxidation to carbon dioxide, instead of only two electrons for a single dehydrogenase enzyme oxidizing ethanol to acetaldehyde, allows for enhanced fuel utilization and higher energy density of the fuel cell. The power density of an enzymatic biofuel can be improved by optimizing/minimizing the enzyme cascade design. In 2009, Arechederra *et al.* reported a bioanode that utilizes a three-enzyme cascade to perform 14-electron oxidation of glycerol to carbon dioxide and achieved a biofuel cell power density of $1.32 mW/cm^2$ when coupled with air breathing platinum cathode.

2.1.2 Minimal Enzyme Cascade

In this project, we focused on efficiently utilizing the energy density through the use of an enzymatic cascade to perform the 24-electron oxidation of glucose to carbon dioxide and water. Mimicking traditional metabolic pathways (i.e., the citric acid cycle)

in living cells can improve the energy density of the biofuel cell.[10] However, the large number of non-energy-producing enzymes in many metabolic enzyme cascades substantially lowers the oxidoreductase/nonoxidoreductase enzyme ratio, and thus, the power density generated per unit area of electrode would be negatively affected. In addition, these natural metabolic pathways utilize NAD(P)-dependent enzymes, and the short lifetime, instability, and difficulty of regeneration of this coenzyme is an issue. The natural metabolic pathways for oxidizing glucose to carbon dioxide (i.e., the full glycolytic pathway and the citric acid cycle) involve 19 enzymes, and only six of those enzymes are oxidoreductases. Therefore, the majority of the enzymes in the cascade are non-power-generating enzymes and would greatly affect the efficiency of this enzymatic pathway if employed at a bioanode to oxidize glucose. Therefore, in this work, a non-natural, minimal six-enzyme cascade was developed to complete the 24-electron oxidation of glucose to carbon dioxide, as shown in Figure 2.1. The cascade consists of four pyrroloquinoline quinone (PQQ)-dependent enzymes (PQQ-dependent glucose dehydrogenase(PQQ-GDH), PQQ-dependent gluconate dehydrogenase, PQQ-dependent alcohol dehydrogenase (PQQ-ADH) and PQQ-dependent aldehyde dehydrogenase(PQQ-AlDH)), aldolase from *Sulfolobus solfataricus*, and oxalate oxidase from barley seedlings.

2.2 Designed Nonnatural Glucose Oxidation Pathways

The nonnatural, minimal glucose oxidation pathway can be divided into three sections or steps. The first step includes a two-enzyme cascade extracted from *Gluconobacter sp*. (PQQ-dependent glucose dehydrogenase and PQQ-dependent

gluconate dehydrogenase) to sequentially oxidize glucose to gluconolactone and then glucuronic acid.[11] The second step is to cleave the ring structure of glucuronic acid with an aldolase extracted from *Sulfolobus solfataricus* to form two smaller molecules, glyceraldehyde and hydroxypyruvate. Since both of those substrates are intermediates in the glycerol oxidation pathway described by Arechederra *et al*.,[12] we use the three enzyme cascade (PQQ-dependent alcohol dehydrogenase, PQQ-dependent aldehyde dehydrogenase, and oxalate oxidase) to complete the oxidation to carbon dioxide and water as the final products.

2.3 Enzyme Isolation from *Gluconobacter*

Since there are no commercial sources for PQQ-GDH, PQQ-gluconate 2-dehydrogenase, PQQ-ADH, and PQQ-AlDH, the enzymes must be extracted in the laboratory. The genus *Gluconobacter* belongs to the group of acetic acid bacteria.[13–15] Acetic acid bacteria are different from other organisms in their ability to oxidize a wide variety of carbohydrates, alcohols, and related compounds.[16–18] PQQ-ADH and PQQ-AlDH used in the designed enzyme cascade are localized in the periplasmic side of the cytoplasmic membrane and function as primary dehydrogenses in the ethanol oxidation respiratory chain. The location of PQQ-ADH and PQQ-AlDH plays an important role in the isolation of the enzymes from *Gluconobacter* species.

There are different vendors providing various strains/lines of *Gluconobacter*. *Gluconobacter sp.* from DSMZ (DSM 3504) and *Gluconobacter sp. 33* from ATCC (ATCC 15163) were compared in order to determine which gives the highest specific activities of each PQQ-dependent enzymes of interest. Both species of *Gluconobacter*

were grown in the same basal media. Also, PQQ-dependent dehydrogenases are membrane-bound in both species, allowing procedures developed for one strain to apply to the other species. All of the lysis and crude purification procedures described are carried out under conditions to prevent inactivation of PQQ-dependent enzymes by adding Ca^{2+} and removing detergents as quickly as possible. Ca^{2+} forms a coordinated complex with PQQ, allowing it to remain as a bound cofactor, which is important for maintaining enzyme activity.[18]

2.4 Aldolase from *Solfolobus Sulfataricus*

Aldolases are enzymes that are able to catalyze an aldol reaction (forming a carbon–carbon bond) or its reverse reaction (cleaving an aldol).[19] In this work, aldolase was utilized to break the carbon–carbon bonds in glucuronic acid and to form two smaller molecules, glyceraldehyde and hydroxypyruvate. Commercially available aldolases are usually a type of fructose-bisphosphate aldolase that catalyze a reverse reaction that splits the aldol, fructose 1,6-bisphosphate, into the triose phosphates, dihydroxyacetone phosphate (DHAP) and glyceraldehyde 3-phosphate (GAP), which is a very similar process as the target reaction for the glucose cascade. Unfortunately, all the commercially available aldolases (aldolase A, B, and C, aldolase from rabbit muscle and aldolase from spinach) are only active toward phosphorylated substrates and show no activity to nonphosphorylated glucuronic acid. However, aldolase extracted from *Solfolobus sulfataricus* has been shown to utilize nonphosphorylated substrates.[20] *Solfolobus sulfataricus* is a hyperthermophilic Archaeon that grows optimally at 80–85 ℃ and pH 2–4. With respect to its pathways of central metabolism, glucose is

oxidized via a nonphosphorylated Entner–Doudoroff pathway, where glucose is oxidized to gluconate, which is then dehydrated to form 2-keto-3 deoxygluconate (KDG). KDG then undergoes an aldol cleavage catalyzed by aldolase. Although glucuronic acid is not the natural substrate of this aldolase, the similarity of the structures of KDG and glucuronic acid and the promiscuity of the enzyme provide the possibility of catalytic activity of aldolase on glucuronic acid. A crude extract of aldolase was obtained via cell lysis, a heating process, and ammonium sulfate precipitation. Enzymatic activity of aldolase toward glucuronic acid was measured with modified thiobarbituric acid (TBA) assay, which will be discussed in the next section.

2.5 Assay Methods

2.5.1 Dichlorophenolindophenol (DCPIP) Assay

The enzymatic activities of PQQ-dependent enzymes toward their specific substrate can be assayed with the redox dye 2,6-dichlorophenol indophenol (DCPIP) and phenazine methosulfate (PMS). The oxidized form of DCPIP (blue) has a maximum absorption at 600 nm and will accept free electrons produced by the catalytic oxidation reaction and be reduced. The reduced form of DCPIP is colorless. Therefore, at a wavelength of 600 nm, the rate change in absorbance of DCPIP correlates to the rate of the compound transitioning from its oxidized form to its reduced form due to free electrons produced by the oxidation of the substrate, thus measuring the rate of the catalytic reaction. The assay reaction can be seen in Figure 2.2.

2.5.2 Bicinchoninic Acid (BCA) Assay

The specific activity of an enzyme is the total activity per mg of enzyme protein. Protein concentration in certain enzyme solutions will be calculated using the BCA assay. This assay is based on the colorimetric detection and quantification of total protein by using the well-known reduction of Cu^{2+} to Cu^{+} by a protein in an alkaline medium with the highly sensitive and selective colorimetric bicinchoninic acid (BCA). The peptide bonds in protein reduce Cu^{2+} ions from the cupric sulfate to Cu^{+}. The amount of Cu^{2+} reduced is proportional to the amount of protein present in the solution. Next, two molecules of BCA chelate with each Cu^{+} ion, forming a purple colored BCA-Cu^{+} that strongly absorbs light at a wavelength of 562 nm. At room temperature, the BCA–Cu^{+} complex is influenced in protein samples by the presence of cysteine/cysteine, tyrosine, and tryptophan side chains. At higher temperatures (37–60 ℃), peptide bonds assist in the formation of the reaction product. BCA reaction mixtures should be incubated at higher temperatures to increase assay sensitivity while minimizing the variances caused by unequal amino acid composition. The concentration of protein present in a solution can be quantified by measuring the absorption spectra and comparing with standard protein solutions of known concentrations.

2.5.3 Thiobarbituric Acid Reactive Substances (TBARS) Assay

Because the aldolase catalytic reaction is a nonredox reaction, redox dye assays will not be suitable to measure the enzymatic activity. A modified TBARS assay was utilized in this process. The reverse reaction of the target aldolase reaction in the designed pathway will form glucuronic acid from hydroxypyruvate and glyceraldehyde.

Glucuronic acid can be peroxidized by H_2SO_4/HIO_4 to form malondialdehyde (MDA) as one of its end products. MDA can further form a pink chromophore with thiobarbituric acid (TBA) to indicate whether the aldolase catalyzed the carbon–carbon bond forming reaction. A schematic of the TBARS assay is shown in Figure 2.3.

2.6 Experimental

2.6.1 Reagents

Reagents used were D-mannitol (Sigma), $(NH_4)_2HPO_4$ (Sigma), NaOH (Sigma), NaH_2PO_4 (Sigma), Na_2HPO_4 (Sigma), NaCl (Sigma), KH_2PO_4 (Sigma), $(NH_4)SO_4$ (Sigma), $MgSO_4 \cdot 7H_2O$ (Sigma), $CaCl_2 \cdot 2H_2O$ (Sigma), $MnCl_2 \cdot 2H_2O$ (Sigma), $Na_2B_4O_7 \cdot 10H_2O$ (Sigma), $ZnSO_4 \cdot 7H_2O$ (Sigma), $CuCl_2 \cdot 2H_2O$ (Sigma), $Na_2MoO_4 \cdot 2H_2O$ (Sigma), casamino acids (BD Medical), lysozyme from egg white (Aldrich), sodium deoxycholate (Sigma), tris-HCl (Sigma), phenylmethanesulfonyl fluoride (PMSF) (Sigma), ethylenediaminetetraacetic acid (EDTA) (Sigma), phenazine methosulfate (PMS) (Sigma), 2,6-dichloroindophenol sodium salt hydrate (DCIP) (Sigma), D-(+) glucose (Sigma), acetaldehyde (Sigma), gluconolactone (Sigma), lithium hydroxypyruvate (Sigma), trichloroacetic acid (TCA) (Sigma), periodic acid (Sigma), sodium arsenite (Sigma), 2-thiobarbituric acid (TBA), dimethyl sulfoxide (Sigma), sodium nitrate (Sigma), 13C-labelled glucose (Sigma), Toray carbon paper TGP-60 (E-Tek), tetrabutylammonium bromide (TBAB) (Sigma), Nafion 1100EW suspension (Aldrich), Triton X-100 (Aldrich), Nafion NRE 212 (Alfa Aesar), *Gluconobacter* sp. (DSMZ), Sulfolobus solfataricus (DSMZ), and oxalate oxidase (Aldrich).

2.6.2 *Gluconobacter* Growth and Enzyme Extraction

Commercially purchased *Gluconobacter sp.* (DSM 3504, ATCC 15163) was cultivated aerobically in a basal media containing yeast extract, D-mannitol, $(NH_4)HPO_4$ and $MgSO_4 \cdot 7H_2O$ at 30 ℃ for 24 h. The cell paste was centrifuged at 12,000 × g for 7 min, then washed twice with 0.9% NaCl and stored at -20 ℃ until use.

Gluconobacter was thawed and suspended in 0.2 M phosphate buffer (pH 7.2) containing 1mM $CaCl_2$, 10% sodium deoxycholate (to 0.5% final concentration), and 1mL of lysozyme (10 mg lysozyme in 1 mL 0.3 M potassium phosphate buffer pH 7.2). The solution was incubated at 4 ℃ with gentle stirring for 1 h followed by ultrasonication using a sonic dismembrator for 1 min at 4 ℃. The solution was then centrifuged for 1 h at 12,000 × g to remove insoluble materials. A 10% $CaCl_2$ solution was added to the supernatant via vortexing (0.5% final concentration) to form a calcium phosphate gel and allowed to equilibrate at 4 ℃ for 45 min. The resultant gel was collected by centrifugation for 20 min at 6,000 × g, resuspended in 0.3 M potassium phosphate buffer (pH 7.2), and stirred gently for 10–20 min to elute bound enzyme. Insoluble material was discarded after centrifugation at 12,000 × g for 30 min.

2.6.3 *Solfolobus Sulfataricus* Growth and Crude Purification of Aldolase

Commercially purchased *Sulfolobus solfataricus* (DSM 1616) was cultivated aerobically in an acidic media containing yeast extract, casamino acids, KH_2PO_4, $(NH_4)SO_4$, $MgSO_4 \cdot 7H_2O$, $CaCl_2 \cdot 2H_2O$, $MnCl_2 \cdot 2H_2O$, $Na_2B_4O_7 \cdot 10H_2O$, $ZnSO_4 \cdot 7H_2O$, $CuCl_2 \cdot 2H_2O$, $Na_2MoO_4 \cdot 2H_2O$, $VOSO_4 \cdot 2H_2O$, and $CoSO_4 \cdot 7H_2O$ at 78 ℃ for 72 h. The cell paste was centrifuged at 12,000 × g for 7 min, then washed twice with 0.9% NaCl

and stored at -20 ℃ until use.

Sulfolobus solfataricus cell paste was resuspended in 20 mM Tris/HCl, pH 8.5, containing 1mM PMSF and 1mM EDTA, at approximately 0.2 g of cells/mL and incubated at 4 ℃ for 30 min, and then cells were broken by ultrasonication using a sonic dismembrator for 1 min at 4 ℃. Soluble cell extract was obtained by centrifugation at 25,000 × g for 1 h at 4 ℃. The insoluble pellet was discarded. The soluble cell extract was heated in a glass test tube (1 cm diameter) in a water bath at 90 ℃ for 15 min. Precipitated proteins were then removed by centrifugation at 13,000 g for 1 h at 4 ℃.

2.6.4 PQQ-Dependent Enzyme Assay Procedure

The enzyme reaction mixture consisted of 1.5 mL of 50 mM potassium phosphate buffer pH 7.3, 0.2 mL of 600 uM PMS, 0.1 mL of 700 uM DCPIP, 0.01 mL of enzyme solution, and 0.2 mL of a 0.2 M substrate solution. For PQQ-alcohol dehydrogenase, the primary substrate was ethanol; for PQQ-aldehyde dehydrogenase, acetaldehyde; for PQQ-glucose dehydrogenase, glucose; and for PQQ-gluconate dehydrogenase, gluconolactone. The change in absorbance during a 2 min interval for each sample was measured at 37 ℃ at time = 0 minutes (A_0) and time = 2 min (A_2) at 600nm on a spectrophotometer. Specific activity was calculated in U/mg. The molar absorptivity (ε) of DCPIP was experimentally determined to be 15. The value of "X" was the amount of protein (mg) in the sample, which was determined by BCA assay. The equation to calculate specific activity in U/mg can be seen below:

$$\frac{U}{mg} = \frac{(A_0 - A_2)/2}{\varepsilon} \times \frac{2.01}{(0.01) \times X/1000}$$

2.6.5 Aldolase TBARS Assay

Aldolase activity was measured using a modification of the TBARS assay. The standard assay temperature in all studies reported in this paper was 78 ℃. Reactions of total volume 250 µL were incubated at 78 ℃ in 50mM sodium phosphate buffer, pH 6.0, with 50 mM hydroxypyruvate and 20 mM D, L-glyceraldehyde and 50 uL of cell extract. After 10 min, 100 µL samples were removed and the reaction stopped by the addition of 10 uL of 12% (w/v) trichloroacetic acid. Precipitated proteins were removed by centrifugation, and 50 uL of the supernatant were then oxidized by the addition of 125 uL of 25 mM periodic acid/0.25 M H_2SO_4 and incubation at room temperature for 20 min. Oxidation was terminated by the addition of 250 uL of 2% (w/v) sodium arsenite in 0.5 M HCl. TBA (1mL, 0.3% (w/v)) was then added and the chromophore developed by heating at 100 ℃ for 10 min. The color was intensified by adding an equal volume of DMSO. The absorbance was read at 549 nm. Assays were performed for both aldolase and a control containing no enzyme (20 mM Tris/HCl, pH 8.5, containing 1mM PMSF and 1mM EDTA solution).

2.6.6 Bioanode Fabrication

The bioanode responsible for complete oxidation of glucose contained a six-enzyme cascade consisting of PQQ-dependent glucose dehydrogenase, PQQ-dependent 2-gluconate dehydrogenase, aldolase, PQQ-dependent alcohol dehydrogenase, PQQ-dependent aldehyde dehydrogenase, and oxalate oxidase immobilized in a TBAB-modified Nafion. The 5 wt.-% TBAB-modified Nafion membrane suspensions were prepared as discussed in Reference.[21] Enzyme/TBAB-modified Nafion casting solutions

were made with 1:1 ratio TBAB-Nafion and enzyme cascade solution. Enzyme ratios were calculated based on specific activity. Casting solutions of 20 mg protein/mL were vortexed in preparation for coating on electrode. A 100 uL aliquot of solution was pipetted onto the electrode, allowed to soak into the Toray paper electrode, and dried in the hood for 12 h. A schematic of the fabricated bioanode coupled with an air-breathing platinum cathode is shown in Figure 2.4.

2.6.7 Physical Cell Apparatus

The biofuel cell test cell consists of an anode compartment and a cathode compartment. The anode compartment of the cell contained approximately 2 mL of pH 6.5 phosphate buffer solution with 100 mM fuel and 6 M $NaNO_3$ electrolyte. The cathode consisted of a 2.5 × 2.5 cm piece of an ELAT electrode with 20% Pt on Vulcan XC-72 (E-Tek) hot pressed to a 3 × 3 cm piece of Nafion NRE212 membrane. Cells were allowed to equilibrate until the electrodes reached maximum open circuit potential. Performance testing was done immediately after equilibration. All data were collected and analysed for the test cell with a CH Instruments 650 potentiostat interfaced to a PC. A schematic of the test cell is shown in Figure 2.5.

2.6.8 Nuclear Magnetic Resonance (NMR) Measurements

NMR is a common qualitative analysis technique employed in electrochemical systems to determine the product of oxidation. We used 100 mM ^{13}C-labelled glucose as fuel and applied a constant voltage to the cell to allow the oxidation to occur and then performed an NMR study on the product of step 1 oxidation and the whole cascade

oxidation. For step 1 oxidation, NMR samples were made by mixing 350 uL of carbon-13 labeled product solution with an equal volume of deuterated water. For the whole cascade study, 0.05 g of NaOH that was allowed to adsorb the CO_2 produced was dissolved in 700 uL deuterated water. Controls were performed without enzyme.

2.6.9 Mass Spectrometry Study

Step 2 of the glucose oxidation pathway is a nonredox reaction. We immobilized aldolase from *Sulfolobus solfataricus* on Toray paper electrode and incubated the electrode in 100 mM glucuronic acid at pH 6.0 for 12 hours. Then we performed mass spectrometry (negative ESI ionization mode, WATERS LCT Premier XE) on this product solution for analysis.

2.7 Results and Discussion

2.7.1 Specific Activities of PQQ-Dependent Enzymes

Each PQQ-dependent dehydrogenase of interest in the crude *Gluconobacter* extract was assayed in the presence of its primary substrates (PQQ-GDH: glucose, PQQ-gluconate 2-dehydrogenase: gluconolactone, PQQ-ADH: ethanol, PQQ-AlDH: acetaldehyde). Specific activity was defined as the total activity toward a certain substrate per mg of protein, and the unit was U/mg. By definition, 1 unit will oxidize 1 μmol of substrate per minute. For biofuel cell applications, it is desirable to have a high specific activity in order to efficiently oxidize fuels to harness chemical energy but not necessarily a stringent specificity toward a substrate. Freshly prepared lysate was tested for enzymatic activity towards several substrates. Results are shown in Table 2.1.

Crude extract from *Gluconobacter sp.* showed activities on all tested substrates which indicated the existence of active PQQ-GDH, PQQ-gluconate 2-dehydrogenase, PQQ-ADH, and PQQ-AlDH. Enzyme was stored in 50 mM potassium phosphate buffer and kept at 4 ℃. Specific activities were measured again after 7 days. Fifty to sixty percent of enzymatic activities were retained for each of the PQQ-dependent enzymes.

2.7.2 Oxidation Pathway Step One

Step one in the designed glucose oxidation pathway utilizes a two-enzyme cascade (PQQ-GDH and PQQ-gluconate 2-dehydrogenase) to perform a two-step oxidation of glucose and form glucuronic acid. To evaluate the two-enzyme cascade in step one, we used a standard test cell containing an air-breathing platinum cathode separated from the analyte by a Nafion 212 PEM, as described in the experimental section. Enzyme extract from *Gluconobacter sp*. was immobilized on a Toray paper electrode with tetrabutyl-ammonium bromide (TBAB)-modified Nafion polymer. In the anodic compartment, a solution of 100 mM ^{13}C labeled glucose in pH 7.2 phosphate buffer was used as fuel. The average open circuit potential was 0.473 ± 0.024 V, and the maximum current density at 0.001V was 0.928 ± 0.106 μA/cm^2. NMR was used to analyze the product solution, as shown in Figure 2.6. Singlet chemical shifts appeared at 173.3 and 179.0 ppm, representing the formation of gluconolactone and glucuronic acid in this process.

2.7.3 Oxidation Pathway Step Two

Aldolase was extracted from *Solfolobus sulfataricus* with methods described in the experimental section. TBARS assay was performed with freshly extracted crude aldolase. Control experiments with no aldolase were also performed, and the results are shown in Figure 2.7. The aldolase sample showed the formation of pink chromophore with TBA while the control did not. The results confirmed the ability of the aldolase to cleave the ring structure of the glucuronic acid and form glyceraldehyde and hydroxypyruvate. Mass spectroscopy was also performed as described in the experimental section. These results also confirmed activity of aldolase toward glucuronic acid (Figure 2.8)

2.7.4. Oxidation of Glucose with Six-Enzyme Cascade

To examine the compatibility of the six-enzyme cascade, enzyme extract from *Gluconobacter sp*. that contained PQQ-dependent glucose dehydrogenase, PQQ-dependent-gluconate 2-dehydrogenase, PQQ-dependent alcohol dehydrogenase, and PQQ-dependent aldehyde dehydrogenase along with aldolase and oxalate oxidase were immobilized onto a Toray electrode with tetrabutylammonium bromide (TBAB)-modified Nafion. A test cell was run, similar to the step one measurement, in 100 mM ^{13}C-labeled glucose in pH 6.5 phosphate buffer solution. Figure 2.9 compares the power curve for the six-enzyme cascade with the power curve for the two-enzyme cascade described before. The average open circuit potential was 0.571 ± 0.012 V, compared to a control biofuel cell with no enzyme on the anode, which had an open circuit potential of 0.143 ± 0.006 V. The maximum current density at 0.001 V was 31.5 ± 6.5 μA/cm^2

for the enzymatic cascade bioanode, compared with 119 ± 8 nA/cm^2 for the nonenzyme control bioanode. The maximum power density was 6.74 ± 1.43 μW/cm^2 for the enzymatic cascade, compared with 9.92 ± 3.37 nW/cm^2 for the nonenzyme control.

When comparing the two-enzyme cascade in step one (glucose dehydrogenase and 2-gluconate dehydrogenase) with the six-enzyme cascade for complete oxidation, the power density increased 46.8-fold, and the current density increased 33.9-fold. This shows the importance of enzyme cascades in deeply oxidizing fuels in enzymatic biofuel cells. To verify that complete oxidation of glucose was achieved and carbon dioxide was produced in the oxidation of glucose, a small NaOH pellet was placed above the fuel solution chamber to absorb ^{13}C-labeled CO_2. NMR results of the pellet (Figure 2.10) showed a peak at 168 ppm, indicating the formation of carbon dioxide in the oxidation process.

In order to quantitatively investigate the conversion of glucose, a bulk electrolysis experiment was carried out to determine the Faraday efficiency (fraction of charge passed to form products in an electrochemical process divided by the charge consumed for that process); coulombic efficiency (fraction of charge passed to form products in an electrochemical process divided by the theoretical charge for that process); and product efficiency (fraction of the amount of product formed in a process divided by the theoretical amount of product formation for that process). All the products formed during operation of the glucose biofuel cell were determined with mass spectrometry. A 2 mL, 1mM glucose solution was used as fuel for the biofuel cell. After 120 h operation at 5mV cell potential, the current density decreased to 2% of the maximum. The theoretical electric charge of the fuel solution was 4.63C (1 mole of glucose can

generate 24×96,485C in principle) and 3.07C of charge had passed during bulk electrolysis process. The Faraday efficiency, Coulombic efficiency, and product efficiency can be calculated by determining the products formed during the biofuel cell operation. The product solution was analyzed with quantitative mass spectrometry, and the results analysis suggests that the product solution has no detectable glucose. It contains gluconic acid (in equilibrium with cyclic ester form gluconolactone in aqueous solution) (0.15mM), glucuronic acid (0.16mM), mesoxalic acid (0.35mM), and oxalic acid (0.2mM) as shown in Figure 2.11. With this information, three efficiencies are calculated:

(1) Product efficiency. The amount of carbon dioxide formed in the process can be calculated by using the total amount of carbon in glucose fuel subtracted by the amount of carbon left in the final product. The calculation result shows that 44.8% of the glucose is completely converted to CO_2.

$$\frac{[6 \times 1mM - (6 \times 0.15mM + 6 \times 0.16mM + 3 \times 0.35mM + 2 \times 0.2mM)]}{6 \times 1mM} = 44.8\%$$

(2) Coulombic efficiency. The calculation result shows that 63% of theoretical maximum amount of charge is transferred during the biofuel cell operation of 120 hours:

$$0.002L \times \frac{96485C}{mole\ e}\left[\left(\frac{1\ mmole\ glucose}{L} \times 0.448\% \times \frac{0.024\ mole\ e}{mmole\ glucose}\right)\right.$$

$$+\left(\frac{0.15}{L} \times \frac{2\ mole\ e}{mmole\ glucose} \times \frac{1\ mole\ glucose}{1000\ mmole\ gluconic\ acid}\right)$$

$$+\left(\frac{0.16\ mmole\ glucuronic\ acid}{L} \times \frac{4\ mole\ e}{mole\ glucose}\right.$$

$$\left.\times \frac{1\ mole\ glucose}{1000\ mmole\ glucuronic\ acid}\right)$$

$$+\left(\frac{0.35\ mmole\ mesooxilic}{L} \times \frac{12\ mole\ e}{mole\ glucose}\right.$$

$$\left.\times \frac{1\ mole\ glucose}{2000\ mole\ mesooxilic\ acid}\right)$$

$$+\left(\frac{0.2\ mmole\ oxilic\ acid}{L} \times \frac{20\ mole\ e}{mole\ glucose}\right.$$

$$\left.\left.\times \frac{1\ mole\ glucose}{3000\ mmole\ oxilic\ acid}\right)\right] / 4.63C$$

$$=2.91C/4.63C = 63.0\%$$

(3) Faraday efficiency. The calculation result shows that 95.0% (2.91*C*/3.07*C*) of charge consumed was transferred to products.

Product analysis shows that this glucose biofuel cell exhibits a good Faraday efficiency of 95%. The biofuel cell was operated till the current density decreased to 2% of its maximum; product efficiency and Coulombic efficiency can be increased by letting the biofuel cell react to lower than 2% current density.

2.8 Conclusions

In this work, glucose was oxidized to carbon dioxide with a simple six-enzyme cascade. PQQ-dependent enzymes were used due to their lack of specificity along with aldolase from *Solfolobus sulfataricus* to cleave the ring structure of glucuronic acid, both of which have not been previously described. This glucose enzymatic bioanode coupled with an air-breathing cathode yielded a maximum power density of 6.74 ± 1.43 $\mu W/cm^2$ and showed a Faraday efficiency of 95%.

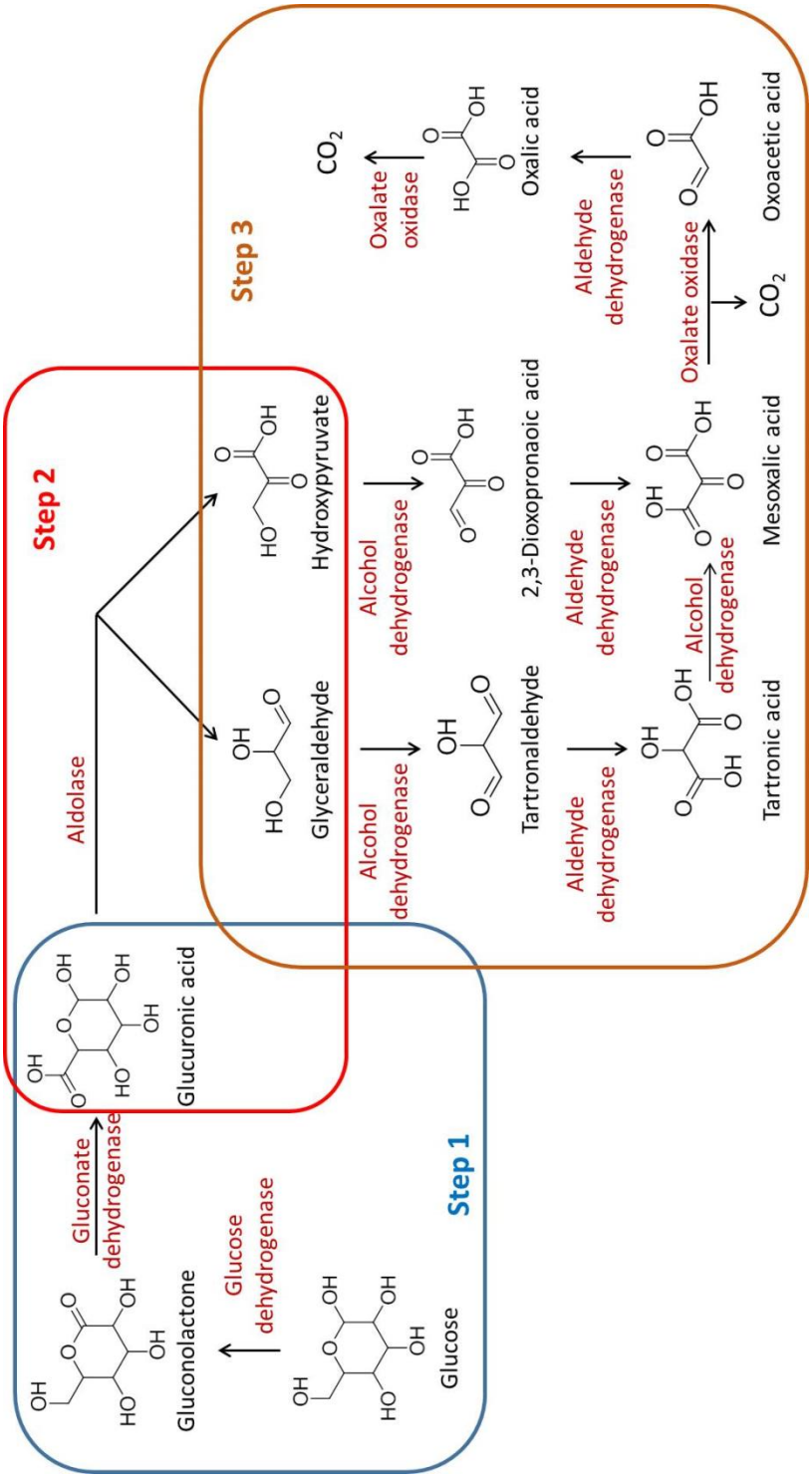

Figure 2.1 Designed oxidation pathways of glucose to carbon dioxide containing a six-enzyme cascade.

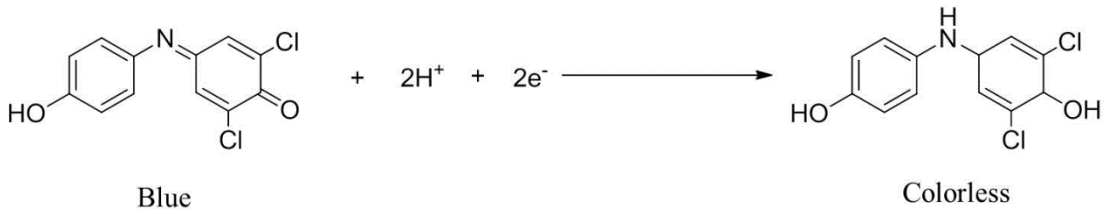

Figure 2.2 The assay reaction of the electron acceptor dye 2,6-dichlorophenol indophenol (DCPIP).

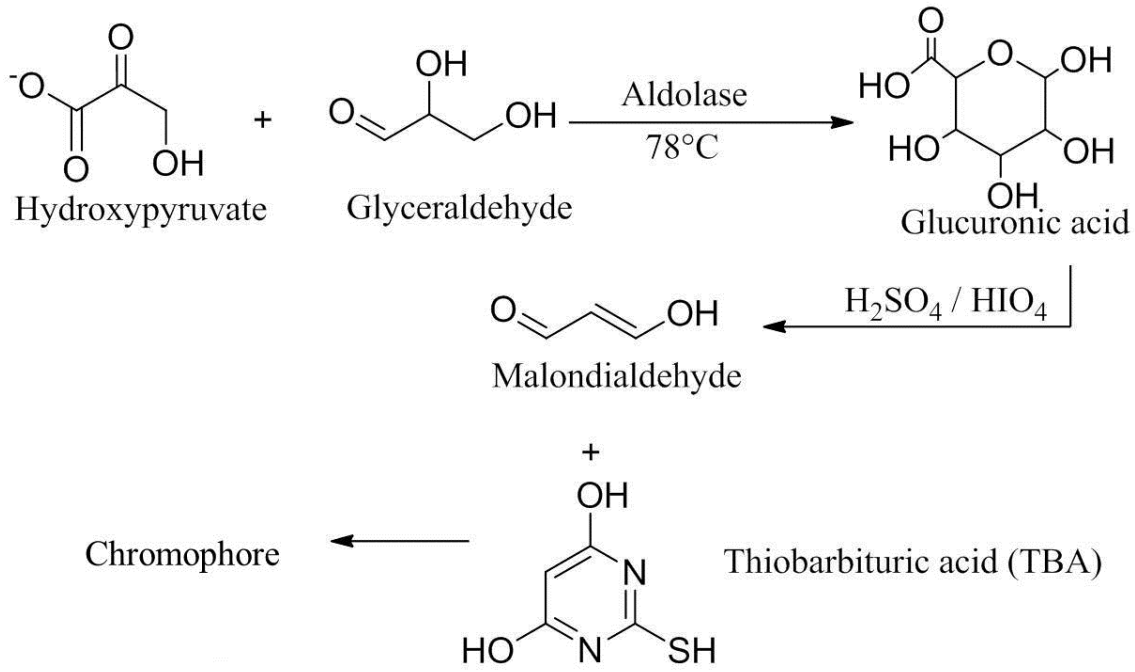

Figure 2.3 Schematic of modified TBARS assay.

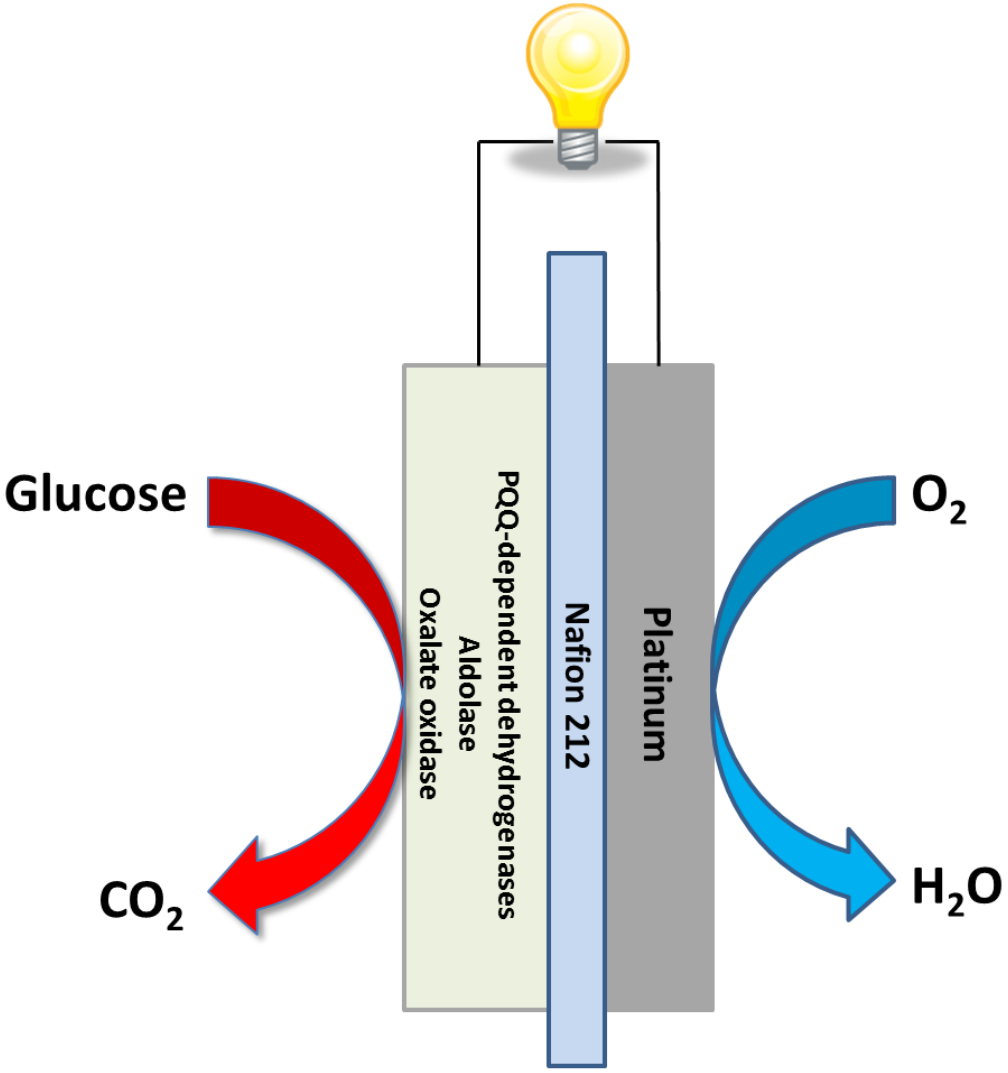

Figure 2.4 A schematic of the fuel cell setup.

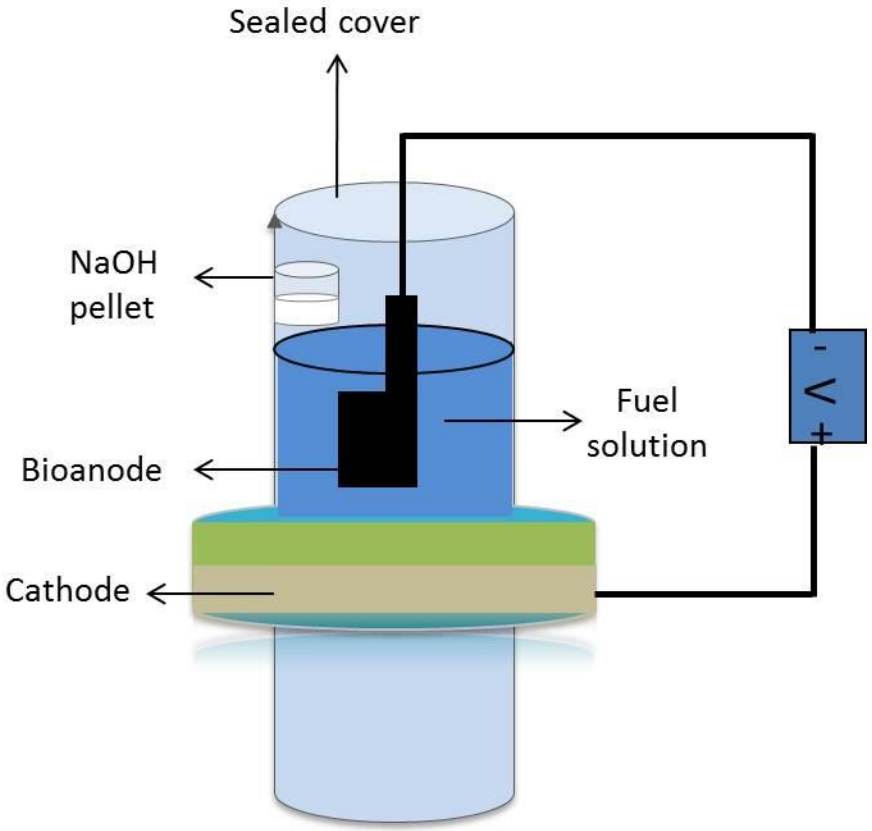

Figure 2.5 A schematic of the test cell setup.

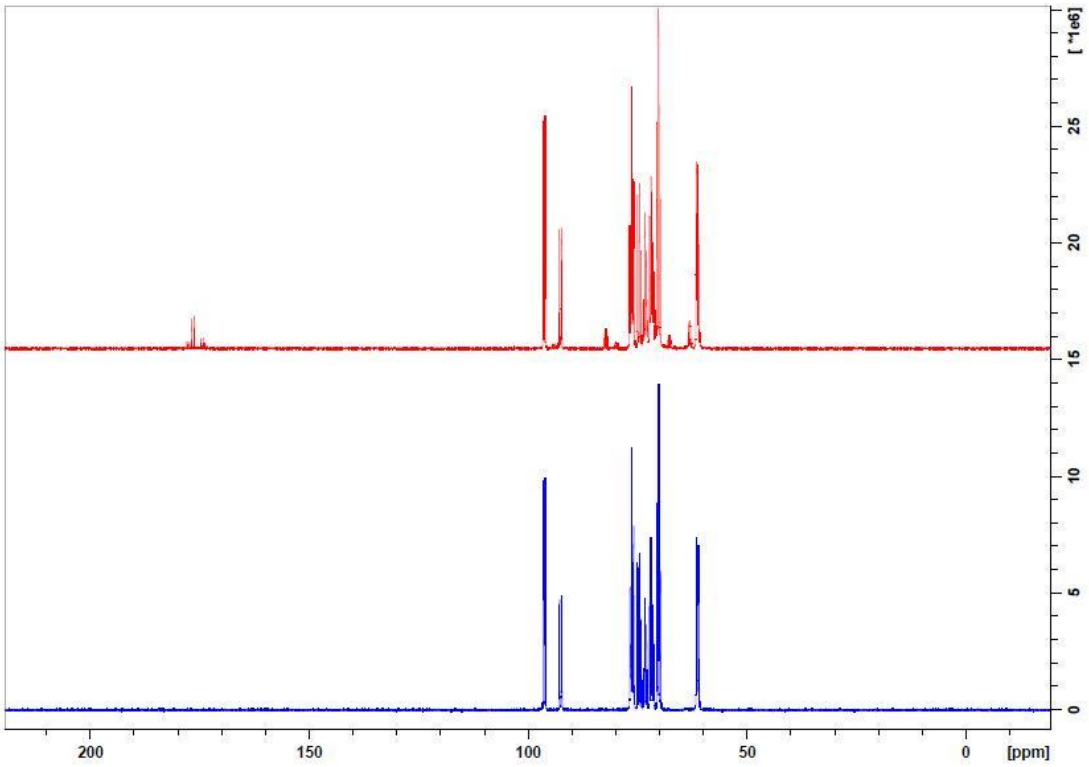

Figure 2.6. ^{13}C NMR results for step 1 (blue: fuel, red: product) fuel and product. New peaks at 173 ppm and 179 ppm indicate the formation of gluconolactone and glucuronic acid.

Figure 2.7. Optical photograph of TBARS assay for aldolase activity.

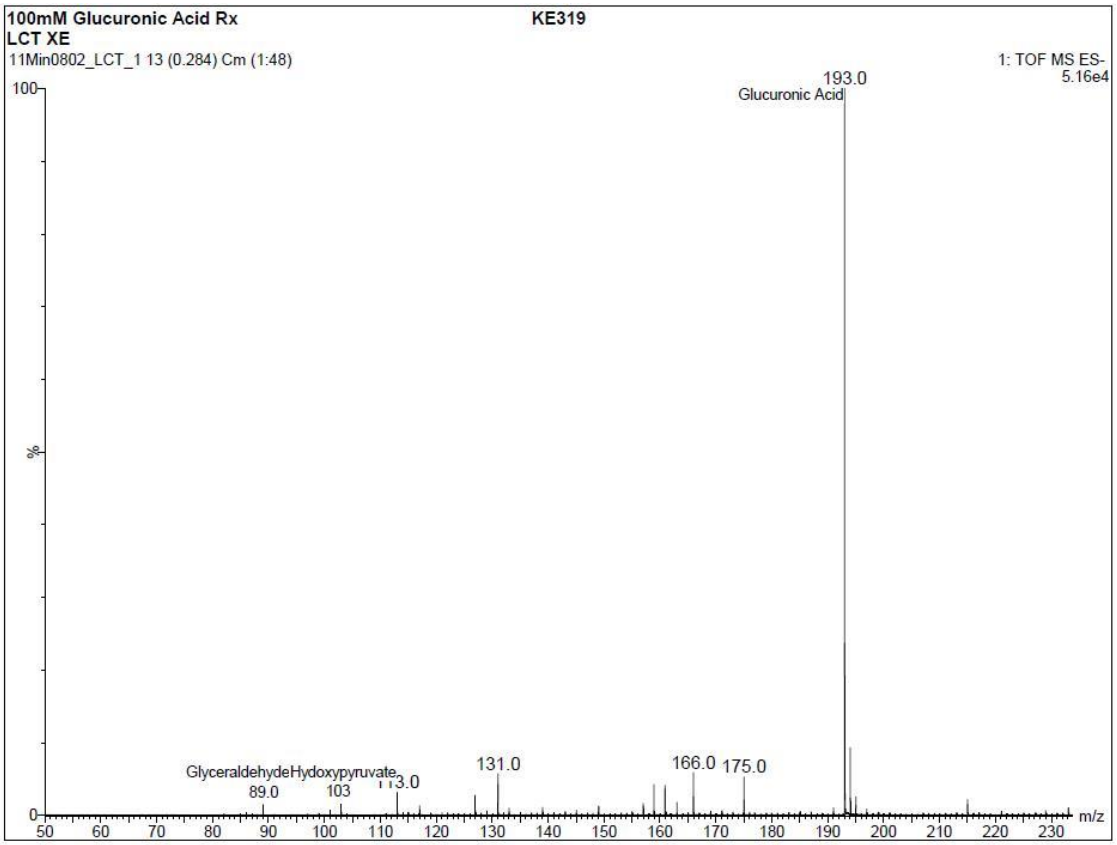

Figure 2.8 Mass spectroscopy results for step 2 product analysis. Peaks of glyceraldehyde (mw: 90.08) and hydroxypyruvate (mw: 104.06) were shown. The sample was run in negative ion mode, which is forming $[M\text{-}H+]^-$; peaks are molecular weight -1.

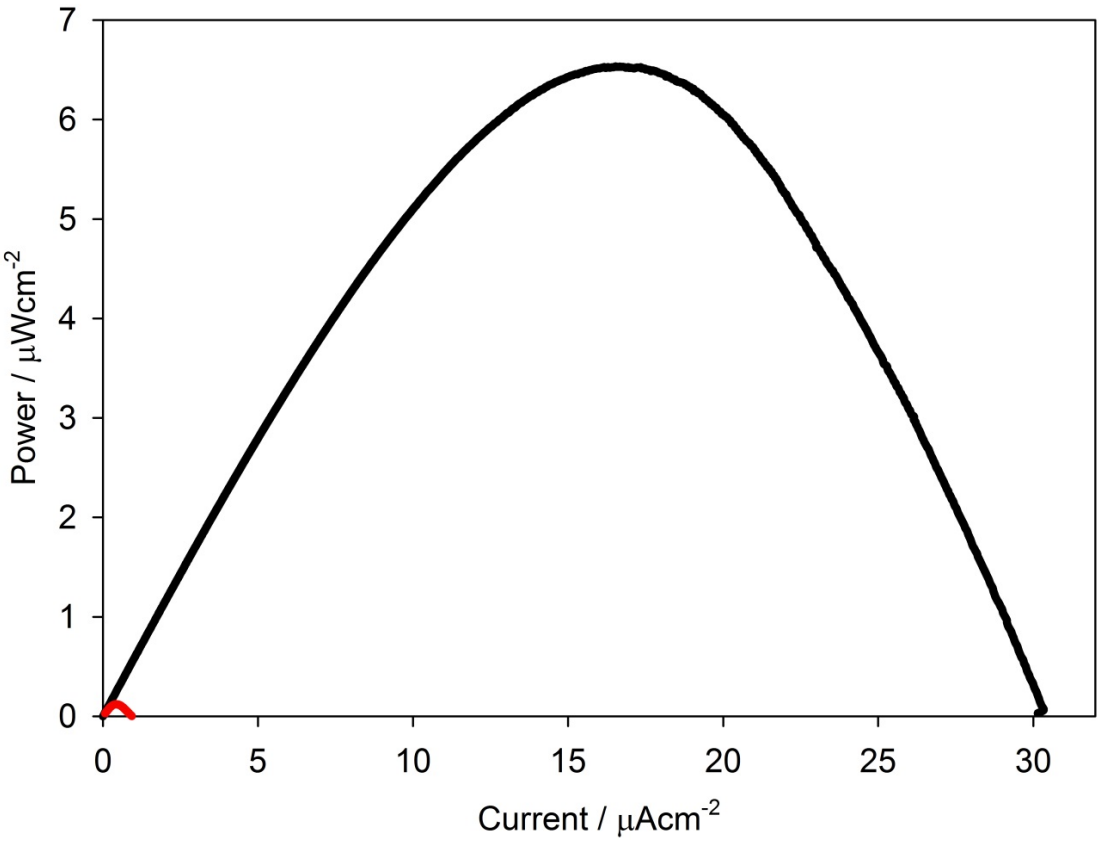

Figure 2.9 Representative power curves and polarization curves for the first-step two-enzyme cascade (red) bioanode and the whole six-enzyme cascade bioanode (black) in a glucose/air biofuel cell using 100mM glucose in phosphate buffer with 6M sodium nitrate supporting electrolyte.

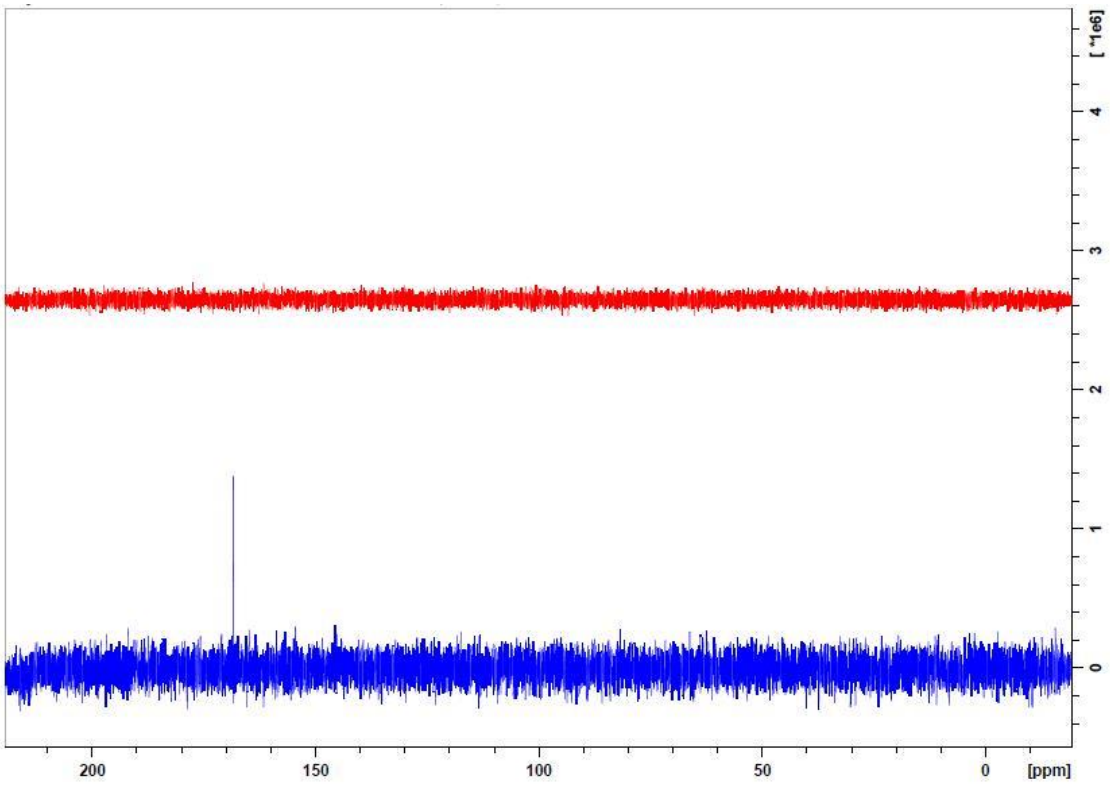

Figure 2.10 NMR spectra for glucose oxidation product of the whole enzyme cascade bioanode. The red signal represents the control sample lacking immobilized enzyme in the anodic compartment, and the blue represents the test sample resulting from the enzymatic cascade anode. A peak at 168 ppm represents carbonate.

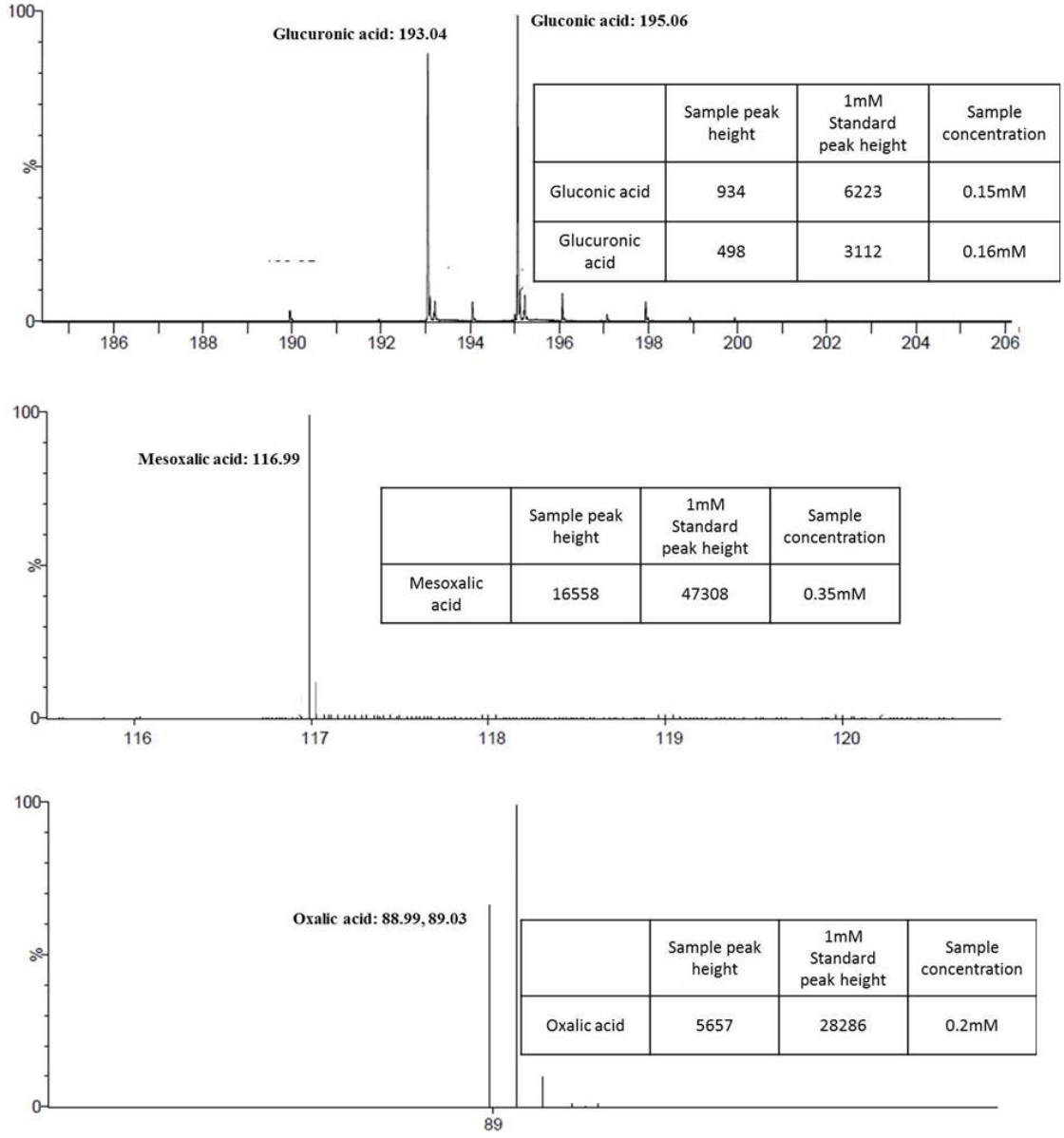

	Sample peak height	1mM Standard peak height	Sample concentration
Gluconic acid	934	6223	0.15mM
Glucuronic acid	498	3112	0.16mM

	Sample peak height	1mM Standard peak height	Sample concentration
Mesoxalic acid	16558	47308	0.35mM

	Sample peak height	1mM Standard peak height	Sample concentration
Oxalic acid	5657	28286	0.2mM

Figure 2.11 Mass spectrometry analysis of bulk electrolysis product solution. Gluconic acid, glucuronic acid, mesoxalic acid, and oxalic acid were detected with concentrations of 0.15 mM, 0.16 mM, 0.35 mM, and 0.2 mM, respectively. Sample was run in negative ion mode which is forming $[M\text{-}H+]^-$; peaks are molecular weight -1. 1mM chemical solutions were used as standards.

Table 2.1 Results of enzyme activity assay for PQQ-dependent dehydrogenases.

Enzyme	Activity (unit/mg)	Activity after 7 days (unit/mg)
PQQ-GDH	1.93 ± 0.34	0.98 ± 0.22
PQQ-gluconate dehydrogenase	2.09 ± 0.48	1.01 ± 0.37
PQQ-ADH	2.95 ± 0.88	1.94 ± 0.52
PQQ-AlDH	2.42 ± 0.48	1.55 ± 0.41

2.9 References

1. Silverman, R. B. *The Organic Chemistry of Enzyme Catalyzed Reactions.* Academic Press: San Diego, 2000.

2. Mano, N.; Fernandez, J. L.; Kim, Y.; Shin, W.; Bard, A. J.; Heller, A. *J. Am. Chem. Soc.* **2003,** *125*, 15290–15294.

3. Saleh, F. S. M., L.; Ohsaka, T. *Sens. Actuators, B* **2011,** *152*, 6–10.

4. Yehezkeli, O.; Tel-Vered, R.; Raichlin, S.; Willner, I. *ACS Nano* **2011,** *5*, 2385–2391.

5. Holland, J.; C., L.; Brozik, S.; Atanassov, P.; Banta, S. *J. Am. Chem. Soc.* **2011,** *133*, 19262–19265.

6. Tanne, C.; Goebel, G.; Lisdat, F. *Biosens. Bioelectron.* **2010,** *26*, 530–535.

7. Li, X.; Zhang, L.; Su, L.; Ohsaka, T.; Mao, L. *Fuel Cells (Weinheim, Ger.)* **2009,** *9*, 85–91.

8. Palmore, G.; Bertschy, H.; Bergens, S. H.; Whitesides, G. M. *J. Electroanal. Chem.* **1998,** *443*, 155–161.

9. Sokic-Lazic, D.; Minteer, S. D. *Biosens. Bioelectron.* **2008,** *24*, 945–50.

10. Sokic-Lazic, D.; Minteer, S. D. *Electrochem. Solid-State Lett.* **2009,** *12*, 26–28.

11. Ivnitski, D.; Atanassov, P.; Apblett, C. *Electroanal.* **2007,** *19*, 1562–1568.

12. Arechederra, R. L.; Minteer, S. D. *Fuel Cells* **2009,** *9*, 63–69.

13. Olijve, W.; Kok, J.J. *Arch. Microbiol.* **1979**, 121, 283–290.

14. De Ley, J.; Gillis, M.; Swings, J. *Bergey's Manual of Systematic Bacteriology,* Williams & Wilkins, **1984;** Vol. 1.

15. Karthikeyan, R.; Sathish, k. K.; Murugesan, M.; Berchmans, S.; Yegnaraman, V. *Environ. Sci. Technol.* **2009,** *43*, 8684–8689.

16. Ameyama, M.; Adachi, O. *Methods Enzymol.* **1982,** *89*, 491–496.

17. Adachi, O.; Shinagawa, E.; Matsushita, K.; Ameyama, M. *Agric. Biol.Chem.* **1982,** *46*, 2859–2863.

18. Ameyama, M.; Shinagawa, E.; Matsushita, K.; Adachi, O. *Agric. Biol. Chem.* **1985,** *49,* 699–709.

19. Rutter, W. J. *J. Biol. Chem.* **1963,** *238,* 6–10.

20. Buchanan, C. L.; Danson, M. J.; Hough, D. W. *Biochem. J.* **1999,** *343*, 8–12.

21. Akers, N.; Moore, C.; Minteer, S. *Electrochim. Acta* **2005,** *50*, 2521–2525.

CHAPTER 3

IMPACT OF THE LINKAGE OF ENZYME TO ELECTRODE ON DIRECT BIOELECTROCATALYSIS

3.1 Background

3.1.1 DET and DET Enzymes

Most oxidoreductase enzymes that have been utilized in biofuel cell applications have not been shown to be able to promote electron transfer by themselves.[1] Small molecular weight redox active compounds[2–5] or immobilized redox polymers[6–9] have been incorporated in the biofuel cell system to mediate the electron transfer from the enzyme to the electrode surface (or vice versa). This approach is termed mediated electron transfer (MET). Although many mediators have been demonstrated to be able to efficiently assist the transfer of electrons, they do have many drawbacks in biofuel cell applications. A "mediatorless" or direct electron transfer (DET) method was much needed in biofuel cell development for the fact that using enzymes that are capable of facile DET eliminates the need for mediator molecules that can be nonselective, decrease stability, and decrease the open circuit potential of the biofuel cell, which limits the optimal performance of the biofuel cell. Since the 1980s, when a number of enzymes were found to be capable of interacting directly with an electrode while

catalyzing the redox reaction of a substrate,[10–15] DET enzymes have drawn the attention of bioelectrocatalysis researches. The first studies of DET enzymes involved examining enzymes such as laccase, which showed the ability to catalyze the four-electron reduction of O_2 to H_2O through direct electron transfer from the electrode surface to the active site. More recently, O_2 reduction at a more neutral pH was observed with the DET-capable enzyme bilirubin oxidase (BOD).[16] Anodic direct bioelectrocatalysis has been rarer. Many of the enzymes that have been shown to perform direct bioelectrocatalysis contain redox active metal centers that perform the intrinsic transfer of electrons.[15] For example, the heme group of several enzymes is capable of existing in several redox states and transfers resultant electrons produced at the active site of the enzyme. One of the prime examples of this has been cellobiose dehydrogenase, which contains a FAD cofactor and a heme center that is capable of direct electron transfer.[17, 18] Another class of heme-containing enzymes that can undergo direct bioelectrocatalysis consists of quinohemoproteins, such as pyrroloquinoline quinone (PQQ)-dependent enzymes.[19–23]

3.1.2 Classification of PQQ-Dependent Enzymes

Pyrroloquinoline quinone (PQQ)-dependent enzymes have shown to be able to catalyze the oxidation of substrates like alcohol, aldehyde, and sugars.[24–26] These quinohemoproteins contain multiheme groups in different subunits, and electrons can be transferred through single-heme or multiheme pathways before they arrive at the surface of the electrode. PQQ-dependent enzymes are generally divided into three types: (1) nonheme containing PQQ-dependent enzymes, such as PQQ-glucose dehydrogenase;

(2) single-heme PQQ-dependent enzymes, such as PQQ-dependent sorbitol dehydrogenase; and (3) multiheme PQQ-dependent enzymes. The most well-known are PQQ-dependent alcohol and aldehyde dehydrogenases. DET was reported to be achieved most frequently with these multiheme biocatalysts, and electron transfer was demonstrated to occur through a single heme or multiheme pathway.[27–29]

3.1.3 Impact of Enzyme Linking Site on DET

The conditions of DET for complex multisubunit proteins are closely related to the proximity and linkage of the enzymes toward the electrode surface for electron tunneling to occur, allowing the biocatalytic reaction to be the limiting process. In the case of quinohemoproteins, the closest heme group in the enzyme to the electrode surface needs to be within electron tunneling distance.[15, 30] For larger proteins, the linking site of the enzyme toward the electrode surface will not only affect the proximity of the redox active site and the electrode surface, but also determines whether the substrate active site is accessible or blocked by the electrode. In the past few years, different methods have been employed to increase the proximity. Conductive polymers,[31] carbon nanotubes (CNTs),[32] and sol-gel/carbon nanotube composite electrodes[33] have been utilized to increase the electrode surface area and roughness, thus decreasing the distance between the redox active site and the electrode surface. However, all of these techniques decrease the electron transfer distance with an anisotropic enzyme linkage, and contributions to electron transfer from differently oriented proteins were not discussed.

3.1.4 Immobilization of PQQ-AlDH via Specific Linking Site

Approaches for isotropic alignment of the DET enzyme on the electrode surface were reported with major methods, including (a) the reconstitute apoenzyme on the preimmobilized cofactor to yield a DET favorable orientation[34, 35] and (b) binding of enzyme molecules through a unique functional group,[36, 37] but most lack in their discussion of electron transfer properties or comparison of electron transfer from different orientations of the same protein.[38, 39] In this work, how the multisubunit, multiheme enzymes' linkages toward the electrode surface will affect the electron transfer rate will be addressed, by aligning PQQ-AlDH on the electrode surface through the six-histidine tag (His-tag) functional group. As mentioned above, PQQ-dependent enzymes have been shown to be capable of DET because of the existence of multiple heme *c* groups that act as DET charge carriers. In this study, PQQ-dependent aldehyde dehydrogenase (PQQ-AlDH) from *Gluconobacter sp.* has been chosen to demonstrate the importance of enzyme orientation. PQQ-AlDH consists of three subunits: one subunit that contains cofactor PQQ and one heme *c* group (subunit I), one subunit that contains three heme *c* moieties (subunit II), and one small subunit that is a peptide that bridges the two larger subunits together and maintains the integrity of the whole protein structure but does not contain any electroactive species (subunit III). Genetically modified PQQ-AlDHs with a 6×His-tag at the N- or C-terminus of each subunit were used for different types of orientation specific immobilization. The strategy of this study is schematically depicted in Figure 3.1.

3.2 Immobilized Metal Ion Affinity Chromatography (IMAC)

Purification of recombinant proteins from host organisms is often a time-consuming task and the rate-limiting step in obtaining proteins from recombinant sources. A well-known solution for simplifying the purification process is to engineer the expressed protein product so as to contain additional amino acids, which convey a unique property to the protein of interest. The property chosen to impart to a protein with a few additional amino acids is the ability to bind transition metals, which allows that protein to be purified using immobilized metal ion affinity chromatography (IMAC).

IMAC is a powerful affinity method introduced in 1975 by Porath *et al*., which takes advantage of the interaction between biomolecules and transition metal ions.[40] In IMAC, metal ions are immobilized on a hydrophilic support that chelates metal ions. Recombinant proteins (target enzyme) with a high affinity for a given metal ion bind through the open coordination sites on the metal ion and are chemically attached to the column, while other proteins without a high affinity for the metal ion pass through the column during the wash. The target protein can be eluted by being replaced by higher affinity molecules. A schematic of interaction between a His-tagged enzyme and Ni-NTA column is shown in Figure 3.2.

3.3 IMAC-Inspired Isotropic Immobilization of Enzymes

To control the linkage of the enzyme toward the electrode surface, a reported method was utilized that was inspired by metal ion affinity chromatography.[41] The flat bare gold surface was exposed to dithiobis(succinimidylpropionate) (DTSP) to form a

monolayer spontaneously with the metal surface through covalent linkage to the sulfur group (Step A). After monolayer formation, the surface with self-assembled monolayer (SAM) was immersed in amino-nitrilotriacetic acid (ANTA, nitrilotriacetic acid containing a side chain with primary amine at the end). The amino group of ANTA reacted with the TSP monolayer to form a carboxamide likage and release an N-hydroxysuccinimide (NHS) group (Step B). The NTA-terminated surface was then ligated to the Ni^{2+} ion via the three carboxylates and the tertiary amine of NTA (Step C). Finally, the enzyme was absorbed to the modified electrode via the coordination of the nitrogen of two of the imidazole side chains of the 6×His-tag. An illustration representative of the modification of the gold electrode is shown in Figure 3.3.

3.4 Electrochemical Impedance Spectroscopy

Electrochemical Impedance Spectroscopy (EIS) was initially applied to the measurement of double-layer capacitance and in ac polarography.[42, 43] Now they are introduced to the characterization of electrode processes and complex interfaces.[44] EIS studies the impedance response to the application of a periodic small amplitude ac signal, and the frequency dependence of this impedance can reveal underlying chemical processes. In this study, the formations of the self-assembled monolayer (SAM) of TSP on the gold electrode surface and the additional layer of ANTA to form the NTA-TSP linker monolayer were monitored with EIS. Electrochemical impedance of the electrode should increase after each modification process.

3.5 Experimental

3.5.1 Reagents

D-mannitol (Sigma), $(NH_4)_2HPO_4$ (Sigma), KOH (Sigma), KH_2PO_4 (Sigma), K_2HPO4(Sigma), KCl (Sigma), KH_2PO_4 (Sigma), $(NH_4)SO_4$ (Sigma), $MgSO_4 \cdot 7H_2O$ (Sigma), $CaCl_2 \cdot 2H_2O$ (Sigma), lysozyme from egg white (Aldrich), sodium deoxycholate (Sigma), 2,6-dicholoroindophenol sodium salt hydrate (DCIP) (Sigma), nickel sulfate (Sigma), 3,3'-dithiodipropionic acid di(N-hydroxysuccinimide ester) (DTSP) (Sigma), 2-mercaptoethanol (Sigma), and amino nitrilotriacetic acid (ANTA) (Sigma) were used as received.

3.5.2 Bioengineered *Gluconobacter* sp. Growth

Six bioengineered *Gluconobacter sp*. (DSM 3504) bacteria were provided by Modular Genetics, Inc., where each bacterium had been engineered to express PQQ-AlDH with a His-tag in a different part of the multisubunit protein. The six resulting enzymes had the His-tag on either the C- or the N-terminus of one of the three subunits (i.e., His-tag on the C-terminus of subunit 1, His-tag on the N-terminus of subunit 2, etc.). Bacteria were cultivated aerobically in a basal media containing yeast extract (5g/L), D-mannitol (10g/L), $(NH_4)_2HPO_4$ (1g/L), and $MgSO_4$ (2g/L) at 30 ℃ for 24 hours, as per previous procedures for the native bacteria. The cell pastes were centrifuged at 12,000×g and then washed twice in 50 mM potassium phosphate buffer and stored at -20 ℃ until use.

3.5.3 Isolation of His-tag PQQ-Dependent AlDHs

All six His-tag PQQ-AlDHs with His-tags on different sites were isolated with the same method. Bioengineered *Gluconobacter* was thawed and suspended in 0.2 M phosphate buffer (pH 7.2) containing 1 mM $CaCl_2$, 10% sodium deoxycholate (to 0.5% final concentration), and 1 mL of lysozyme (10 mg lysozyme in 1 mL 0.3 M pH 7.2 potassium phosphate buffer). The solution was incubated at 4 ℃ with gentle stirring for 1 h followed by ultrasonication using a sonic dismembrator for 1 min at 4 ℃. The solution was then centrifuged for 1 h at 12,000 × g to remove insoluble materials. Crude extract was dialyzed against 0.1 M potassium phosphate buffer containing 500 mM KCl, 10 mM imidazole, and 10 mM mercaptoenthanol overnight.

Immobilized metal ion affinity chromatography (IMAC) (Thermo Scientific) was utilized to purify target His-tag proteins with 10 mM imidazole equilibration buffer, 50 mM imidazole wash buffer, and 500 mM imidazole elution buffer. Eluates were washed with 50 mM potassium phosphate buffer to remove imidazole residue, which can interfere with enzyme activity assay and electrode modification. Purity of enzymes was determined with native protein gels and SDS-PAGE gels.

3.5.4 Electrophoresis Gels

Electrophoresis methods were used to determine the purity of the enzymes after immobilized metal ion affinity chromatography (IMAC). Four to sixteen percent native Bis-Tris gel (Invitrogen) was run in a water-cooled, dual-gel vertical system electrophoresis apparatus (VWR) for 40 minutes, starting at 100 mA/gel ending at 40 mA/gel at 150 V and stained with Coomassie. The gel was run with His-IIC and

standard (including B-phycoerythrin, 242 kDa; lactate dehydrogenase, 146 kDa; bovine serum albmin, 66 kDa; soybean trypsin inhibitor, 20kDa.). A 3–20% SDS-PAGE gel stained with Coomassie was also run for samples extracted from each step of the purification process. The Standard includes β-galactosidase, 116 kDa; bovine serum albumin, 66 kDa; carbonic anhydrase, 29 kDa; soybean trypsin inhibitor, 20kDa; and α-lactalbumin, 14.2kDa.

3.5.5 Surface Modification of Gold Electrode

The SAM electrode modification method was reported by Ataka *et al*.[41] Polished gold electrodes were exposed to 1 mg/ml dithiodis(succinimidylpropionate) (DTSP, Fluka) in DMSO for 30 minutes. DTSP forms a monolayer on gold through covalent linkage to the sulfur group. The self-assembled monolayer (SAM) was then immersed in an aqueous solution of 150mM amino-nitrilotriacetic acid (ANTA, Sigma) in 0.5 M K_2CO_3 buffer (pH 9.8). Excess ANTA was removed with ultrapure water washing. The TSP-NTA modified electrode was then incubated with 50 mM $NiSO_4$ (Sigma) to ligate Ni^{2+} ion via the three carboxylates and the terminal amine of NTA. Finally, the TSP-NTA-Ni modified electrode was incubated with 1 mg/ml His-tag PQQ-AlDH solutions for 12 hours. PQQ-AlDHs attached to the Ni–NTA moiety through the coordination of the two nitrogens of the imidazole side chains of the 6×His-tag.

3.5.6 Enzyme Activity Assay

The enzyme reaction mixture consists of 1.5 mL of 50 mM pH 7.3 potassium phosphate buffer, 0.2 mL of 600uM PMS (phenazine methosulfate), 0.1 mL of 700 uM

DCIP (dichlorophenolindophenol), 0.01 mL of enzyme solution, and 0.2 mL of a 0.2 M substrate solution. For PQQ-dependent aldehyde dehydrogenase, acetaldehyde and glyceraldehyde were used as substrates. The change in absorbance during a 2 min interval for each sample was measured at 37 ℃ at time = 0 minutes and time = 2 min at 600 nm on a Genesys 20 spectrophotometer. Specific activity was calculated in U/mg, where one unit corresponds to converting one micromole of substrate per minute. The molar absorptivity (ε) of DCIP was experimentally determined to be 30.

Immobilized enzyme concentration was measured with a modified UV spectrophotometric protein assay utilizing the 280 nm characteristic protein absorbance peak on a Thermo Evolution 260 Bio. Each type of recombinant PQQ-AlDHs was immobilized on 1 cm^2 TSP-Ni-NTA modified gold electrode and then washed off with 1 mL of 500 mM imidazole in 50 mM phosphate elution buffer. UV absorbances of the wash solutions at wavelength of 280 nm and 260 nm (A_{280} and A_{260}) were measured with elution buffer used as the blank. Protein concentration was measured with the equation $[protein](mg/ml) = 1.55 \times A_{280nm} - 0.76 \times A_{260nm}$.

3.5.7 Electrochemical Measurements

Cyclic voltammetry (CV) was performed on a CH Instruments 611C potentiostat. Platinum and Ag/AgCl electrodes were used as counter and reference electrodes and all measurements were performed in 50 mM pH 7.4 potassium phosphate buffer with 0.1M sodium nitrate as supporting electrolyte. Electrochemical impedance spectroscopy was measured in the same buffer solution, and this measurement was performed with a Bio-Logic 150SP potentiostat.

3.6 Results and Discussion

3.6.1 *Gluconobacter* Growth and Recombinant PQQ-AlDH Purifications

Six types of bioengineered *Gluconobacter sp*. were cultured in a fermentation system (yielded 1.8-2 g/L bacteria for each type), and six types of recombinant PQQ-AlDHs, each have a 6×His-tag label on different sites of the protein, have been expressed and purified with IMAC method. Two of the constructs of PQQ-AlDH have the His-tag at the C- and N- terminus of subunit I (His-IC, His-IN), which is the active site subunit and contains a single heme c group. His-IIC and His-IIN represent two of the constructs of PQQ-AlDH that have the His-tag at the C- and N-terminus of subunit II, which is a multiple heme c subunit. There are also two constructs of PQQ-AlDH with His-tag at C- and N-terminus of the subunit III (His-IIIC and His-IIIN) which is a peptide subunit that provides structural integrity.

3.6.2 His-tag PQQ-AlDH Activity and Purity Measurements

Monitoring specific activity change through the purification process is a way of determining the magnitude of purification.[23] PQQ-AlDH is a promiscuous enzyme, which means that it shows activity on a broad scope of endo- and exogenous aldehydes. Six recombinant PQQ-AlDHs' specific activities toward two aldehydes (acetaldehyde and glyceraldehyde) were monitored before and after the purification processes, as shown in Table 3.1. Comparing the specific activities before and after IMAC, results showed a roughly 10-fold purification with IMAC with all the six His-tagged AlDHs. All recombinant AlDHs showed slightly higher activity toward glyceraldehyde than acetaldehyde. Therefore glyceraldehyde was used as the enzyme substrate for all further

electrochemical and spectroscopic measurements. The purity of recombinant enzymes after IMAC was determined with electrophoresis methods. A representative native Bis-Tris gel that was run with His-IIC and standard is shown in Figure 3.4A. A clear single band representing His-IIC AlDH was found between 66 and 146 kDa. A representative SDS-PAGE gel that was run with the same enzyme and standard is shown in Figure 3.4B. Purified His-IIC showed three clear bands representing each subunit of the protein.

3.6.3 Gold Electrode Modification

The gold electrode surface has been modified by several steps to form a Ni-NTA-terminated self-assembled monolayer (SAM). In order to monitor the process of the gold electrode modification, electrochemical impedance spectroscopy (EIS) was utilized to monitor the impedance change after each SAM formation step. The results are shown in Figure 3.5. A Randles circuit (Figure 3.5) was proposed to model interfacial electrochemical reactions in presence of semi-infinite linear diffusion of electroactive species to flat electrode surfaces.[1] A Randles model consists of a solution resistance R_s, which is in series with the parallel combination of the double-layer capacitance C_{dl} and an impedance of a faradaic reaction. This model was chosen because it represents the flat gold electrode surface and it contains an active charge transfer resistance (R_{CT}), which is a parameter to monitor the formation of monolayer on the gold electrode surface. A specific electrochemical element of diffusion W (Warburg element) was added to represent the diffusion of the redox probe hydroquinone.

Experimental data were fitted with the Randles circuit model (Figure 3.5) and

charge transfer resistance; double layer capacitance and solution resistance were calculated with each modification step. The fitting results show that the solution resistance (R_s) was around 250 Ohm. With the adding of TSP on the bare gold electrode, the charge transfer resistance (R_{CT}) increased by 8 kOhm, and the NTA addition of TSP monolayer increased the resistance by 10 kOhm. The results indicate successful modification of the gold electrode with each modification step.

To further prove the formation of the linker layer and its ability to chelate metal ions, cyclic voltammetry was performed with a NTA-TSP modified electrode with Cu^{2+} to compare with previously reported immobilized Cu^{2+} oxidation potential.[45] A reversible peak at 0.2 V versus Ag/AgCl was found, which corresponds to the one electron oxidation from Cu(I) to Cu(II), which matches with the reported value (Figure 3.6). This result shows that the linker layer was formed on the gold electrode surface and can successfully chelate metal ions.

3.6.4 Immobilized Enzyme Activity Measurements

In order to demonstrate that active His-tag enzymes were successfully attached to modified electrodes, immobilized enzyme activity assays (DCPIP assay described above) were performed. His-tag enzyme loaded electrodes were exposed to assay solutions for 60 minutes and absorbance changes at 600 nm wavelength were recorded. This experiment was performed with the sole purpose of demonstrating that active enzymes attached to the modified electrodes. Assay results are shown in Table 3.2. Glyceraldehyde was used as enzyme substrate in the assays. All immobilized enzyme assay results showed that all immobilized recombinant PQQ-AlDHs have a statistically

significant absorbance change compared to control except for His-IIC, which indicates that five active His-tag PQQ-AlDHs (His-IC, His-IN, His-IIN, His-IIIC, and His-IIIN) were successfully immobilized on modified gold electrodes. Whether His-IIC was successfully coupled with the modified gold electrode needed to be further measured with a protein concentration assay to determine the enzyme density on the electrode. In order to measure the enzyme immobilized density on the electrode for each of the six recombinant enzymes, we modified 1cm×1cm gold foils as described above with six recombinant enzymes. Then we washed off the His-tag enzymes with 500 mM imidazole solution. After washing, the enzymes were rinsed with phosphate buffer to get rid of imidazole, and the protein concentrations were measured with absorbance at 280 nm and are shown in Table 3.2.

Protein concentration assays showed that all recombinant PQQ-AlDHs attached to the modified gold electrode with a density of 7.0–8.5 $\mu g/cm^2$, except for His-IIC, which showed no significant enzyme was immobilized on the electrode. This could be that the C-terminus of subunit II is sterically unreachable by NTA-Ni. By coupling the results of the DCPIP assays and protein concentration assays, specific activities of immobilized His-tag PQQ-AlDHs were calculated. From the results, we can determine that subunit III and subunit II N-terminus tagged PQQ-AlDHs showed close to free enzyme specific activity, which means immobilization did not deactivate the enzyme, and the substrate was accessble to the enzyme. Subunit I labeled PQQ-AlDH showed lower specific activity. Enzyme activities in free solutions after IMAC purification showed similar results for all six samples, which indicates that the His-tag is not or minimally affecting the kinetics of the enzyme. This can only be explained by change of substrate

accessibility and minor conformational changes when enzymes are immobilized on the electrode surface. In order to rule out the possibility of nonspecific binding of enzymes on the electrode, an immobilized assay with native enzyme was performed. Results showed no enzyme was bound to the modified electrode surface (same results as blank).

3.6.5 Electrochemical Properties of Surface-Tethered PQQ-AlDHs

The ability of the enzyme to do direct electron transfer (DET) was investigated with different orientations of PQQ-AlDHs. Electron transfer was probed by cyclic voltammetry (CV). CVs were measured with glyceraldehyde substrate at various concentrations. TSP-NTA-Ni modified gold electrodes without enzyme loading were used as the control.

Cyclic voltammograms of linker modified electrodes (control electrodes without enzymes) with a wider scan window showed an oxidation peak at around +500 mV versus Ag/AgCl (Figure 3.7A). This peak was identified as the oxidation peak of Ni ion catalyzing oxidation of glyceraldehyde. PQQ-dependent aldehyde dehydrogenase should have a oxidation peak at around 190 mV versus Ag/AgCl[46] because the electron transfer is believed to occur through one of the heme c groups in subunit II, which has a potential of 190 mV vs Ag/AgCl. A smaller window scan was performed on the control electrodes, and no peak was observed in the range of -150 mV to 450 mV (Figure 3.7B). Therefore, all studies of enzyme modified electrodes used this scan window. In order to rule out the possibility of nonspecific binding of enzyme on electrode, electrochemistry of the electrodes with native enzyme was tested. CVs showed no catalytic peak in the scan range.

After tethering His-tag enzymes to the modified electrode surface, electrodes were tested in different concentrations of glyceraldehyde substrate solution. CVs of His-IC and His-IN are shown in Figure 3.8. Electrons can be transferred either via the single heme-c group in subunit I and then directly to electrode surface or through the multiple heme-c groups in subunit II before being released by the protein to the electrode. With subunit I tagged PQQ-AlDH, electron transfer to the gold electrode surface via the single heme-c group in subunit I is a reasonable prediction. CVs of His-IC showed a small catalytic peak at 203 $\pm$ 4 mV versus Ag/AgCl, while His-IN showed no peak in this scan window. The electrochemical measurement results are indicating that even though the two His-tags are on the same subunit, the N- and C-terminus are giving different orientations of the enzyme toward the electrode, which result in different heme-to-electrode distances.

The N-terminus His-tag is far from the heme-c group in subunit I, which yields a longer space between the heme-c and the gold electrode surface. Plots of peak current versus concentration and the Lineweaver–Burk curve of His-IC modified electrodes are shown in Figure 3.9. The calibration curve of His-IC follows Michaelis–Menton kinetics and Lineweaver–Burk gives K_m of 3.89 $\pm$ 0.52 mM and V_{max} of 1.19 $\pm$ 0.16 nA and reported wild-type PQQ-AlDH K_m is 12 mM.[47] The results show that His-IC orientation is capable of DET; however, the electron transfer rate is low. This can be explained as the substrate accessibility to the enzyme active site was inhibited with this orientation arrangement, and the distance between the single heme c group and the gold surface was too long for efficient electron tunneling. His-IN showed no ability for direct electron transfer, which is in accordance with the previous low immobilized enzyme

activity assays, combined with the fact that this orientation is unfavorable for efficient DET since the PQQ active site is in this general area of subunit I.

CVs of His-IIC and His-IIN are shown in Figure 3.10. Subunit II is the subunit with multiple heme-c groups. In those two orientations, enzymes are tethered to the electrode surfaces by connecting subunit II to the Ni-NTA linker, so electron transfer can occur through the PQQ cofactor to multiple heme-c groups and to electrode surface via the closest heme-c group. CVs of His-IIN show a catalytic peak at +229 mV versus Ag/AgCl, which exhibits direct electron transfer, while His-IIC shows no peak in this scan range, which is expected since the immobilized enzyme assays showed no significant protein was bound to the gold electrodes. A calibration curve and Lineweaver–Burk plot of the electrochemical assay data for His-II-N modified gold electrodes are shown in Figure 3.11.

The calibration curve of His-II-N modified gold electrodes also follows Michaelis–Menton kinetics, and the Lineweaver–Burk curve gives K_m of 5.07 ± 0.49 mM and V_{max} of 7.94 ± 0.63 nA. His-II-N modified gold electrodes show a six-fold DET rate increase over His-I-C modified gold electrodes. This is expected since the multiple heme-c subunit is attached to electrode surface allowing for facile electron transfer, and yet the PQQ subunit (subunit I) is still exposed to the substrate.

CVs of His-IIIC and His-IIIN modified gold electrodes are shown in Figure 3.12. Subunit III is the peptide subunit, which has only a structural function. With this subunit attached to the electrode surface, no heme-c group or PQQ cofactor is in good proximity with the electrode surface, so the CVs showed no peak structure and no direct electron transfer.

For the purpose of direct comparison, His-IC, His-IIN and His-IIIN modified gold electrodes are chosen to represent different enzyme orientations toward the electrode. The His-III-N electrode showed no catalytic peak in the scan range. This result is in accordance with our prediction; with the peptide subunit anchored on the modified surface, the heme-containing subunits are stretched away from the electrode surface resulting in a long heme-to-electrode distance, which prevents electron transfer from occurring. The His-I-C electrode showed a small oxidation peak (1.01 ± 0.11 nA) at 203 ± 9 mV versus Ag/AglCl and a clearer reduction peak at 123 ± 6 mV versus Ag/AgCl. Compared to the oxidation potential of the His-IIN electrode (229 ± 4 mV versus Ag/AgCl) and the reduction potential of 98 ± 2 mV versus Ag/AgCl, the oxidation potential shifted by 26 mV, and the reduction potential shifted by 25 mV, which can be caused by different internal electron transfer pathways.

The His-IIN modified gold electrode showed a 6.6-fold catalytic current increase (6.71 ± 0.52 nA vs. 1.01 ± 0.11 nA), which indicates this linkage is preferable for fast electron transfer. Our explanation for this result is that His-II-N gives good accessibility of the substrate to the active site of the enzyme, and electrons can be rapidly transferred via multi-heme-c groups and released to the electrode surface from the closest heme-c group. This orientation has comparativly small tunneling distance. The His-IC has its active site buried close to the electrode surface, so it is more difficult for the substrate to diffuse to the active site and the electrons produced at the active site to transfer to the single heme-c group in subunit one and then transfer to the gold electrode, which is a less optimal pathway.

In order to categorize an enzyme to be DET, there are usually two prerequisites to

be obeyed: the first is that an electrochemical signal should be exhibited in the absence of the substrate molecules, which only reveals the electrochemistry of the enzyme-bound electron carrier. The second is that in the presence of the substrate, a catalytic current should be seen. However, on ordinary graphite/glassy carbon electrodes, very rarely is the first prerequisite fulfilled because of the large background current; the prime example is laccase.[2] The capacitive current of such electrodes is high due to the rather high roughness factor of the electrodes. The surface coverage of a redox enzyme is rather low (50–60 pmol/cm^2 for His-PQQ-AlDH). The Faradaic current is thus hard to see on top of the large background current. In order to investigate the direct electron transfer property of His-IIN, the cyclic voltammetry was modeled with DigiElch simulation software.

Simulation parameters were input as shown below:

Charge transfer reaction: Ox + 2e = Red, $E^\circ = 0.2$V (Representing redox reaction of enzyme).

Chemical reaction: Ox + S = Red + P, K_{eq}= 100 $K_f = 6.25\times10^6$, and $K_b = 6.25\times10^4$ (S: substrate, P: product).

Enzyme concentration 4×10^{-11} mol/L and enzymes are all surface adsorbed.

Solution resistance: 30 Ohm, capacitance: 1×10^{-6} F, scan rate and scan range are the same as actual experiments.

First, CV without capacitance and substrate was simulated, as shown in Figure 3.13A, then capacitance was included in simulation, and CVs with difference concentrations of substrates were simulated, as shown in Figure 3.13B. The calibration curve was shown in Figure 3.13C. The simulation results show that without capacitive

current, a clear redox peak can be observed with peak current of 4.5 pA, which represents the electrochemical communication between the enzyme (heme-c group) and electrode without substrate (DET prerequisite 1). When 1×10^{-6} F of capacitance is added to the system, this small peak can no longer be observed on top of the much larger capacitive current. When substrate is added, positive feedback occurs and catalytic current at nanoamp scale can be observed (DET prerequisite 2), which indicates bioelectrocatalysis. The simulation results were plot in the calibration curve and compared to experiment results (Figure 3.9C), two calibration curves showed great similarity. The differences in shape between the simulated CVs and experiment CVs (Figure 3.13B) are due to the fact that in an actual experiment, there is also oxygen reduction at potential lower than -0.1 V and Ni ion catalyzing glyceraldehyde oxidation starting from 0.5 V.

3.7 Conclusions

In this work, we have addressed the importance of enzyme orientation for efficient direct electron transfer to occur. Control of the orientation has been achieved by specifically binding six PQQ-AlDHs to Ni-NTA-modifed gold electrodes via His-tags on different subunits of the enzymes. Capability of DET of each orientation arrangement was measured with cyclic voltammetry. It was demonstrated that only with PQQ-AlDH oriented to expose its active site to substrate and good proximity between heme-c groups to the electrode, efficient DET is observed. Thus, proper orientation is mandatory for efficient direct electron transfer to occur.

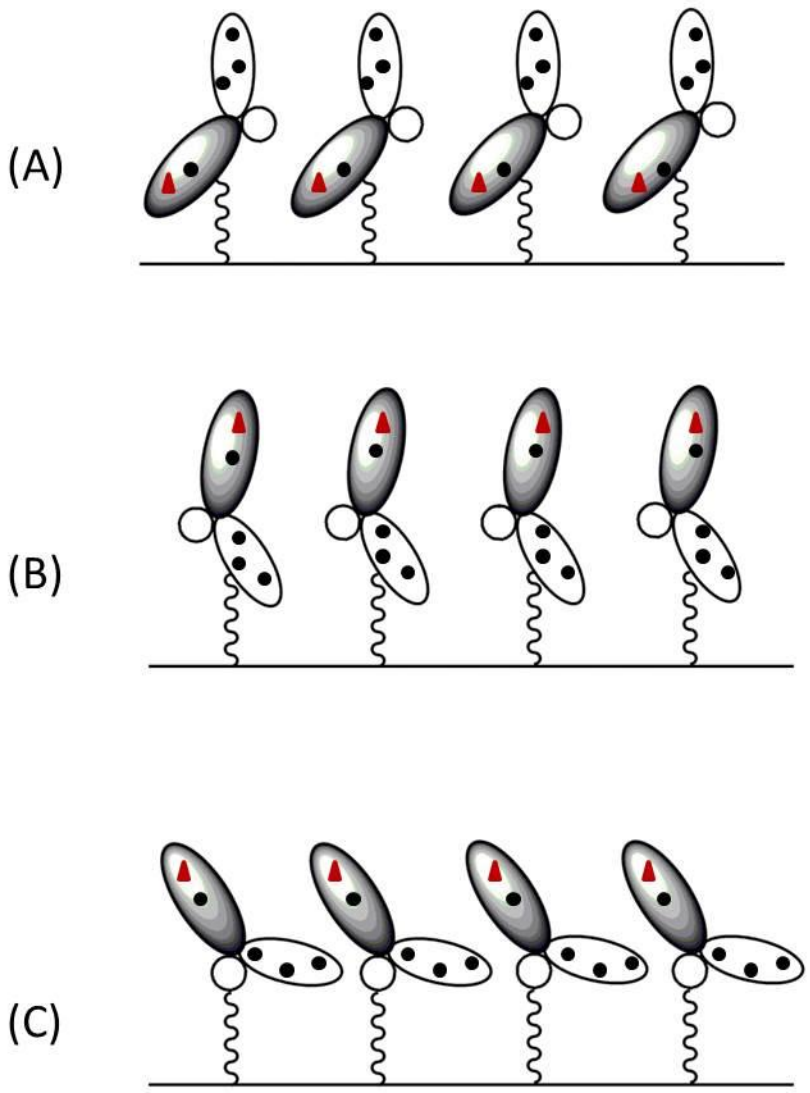

Figure 3.1 Schematic illustration of His-tag PQQ-AlDH with His-tag orientation controlled via immobilization on electrodes, where the black circles represent heme-c groups, the red trangles represent PQQ cofactors, and the colored subunit represents the active site subunit (subunit I). (A) His-tag on subunit I as the linking site, (B) His-tag on subunit II as the linking site, and (C) His-tag on subunit III as the linking site.

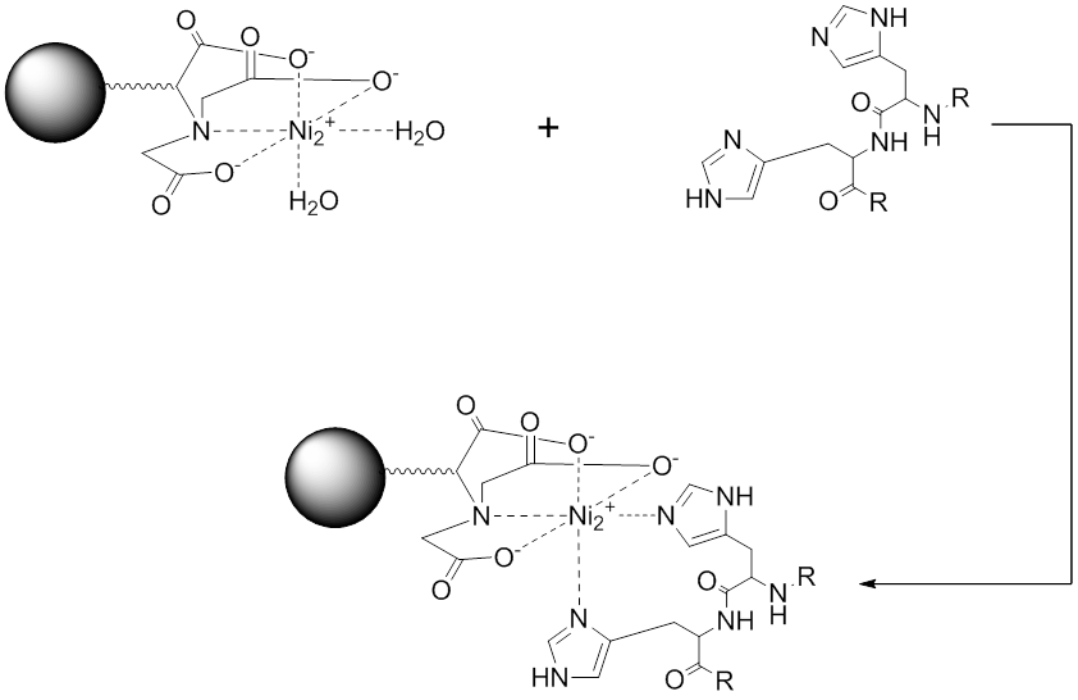

Figure 3.2 Schematic representative of the interaction between a His-tagged protein and Ni-NTA column resin.

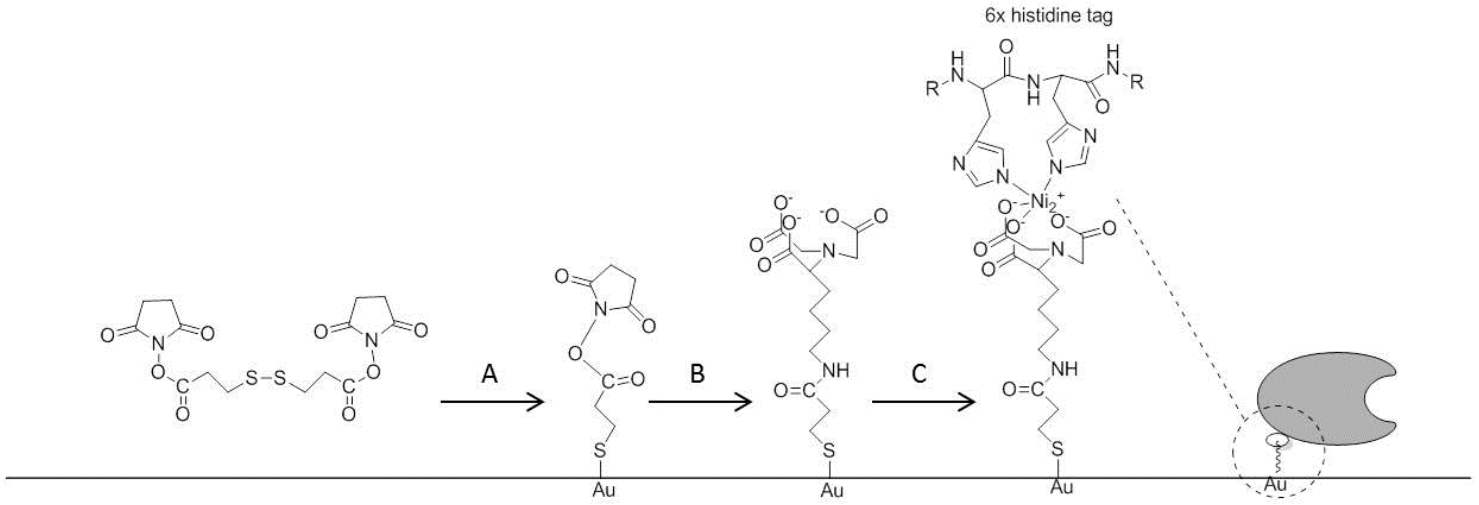

Figure 3.3 Schematic representative of the gold electrode surface modification process. (A) Self-assembly of the TSP monolayer on a flat gold electrode surface. (B) Cross-linking of ANTA with the TSP monolayer. (C) Ligation of Ni^{2+} ion and adsorption of recombinant PQQ-AlDH on the modified electrode surface via the His-tag site.

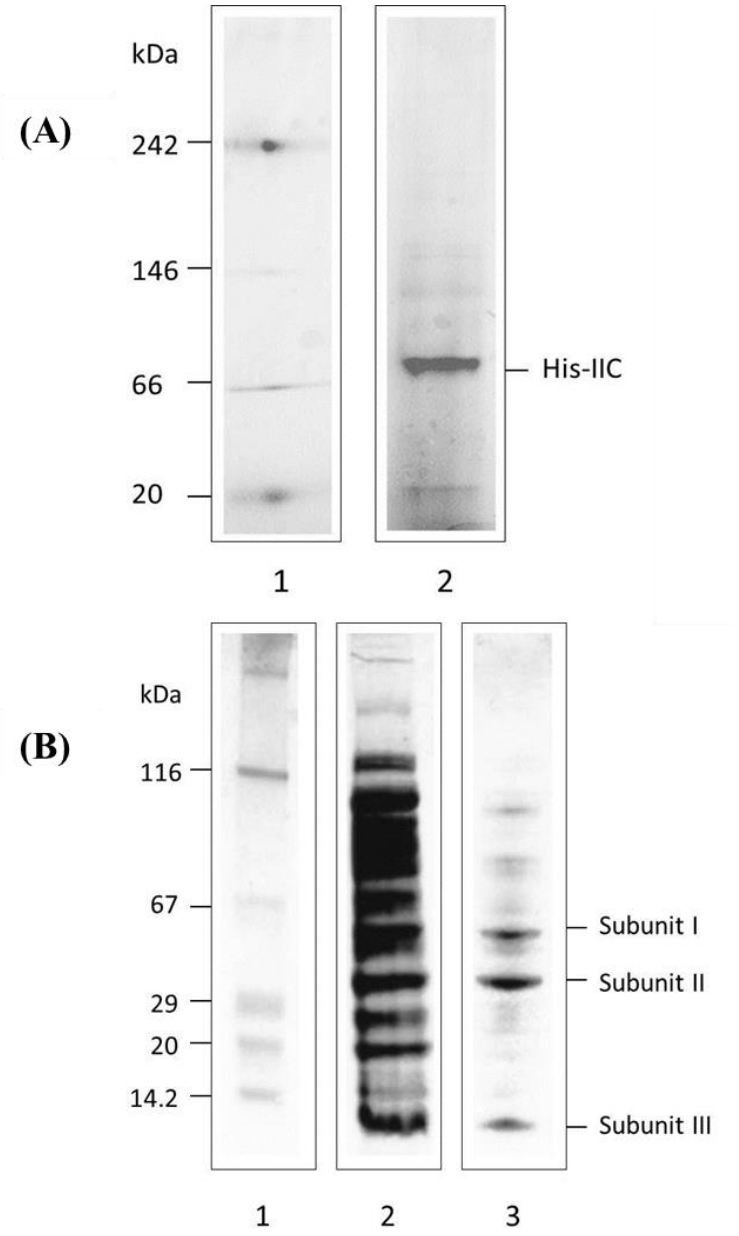

Figure 3.4 Electrophoresis study of purified His-IIC. (A) A 4–16% native gel stained with Coomassie showing (1) standard including B-phycoerythrin, 242 kDa; lactate dehydrogenase, 146 kDa; bovine serum albmin, 66 kDa; soybean trypsin inhibitor, 20kDa and (2) His-IIC sample. (B) A 3–20% SDS-PAGE gel stained with Coomassie showing: (1) standard including β-galactosidase, 116 kDa; bovine serum albumin, 66 kDa; carbonic anhydrase, 29 kDa; soybean trypsin inhibitor, 20kDa; and α-lactalbumin, 14.2kDa; (2) crude lysate from bacteria lysis; and (3) His-IIC sample.

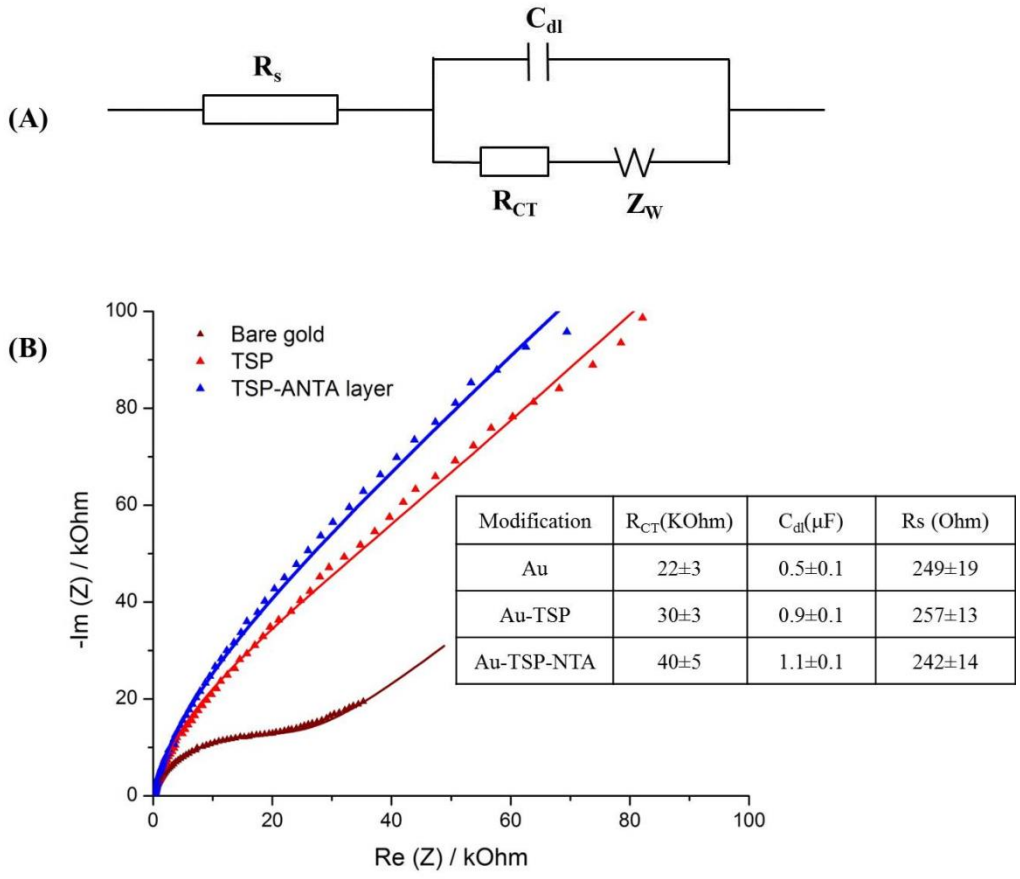

Modification	R_{CT}(KOhm)	C_{dl}(μF)	Rs (Ohm)
Au	22±3	0.5±0.1	249±19
Au-TSP	30±3	0.9±0.1	257±13
Au-TSP-NTA	40±5	1.1±0.1	242±14

Figure 3.5 Electrochemical Impedance Spectroscopy results and fitting. (A) Schematic representatibe of Randles circuit. (B) Impedance spectra in Niquist impedance plot; dotted lines represent experimental data, and solid lines show the curves fitted to the equivalent circuit.

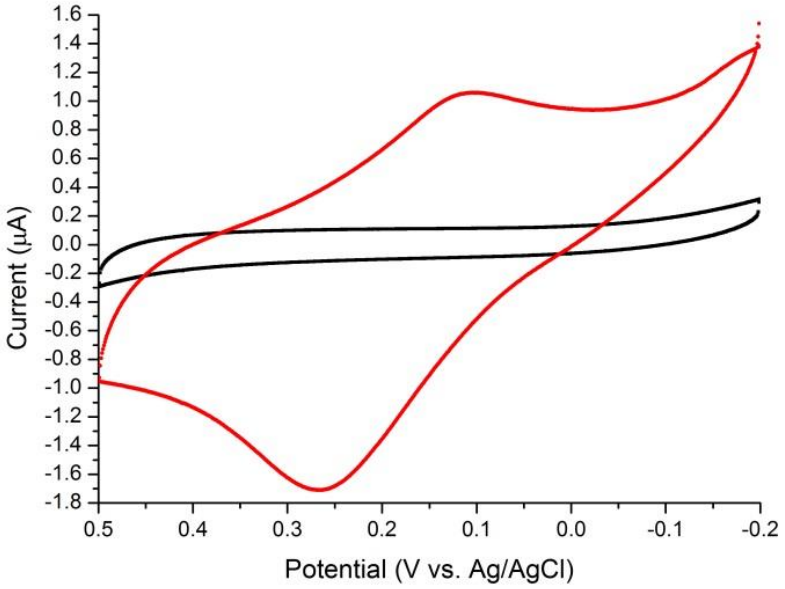

Figure 3.6 Detection of chelated copper to the TSP-ANTA-modified gold electrodes. Black line is TSP-NTA modified electrode, and red line is TSP-NTA-Cu. Measurements were performed in 50 mM pH7.0 phosphate buffer at scan rate of 50 mV/s.

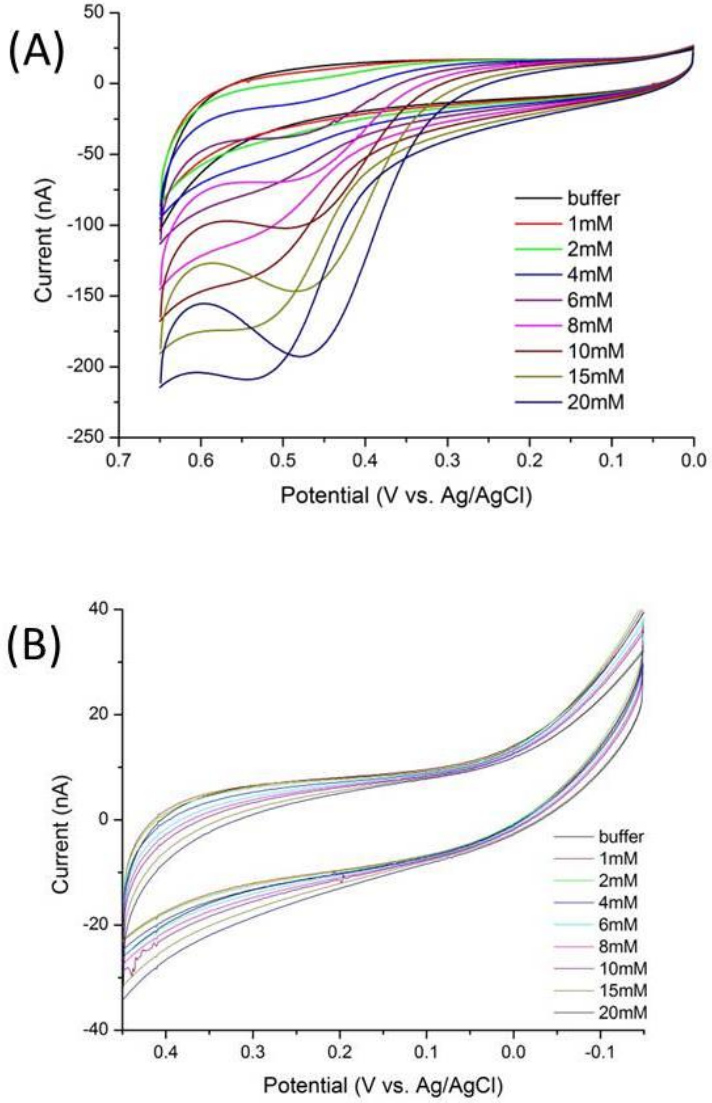

Figure 3.7 Cyclic voltammograms of TSP-NTA-Ni-modified gold electrode (control) in different concentrations of glyceraldehyde. Scan rate is 5 mV/s. (A) CVs of control electrodes with a scan window of 0 mV to +650 mV. (B) CVs of control electrodes with a scan window of -150 mV to +450 mV.

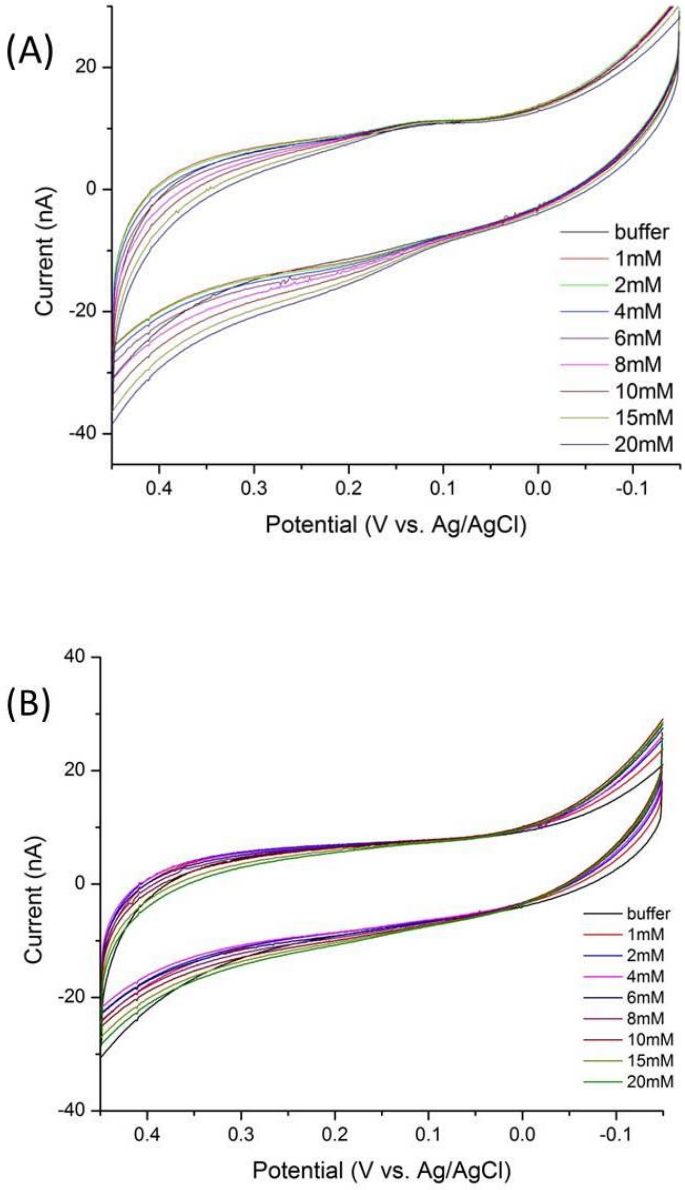

Figure 3.8 Cyclic voltammograms of (A) His-IC and (B) His-IN modified gold electrodes in a 50 mM pH 7.4 phosphate buffer with 0.1 M KNO_3 supporting electrolyte at a scan rate of 5 mV s^{-1}. Concentrations correspond to increasing concentrations of glyceraldehyde.

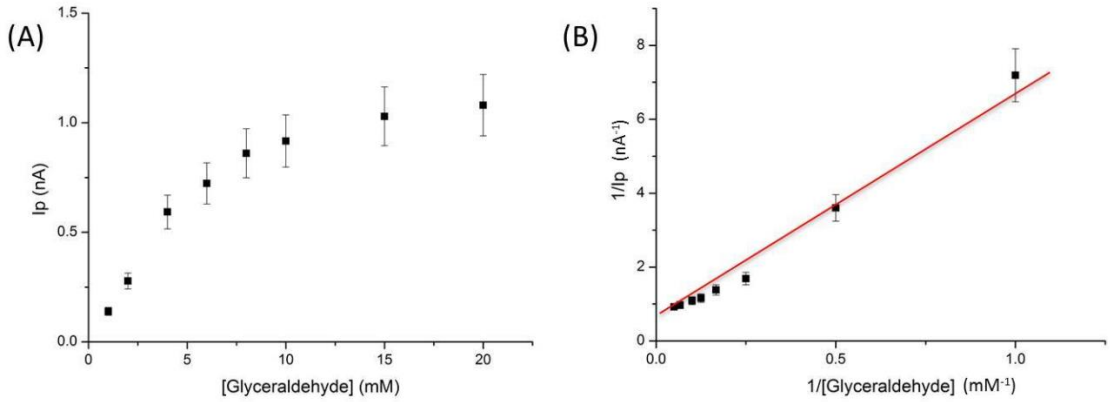

Figure 3.9 Calibration curve of peak current versus concentration of glyceraldehyde (A) and Lineweaver–Burk curve (B) of His-I-C modified gold electrodes.

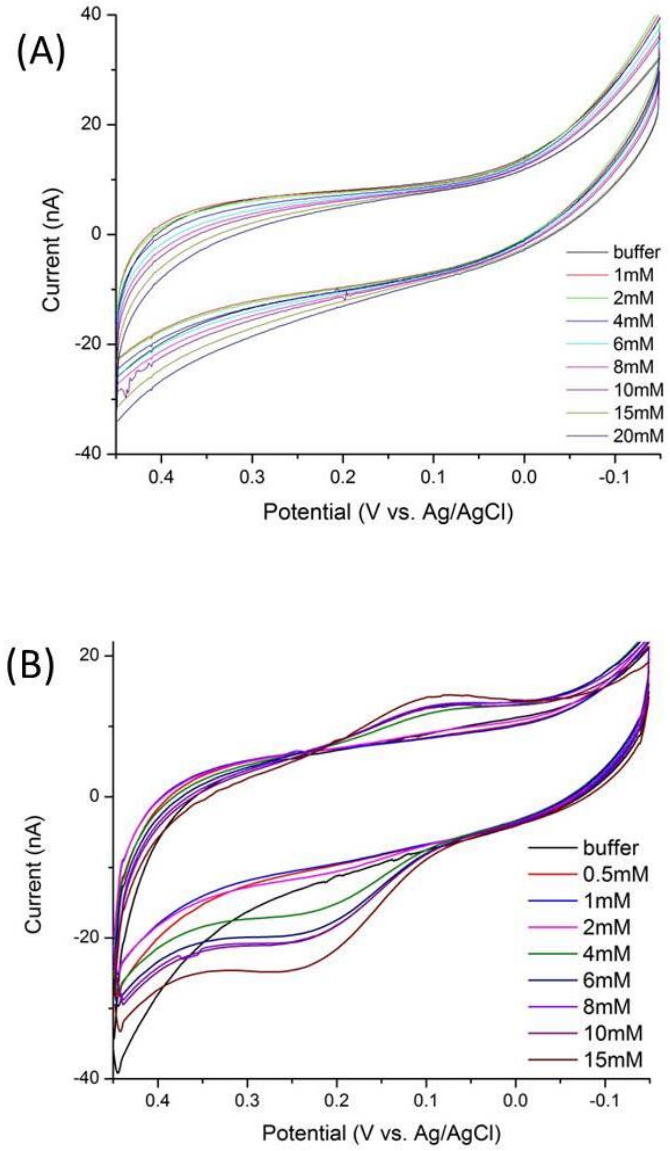

Figure 3.10 Cyclic voltammograms of (A) His-II-C and (B) His-II-N modified gold electrodes in 50 mM pH 7.4 phosphate buffer with 0.1 M KNO_3 supporting electrolyte at a scan rate of 5 mV s^{-1}. Concentrations correspond to increasing concentrations of glyceraldehyde.

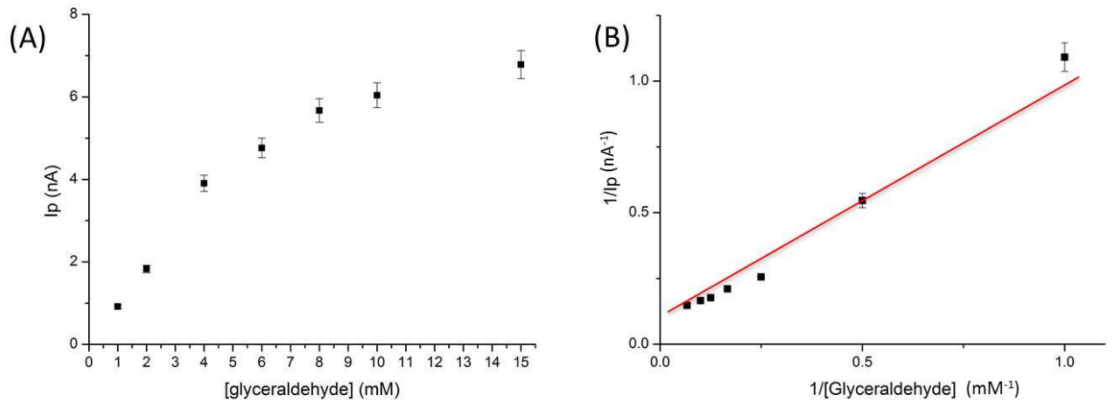

Figure 3.11 Calibration curve of peak current versus concentration of glyceroladehyde (A) and Lineweaver–Burk curve (B) of His-II-N modified gold electrodes.

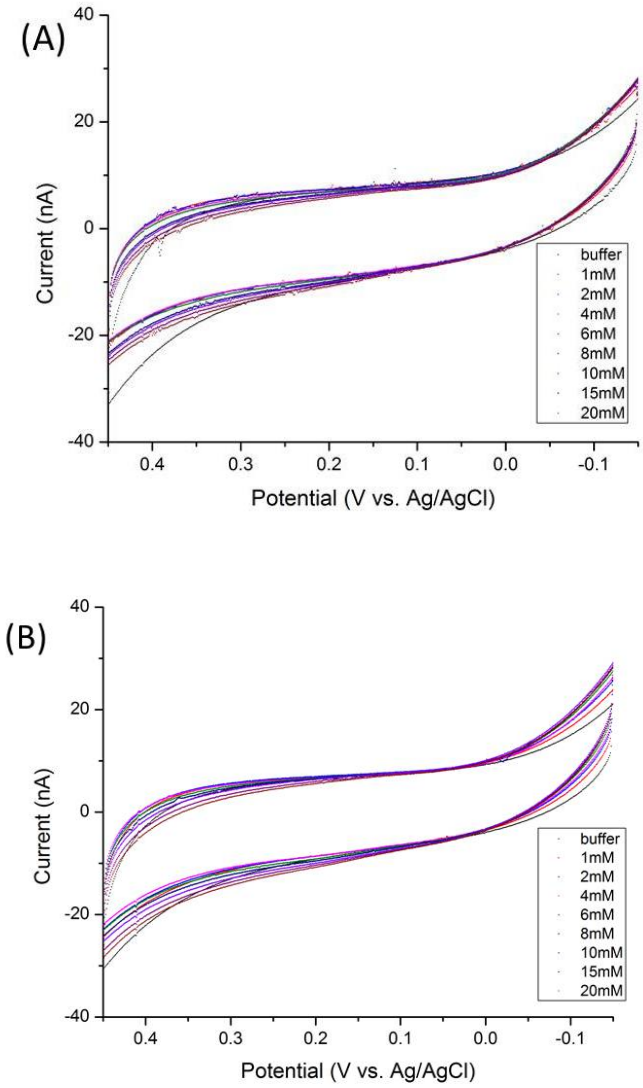

Figure 3.12 Cyclic voltammograms of (A) His-III-C and (B) His-III-N modified gold electrodes in 50 mM pH 7.4 phosphate buffer with 0.1 M KNO_3 supporting electrolyte at a scan rate of 5 mV s^{-1}. Concentrations correspond to increasing concentrations of glyceraldehyde.

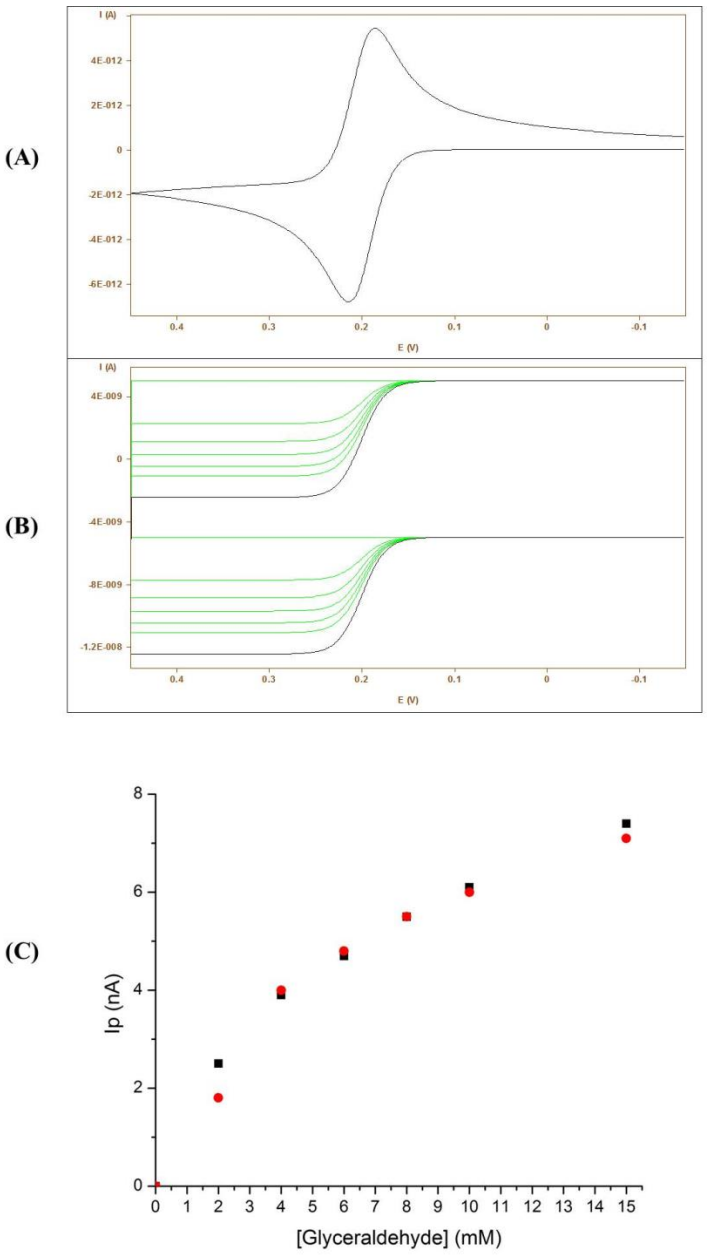

Figure 3.13 Cyclic voltammetry simulation results of His-IIN AlDH. (A) Simulation of cyclic voltammetry without substrate and capacitance. (B) simulation of cyclic voltammetry with capacitance of 1×10^{-6}F and substrate concentration from 0 mM to 15 mM. (C) Calibration curve of simulation results (black dots) and experimental results (red dots).

Table 3.1 Specific activity assay results for six recombinant PQQ-AlDHs before and after purification via affinity chromatography with both acetaldehyde and glyceraldehyde as substrates.

		His-IC (U/mg)	His-IN (U/mg)	His-IIC (U/mg)	His-IIN (U/mg)	His-IIIC (U/mg)	His-IIIN (U/mg)
Before IMAC	Acetaldehyde	0.25±0.07	0.33±0.11	0.39±0.12	0.25±0.08	0.32±0.10	0.34±0.11
	Glyceraldehyde	0.37±0.12	0.35±0.14	0.41±0.18	0.31±0.09	0.34±0.11	0.44±0.19
After IMAC	Acetaldehyde	2.63±0.31	2.71±0.34	2.76±0.25	3.40±0.35	3.06±0.25	3.24±0.31
	Glyceraldehyde	3.43±0.33	4.64±0.48	3.37±0.39	3.65±0.33	3.42±0.22	3.91±0.34

Table 3.2 Enzyme immobilization density and specific activity of six recombinant PQQ-AlDH on modified gold electrodes.

Enzymes	His-I-C	His-I-N	His-II-C	His-II-N	His-III-C	His-III-N	Control
Change in Abs	0.056±0.012	0.019±0.011	0.004±0.001	0.245±0.035	0.192±0.011	0.213±0.017	0.000±0.002
Enzyme density ($\mu g/cm^2$)	8.5	7.0	0.7	8.5	8.5	7.0	0.7
Specific activity (Unit/mg)	0.73±0.16	0.20±0.11	0.63±0.16	3.21±0.52	2.52±0.14	2.23±0.18	0.00±0.32
Protein surface coverage ($nmol/cm^2$)	0.06	0.05	0.005	0.06	0.06	0.05	0.05

3.8 References

1. Moehlenbrock, M. J.; Minteer, S. D. *Chem. Soc. Rev.* **2008,** *37*, 1188–1196.

2. Chaubey, A.; Malhorta, B. D. *Biosens. Bioelectron.* **2002,** *17*, 441–456.

3. Chuang, C. L.; Wang, Y. J.; Lan, H. L. *Anal. Chim. Acta* **1997,** *353*, 37–44.

4. Nishikiori, H. K.; Kano, K.; Tsujimura, K. *Jpn. Kokai Tokkyo Koho* **2008,** 14, 359–364.

5. Meredith, M. T.; Glatzhofer, D.; Kao, D.-Y.; Schmidtke, D. W.; Hickey, D. *J. Electrochem. Soc.* **2011,** *158*, 166–174.

6. Tran, T. O.; Lammert, E. G.; Chen, J.; Merchant, S. A.; Brunski, D. B.; Keay, J. C.; Johnson, M. B.; Glatzhofer, D. T.; Schmidtke, D. W. *Langmuir* **2011,** *27*, 6201–6210.

7. Bunte, C.; Prucker, O.; Konig, T.; Ruhe, J. *Langmuir* **2010,** *26*, 6019–6027.

8. Gallaway, J. W.; Calabrese Barton, S. A. *J. Electroanal. Chem.* **2009,** *626*, 149–155.

9. Stoica, L.; Dimcheva, N.; Ackermann, Y.; Karnicka, K.; Guschin, D. A.; Kulesza, P. J.; Rogalski, J.; Haltrich, D.; Ludwig, R.; Gorton, L.; Schuhmann, W. *Fuel Cells* **2009,** *9*, 53–62.

10. Allen, P. M.; Allen, H.; Hill, O.; Walton, N. J. *J. Electroanal. Chem.* **1984,** *178*, 69–86.

11. Frew, J. E.; Hill, H. A. O. *Eur. J. Biochem.* **1988,** *172*, 261–269.

12. Degani, Y.; Heller, A. *J. Am. Chem. Soc.* **1988,** *110*, 2615–2620.

13. Gorton, L.; Jonsson-Pettersson, G.; Csoregi, E.; Johansson, K.; Dominguez, E.; Marko-Varga, G.; Persson, B. *Analyst* **1992,** *117*, 1235–1241.

14. Varfolomeev, S. D.; Kurochkin, I. N.; Yaropolov, A. I. *Biosens. Bioelectron.* **1996,** *11*, 863–871.

15. Ghindilis, A. L.; Atanasov, P.; Wilkins, E. *Electroanalysis* **1997,** *9*, 661–674.

16. Xu, F.; Shin, W. S.; Brown, S. H.; Wahleithner, J. A.; Sundaram, U. M.; Solomon, E. I. *Biochim. Biophys. Acta, Protein Struct. Mol. Enzymol.* **1996,** *1292*, 303–311.

17. Stoica, L.; Ruzgas, T.; Ludwig, R.; Haltrich, D.; Gorton, L. *Langmuir* **2006,** *22*, 10801–10806.

18. Tasca, F.; Gorton, L.; Harreither, W.; Haltrich, D.; Ludwig, R.; Noll, G. *J. Phys. Chem. C* **2008,** *112*, 9956–9961.

19. Duine, J. A. *Eur. J. Biochem.* **1991,** *200*, 271–284.

20. Ikeda, H.; Kobayashi, D.; Matsushita, F.; Sagara, T.; Niki, D. *J. Electroanal. Chem.* **1993,** *361*, 221–228.

21. Torimura, M.; Kano, K.; Ikeda, T.; Ueda, T. *Chem. Lett.* **1997,** *6*, 525–526.

22. Laurinavicius, V.; Razumiene, J.; Ramanavicius, A.; Ryabov, A. *Biosens. Bioelectron.* **2004,** *20*, 1217–1222.

23. Treu, B. L.; Minteer, S. D. *Bioelectrochemistry* **2008,** *74*, 73–77.

24. Lapenaite, I.; Kurtinaitiene, B.; Razumiene, J.; Laurinavicius, V.; Marcinkeviciene, L.; Bachmatova, I.; Meskys, R.; Ramanavicius, A. *Anal. Chim. Acta* **2005,** *549*, 140–150.

25. Yuhashi, N.; Tomiyama, M.; Okuda, J.; Igarashi, S.; Ikebukuro, K.; Sode, K. *Biosens. Bioelectron.* **2005,** *20*, 2145–2150.

26. Schmid, R. D.; Urlacher, V. B. *Modern Biooxidation*, Eds. Wiley-VCH, 2007; Vol.13.

27. Aquino Neto, S.; Suda, E. L.; Xu, S.; Meredith, T. M.; De Andrade, A. R. *Electrochim. Acta* **2013,** *87*, 323–329.

28. Arechederra, R. L.; Minteer, S. D. *Electrochem. Acta* **2009,** 54, 7268–7272.

29. Treu, B. L.; Minteer, S. D. *Polym. Mater. Sci. Eng.* **2005,** *92*, 192–193.

30. Barton, S.; Gallaway, J.; Atanassov, P. *Chem. Rev.* **2004,** *104*, 4867–4886.

31. Aquino Neto, S.; Suda, E.; Xu, S.; Meredith, M. T.; De Andrade, A. R.; Minteer, S. D. *Electrochem. Acta* **2013,** *87*, 323–329.

32. Zebda, A.; Gondran, C.; Le Goff, A.; Holzinger, M.; Cinquin, P.; Cosnier, S. *Nat. Commun.* **2011,** *2*, 370–371.

33. Lim, J.; Ciriglinano, N.; Wang, J.; Dunn, B. *Phys. Chem. Chem. Phys.* **2007,** *9*, 1809–1814.

34. Willner, I.; Heleg-Shabtai, V.; Blonder, R.; Katz, E.; Tao, G.; Buckmann, A. F.; Heller, A. *J. Am. Chem. Soc.* **1996,** *118*, 10321–10322.

35. Zayats, M.; Katz, E.; Baron, R.; Willner, I. *J. Am. Chem. Soc.* **2005,** *127*, 12400–12406.

36. Pardo-Yissar, V.; Katz, E.; Willner, I.; Kotlyar, V. S.; Sanders, C.; Lill, H. *Faraday Discuss.* **2000,** *116*, 119–134.

37. Katz, E. *J. Electroanal. Chem.* **1994,** *365*, 157–164.

38. Johnson, D.; Martin, L. *J. Am. Chem. Soc.* **2005,** *127*, 2018–2019.

39. Holland, J.; C., L.; Brozik, S.; Atanassov, P.; Banta, S. *J. Am. Chem. Soc.* **2011,** *133*, 19262–19265.

40. Porath, J.; Carlsson, J.; Olsson, I.; Belfrage, G. *Nature* **1975,** *258*, 598–599.

41. Ataka, K.; Giess, F.; Knoll, W.; Naumann, R.; Haber-Pohlmeier, S.; Richter, B.; Heberle, J. *J. Am. Chem. Soc.* **2004,** *126*, 16199–206.

42. Liu, Y.; Jiang, H., *Electroanalysis* **2006,** *18*, 1007–1013.

43. Kiss, I. Z.; Kazsu, Z.; Gaspar, V. *J. Phys. Chem. A* **2005,** *109*, 9521–9527.

44. Zhao, J.-W.; Kong, X.-G.; Shi, W.-Y.; Shao, M.-F.; Han, J.-B.; Wei, M.; Evans, D. G.; Duan, X., *J. Mater. Chem.* **2011,** *21*, 13926–13933.

45. Haddour, N.; Cosnier, S., *J. Am. Chem. Soc.* **2005,** *127*, 5752–5753.

46. Toyama, H.; Mathews, F. S.; Adachi, O.; Matsushita, K. *Arch. Biochem. Biophys.* **2004,** *428*, 10–21.

47. Fukaya, M.; Yayama, K.; Okumura, H.; Kawamura, Y.; T., B. *Appl. Microbiol. Biotechnol.* **1989,** *32*, 176–180.

CHAPTER 4

UTILIZATION OF CONDUCTING POLYMER FOR DET ENZYME IMMOBILIZATION

4.1 Background

4.1.1 Conducting Polymer Introduction

For a long time, polymers have played a central role in electric insulator studies.[1] This role has changed since the discovery of poly(sulphur nitride) [$(SN)_x$] in 1975, which becomes superconducting at low temperatures,[2] and the discovery of the conjugated conducting polymer of doped polyacetylene with relatively high electrical conductivity (~10^3 S/cm) at room temperature in 1977.[3] This sparked extensive research in the application of conjugated polymers in diverse fields such as electronics,[4] energy storage,[5] catalysis,[6] chemical sensing,[7] biochemistry,[8] and corrosion control.[9] Significant advances in improving the electrical, optical, and mechanical properties while simultaneously enhancing processability and stability have been achieved by cross-disciplinary collaborations between chemists, physicists, materials scientists, and engineers.[10]

Conjugated polymers have shown many unusual electronic properties, such as electrical conductivity,[11] low energy optical transitions,[12] low ionization potential,[13] and

high electron affinity.[14] Those unique properties are caused by the π-electron backbone structure of the polymers. The extended π-conjugated systems of the conducting polymers have single and double bonds alternating along the polymer chain. The conducting polymers belonging to polyenes or polyaromatics such as polyaniline, polyacetylene, polypyrrole, polythiophene, and polyphenylene classes have been studied extensively (Figure 4.1). Among all the above classes, the polyaniline family is of much interest because of its simple synthesis, unique conduction mechanism, and good environmental stability in the presence of oxygen and water.[15, 16]

The mechanism of electrical conduction in conjugated polymers is very complicated since those polymers exhibit conductivity across a range of over 10 orders of magnitude, and many involve different conduction mechanisms within different regimes. Conjugated polymers show enhancement of electrical conductivity by several orders of magnitude by the molecular doping process. The concepts of "solitons," "polarons," and "bipolarons" have been used to explain the conducting phenomena in these systems.[17, 18] Generally speaking, the electrical conductivity of conjugated polymers is determined by factors including polaron length, the conjugation length, the overall chain length, and by the charge transfer to adjacent molecules.[19]

4.1.2 Polyaniline as Conducting Polymer

Polyaniline is one of the oldest conducting polymers known. It was first prepared over 150 years ago by Letheby in 1862 by anodic oxidation of aniline in sulphuric acid.[20] However, only since the early 1980s has polyaniline captured intense research attention due to the rediscovery of high electrical conductivity. The general expression

of polyaniline structure can be expressed as shown in Figure 4.1A. The y-value varies from 1 to 0. Polyaniline is in its fully reduced form when the y-value is 1, and this form of polyaniline is named "polyleucoemeraldine." When the y-value is 0, the structure is called polypernigraniline, which is the fully oxidized form of polyaniline with imine links instead of amine links. The polyemeraldine form, where y-value is 0.5 represents the form of polyaniline when it is a mixture of the other two states. It is often referred to as polyemeraldine base when it is neutral or polyemeraldine salt when it is doped (protonated), with the imine nitrogen atoms protonated by an acid. The polyaniline polymers are only conductive when in the form of protonated polyemeraldine or polyemeraldine salt whose conductivity is around 15 S/cm,[21] whereas the conductivity of polyemeraldine base is around 10^{-5} S/cm.[22]

The electrical conductivity of polyaniline is determined by the oxidation state of the polymer, degree of protonation, electronic structure, and types of dopants.[23] The protonated polyaniline is most conducting in the polyemeraldine oxidation state. The precise degree of the protonation of the highest conductivity is, however, dependent on the pH of the media equilibrated with the polyaniline for protonation. Therefore, polyaniline is more conductive in a strong acidic environment, and the conductivity decrease drastically when it is in neutral or basic solution. The heavy dependence of the polyaniline electrical conductivity on environment pH can be diminished by using so called "self-doped" polyaniline. Self-doped polyaniline represents one of the most unique types of polyaniline derivatives. These polyaniline structures bear aniongenic functional groups such as –COOH,[24] -OH,[25] and $-SO_3H$[26] directly or spacer bound to the aromatic ring. In those "self-doped" polyaniline structures, the protonation of the parent

polyemeraldine can be performed by the proton exchange from the aniongenic functional groups instead of the external environment. This greatly expands the pH range in which the polymers remain conductive. Among those "self-doped" polyanilines, sulfonated polyaniline has been given special interest because the sulfonic acid group is a strong acid and because there is a large variety of sulfonated aromatic amines commercially available. By introducing the sulfonic group into polyaniline parent structures, the polymers show many distinctive properties, such as electrochemical activity in alkaline and neutral media, the property of self-doping, and the fact that the polymer electrical conductivity remains stable when treated with aqueous solutions at pH $\geq$ 4.[27] Representative commercially available sulfonated anilines and the sulfonated polyanilne self-doping process are shown in Figure 4.2.

4.1.3 Polyaniline for Enzyme Immobilization

Stable and convenient immobilization of enzymes on conducting surface (electrodes) with complete retention of their biological recognition properties is a crucial problem for the commercial development of biosensors or biofuel cells.[28, 29] Self-doped polyanilines, which provide fair conductivity (1–10 S/cm) at neutral pH, are potentially capable of forming the appropriate environment for enzyme immobilization at the electrode surface and provide electrical interactions with metallic or carbon electrode surface.[30] Most of the conventional procedures for biomolecule immobilization such as cross-linking and entrapment in gels or membranes suffer from a low electron transfer rate for direct electron transfer (DET) enzymes because it cannot provide close enzyme-electrode proximity, which is crucial for DET enzyme

bioelectrocatalysis. This problem can be solved by covalently bonding enzyme molecules to conducting polymers, which can significantly decrease the enzyme-electrode surface distance.[31]

The strategy for covalently bonding enzymes to a polyaniline conducting polymer is to copolymerize two different aniline derivatives. One sulfonated aniline derivative (2-methoxyaniline-5-sulfonic acid, MASA) is used for improving polymer conductivity and one carboxylated aniline derivative (3-aminobenzoic acid) is used for enzyme immobilization.[31] The carboxylic groups in the polymer film can be activated by *N*-(3-Dimethylaminopropyl)-*N*′-ethylcarbodiimide hydrochloride (EDC) and *N*-hydroxysuccinimide (NHS) to be able to react with the primary amine groups in proteins to form covalent bonds. The schematic illustration of the copolymerization is shown in Figure 4.3.

4.2 Polyaniline Synthesis

4.2.1 Polymerization Mechanism

Polyaniline is generally synthesized by aniline monomer oxidation with either chemical reaction with an oxidant or through the electrochemistry route. Other synthesis routes are proposed such as plasma polymerization,[32] autocatalytic polymerization,[33] or inverse emulsion polymerization.[34] With different polyaniline synthesis methods, a multitude of polymerization mechanisms were induced. The electrochemical polymerization and chemical oxidative polymerization mechanisms are the most studied, and a close similarity can be found for both polymerization methods.[35]

The polymerization mechanism corresponds to a polycondensation process

because it proceeds by steps. A schematic representative of the mechanism is shown in Figure 4.4. The polymerization is initiated by an oxidation step, which leads to the radical cation formation by electron transfer from the 2 s energy level of the aniline nitrogen atom (Figure 4.4A). This step is the kinetic rate limiting step. Then, the reaction is autocatalyzed. The aniline radical cation formed in the first step has three resonance structures (Figure 4.4B), and the resonance form (b) is the more reactive than the other two due to (1) substituent inductive effect and (2) absence of steric hindrance. The next step would be the so called "head to tail" reaction between the radical cation and the resonance form (b) in acidic medium to form a dimer. Then, the dimer is oxidized to form a new radical cation to react either with the radical cation monomer or with the radical cation dimer to form, respectively, a trimer or a tetramer with the same mechanism described previously, and the reactions go on to form the polymer (Figure 4.4C).

4.2.2 Electrochemical Synthesis of Polyaniline

Different electrochemical methods were used for polyaniline synthesis: (1) the galvanostatic method to apply a constant current,[36] (2) the potentiostatic method with constant potential pulses,[37] and (3) the potentiodynamic method, where potential applied varies with time, such as cyclic voltammetry.[38] For all three electrochemical methods above, a three-electrode assembly is required: a working electrode where the polymerization reaction takes place, a counter electrode, or auxiliary electrode, which in often cases is platinum mesh or grid. And a reference electrode such as a Ag/AgCl or a saturated calomel electrode (SCE). Polyaniline can be deposited on many working

electrodes such as metals (Pt,[39] Cu,[40] Fe,[41] Au,[42] stainless steel[43]), conducting glass[44] (glass covered by indium-doped tin oxide (ITO) electrode), and carbon based electrodes (graphite,[45] carbon fiber,[46] carbon nanotubes[47]). Compared to chemical synthesis, electrochemical method presents many advantages: (1) clean synthesis, where no extraction from the monomer-solvent-oxidant mixture is necessary, (2) thickness and doping being controlled by electrode potential applied, and (3) simultaneous synthesis and deposition of the polymer thin layer.

In 2012, Schubart *et al.* reported a glucose bioanode where the nonheme-containing PQQ-dependent glucose dehydrogenase (PQQ-GDH) was covalently bound to an electro-polymerized polyaniline copolymer film on a multiwalled carbon nanotube (MWCNT)-modified gold electrode and observed electron transfer between the PQQ-GDH and electrode surface.[31] In this study, bioanodes based on carbon fiber paper electrode are prepared. To promote the electric contact of the multiple heme containing PQQ-dependent alcohol (PQQ-ADH) dehydrogenase and PQQ-dependent aldehyde dehydrogenase (PQQ-AlDH) to the electrode surface, a layer of sulfonated polyaniline is synthesized onto the carbon fiber electrode surface. The polymer film is prepared by electropolymerization of different aniline derivatives by a cyclic voltammetry method. The preparation method is optimized with respect to the electrical communication of the proteins to the electrode.

4.3 Experimental

4.3.1 Reagents

D-mannitol (Sigma), $(NH_4)_2HPO_4$ (Sigma), KOH (Sigma), KH_2PO_4 (Sigma), K_2HPO4(Sigma), KCl (Sigma), KH_2PO_4 (Sigma), $(NH_4)SO_4$ (Sigma), $MgSO_4 \cdot 7H_2O$ (Sigma), $CaCl_2 \cdot 2H_2O$ (Sigma), lysozyme from egg white (Aldrich), CHAPS (Sigma), 2,6-dicholoroindophenol sodium salt hydrate (DCIP) (Sigma), EDC hydrochloride (Sigma), *N*-hydroxysuccinimide (NHS) (Sigma), methylene chloride (Sigma), 3-aminobenzoic acid (ABA) (Sigma), 2-methoxyaniline-5-sulfonic acid (MASA) (Sigma) and MES (Sigma) were used as received.

4.3.2 PQQ-Dependent DET Enzymes Extraction

Gluconobacter sp. (DSM 3504, ATCC 15163) was grown the same way as described in the Chapter 2 Experimental section. After cultivation, 5g of *Gluconobacter* was thawed and suspended in 0.2 M phosphate buffer pH 7.2, 1 mM $CaCl_2$, 10% CHAPS (to 0.5% final concentration), and 1 mL of lysozyme (10 mg lysozyme in 1mL 0.2M phosphate buffer pH 7.2, 1 mM $CaCl_2$). The solution was incubated at 4 ℃ with gentle stirring for 1 h followed by ultrasonication using a sonic dismembrator for 2 min at 4 ℃. The solution was then centrifuged for 1 h at 12,000 × g to remove insoluble materials. Resulting enzyme lysate was used directly for enzyme immobilization.

4.3.3 Copolymerization of Aniline Derivatives

Toray paper electrodes were cleaned by sonication in methanol for 45 minutes (15 minutes per sonication, 3 times cleaning). Toray paper electrodes were then dried in air

and then equilibrated in 1 M H_2SO_4 solution containing 0.1 M KNO_3. Cyclic voltammetry was chosen as the electrochemical polymerization method. In a solution of a total concentration of 0.1 M aniline derivatives in 1 M H_2SO_4 solution containing 0.1 M KNO_3, the polymerization was done. The Ag/AgCl electrode was used as a reference electrode, and a platinum mesh electrode was used as a counter electrode.

4.3.4 Polymer Carboxylic Group Activation and Enzyme Immobilization

After polymer synthesis the electrode was rinsed with DI water. For covalent coupling of the PQQ-dependent enzymes the carboxylic groups of m-aminobenzoic acid were active by 25 mM NHS and 100 mM EDC for 15 minutes. Activation was performed in both aqueous MES buffer and organic solvent CH_2Cl_2 for comparison. For enzyme immobilization the electrode was incubated with a PQQ-dependent enzymes solution of 5 mg/ml for overnight. Finally the electrode was washed 3 times with 50 mM MES buffer pH 6.5 containing 1 mM $CaCl_2$ and stored at 4 ℃ until use.

4.3.5 Electrochemical Measurements

Electropolymerization was performed on a Digi-Ivy DY2300 potentiostat, and electrochemical measurements of the modified electrodes were performed on a CH Instruments 1030 potentiostat. Platinum and Ag/AgCl electrodes were used as counter and reference electrodes. All polymerizations were performed in 1 M H_2SO_4 solution containing 0.1 M KNO_3, all electrochemical measurements of modified electrodes were performed in 50 mM MES buffer pH 6.5 containing 0.1 M KNO_3.

4.4 Results and Discussion

4.4.1 Electrode Polymerization

As described previously, the initial step of polymerization is oxidizing aniline derivatives to form radical cations. This is the rate limiting process; thus finding the appropriate cyclic voltammetry scan window to efficiently form radicals is crucial for electropolymerization. Before the copolymerization of two aniline derivatives, polymerizations of each aniline derivative monomer were studied to find their significant polymerization peaks. Eighty mM of 2-methoxyaniline-5-sulfonic acid (MASA) and 20 mM of 3-aminobenzoic acid (ABA) were polymerized in 1 M H_2SO_4 solution with 0.1 M KNO_3, respectively. Scan windows of 0.45 V–0 V, 0.6 V–0 V, and 0.8 V–0 V (versus Ag/AgCl, scan rate 100 mV/s) were chosen. Results are shown in Figure 4.5. The cyclic voltammograms of MASA polymerization showed that for scans of 0.45 V–0 V and 0.6 V–0 V versus Ag/AgCl windows, no polymerization peaks were observed, but when the upper limit of the scan window was raised to 0.8 V, two distinct reversible polymerization peaks appeared at around 0.5 V and 0.6 V versus Ag/AgCl. The results indicated that MASA can be oxidized to radical cation only at a potential around 0.8 V, and potentials lower than this cannot efficiently produce radicals for the following polymerization steps. Similar results were obtained for ABA polymerization; two new peaks at 0.35 V and 0.5 V versus Ag/AgCl appeared when the scan upper limit was raised to 0.8 V versus Ag/AgCl and those peaks were not observed when scan windows of 0.45 V–0 V and 0.6 V–0 V versus Ag/AgCl were used. The next step is to copolymerize two aniline derivatives to form a polymer film on the electrode surface that contains both sulfonic groups and carboxylic groups. A polymerization solution

containing 80 mM MASA and 20 mM ABA in 1 M H_2SO_4 solution with 0.1 M KNO_3 was used for copolymerization. The cyclic voltammograms of copolymerization showed significant polymerization peaks from both MASA and ABA, indicating that the two aniline derivatives are successfully polymerized together to form a polymer film on Toray paper electrode surface.

In order to optimize the copolymerization process, a further study of electropolymerization was performed. The polymerization cyclic voltammograms were compared with scan windows of 0.8 V–0 V, 0.85 V–0 V, and 0.9 V–0 V. As shown in Figure 4.6A, a 30-cycle polymerization 0.9 V–0 V scan showed an increase of polymerization peak height of 25-fold compared to a 0.8 V–0 V scan window. With this knowledge, the optimized polymerization window has been set to be 0.9 V–0 V. In order to test the polyaniline electrical conductivity at neutral pH environment, the polymerized electrode was tested in MES buffer pH 6.5. As shown in Figure 4.6B, two distinct redox peaks at 0.3 V and 0.5 V can be observed in the cyclic voltammogram. Those two peaks represent the conversion of the fully reduced form polyleucoenmeraldine to mixed state polyemeraldine and the conversion between polyemeraldine and the fully oxidized form polypernigraniline. The results suggest that this polyaniline configuration is electrical conductive at neutral pH, which is suitable for enzyme electrocatalysis.

4.4.2 Polymer Carboxylic Group Activation Results

For the covalent coupling of PQQ-dependent enzymes to the polymer, the carboxylic groups in the polymer film should be activated. To activate carboxylate

complexes means to prepare amine-reactive esters of carboxylate groups for crosslinking. Carboxylates are usually activated with a carbodiimide such as *N*-(3-Dimethylaminopropyl)-*N′*-ethylcarbodiimide (EDC) in the presence of *N*-hydroxysuccinimide (NHS). The activation reaction scheme is shown in Figure 4.7. Carboxylate reacts with EDC to form a very unstable *o*-acylisourea intermediate, which is ready to react with a primary amine to form a stable conjugated amide bond.[48] This intermediate can also react with NHS to form a more stable intermediate, which can also react with complexes with primary amine group.[49] Although NHS is not required for carbodiimide reactions, their using greatly enhances coupling efficiency, and using NHS makes it possible to perform a two-step reaction. However, in water-based activation solutions, hydrolysis of activation intermediates is always a problem. Even more stable NHS ester will hydrolyze back to carboxylate form within hours or minutes, depending on water-content and pH of the reaction solution. NHS esters have a half-life of 1 hour at pH 7 and 10 minutes at pH 8.[50] This might greatly affect the activation efficiency and result in limited binding sites for proteins to be immobilized on electrode.

Carboxylate activation can be performed in both aqueous and organic solvents. Both EDC and NHS have better solubility in water based solutions than the organic solvent, but using organic solvents can rule out the possibility of hydrolysis of the activated esters. In order to find the optimal activation method for the carboxylic acid groups on polyaniline film, parallel experiments were carried out with three different activation routes. All Toray paper electrodes were polymerized with the same method (0.02 M ABA, 0.08 M MASA in 1 M H_2SO_4, 0–0.9 V scan, 15 cycles). Then

polymerized electrodes were divided into three groups for three different activation methods: (A) two step activation, where electrodes were incubated with 100 mM EDC, 25 mM NHS in MES buffer pH 6.5 and 0.1 M KCl for 15 minutes and rinsed with DI water before being transferred to enzyme solution (0.2M phosphate buffer pH 7.2, 1mM $CaCl_2$); (B) two step activation, where electrodes were incubated with 30 mM EDC, 10 mM NHS dissolved in CH_2Cl_2 for 15 mintutes, then dried with nitrogen gas before being transferred to enzyme solution; and (C) one step activation, where electrodes were incubated with 100 mM EDC, 25 mM NHS in enzyme solution.

For the three activation methods, the same *Gluconobacter* crude extract solution was used and the same enzyme incubation time was performed (3 hours). During this process, in method (A), activation solution and enzyme solution kept clear throughout the activation and enzyme immobilization process. In method (B), activation solution turned a little yellow and the polyaniline film on Toray electrodes was a little washed off, indicating the polymer film might be dissolved in organic solvent. In method (C), the enzyme solution turned cloudy 5 minutes after the polymerized electrodes were immersed and white precipitate was formed during the incubation. All electrodes were dried at 4 ℃ for overnight before the test. Test results (Figure 4.8) showed that only the electrode activated with method (A) showed electrocatalytic responses. Electrode activated with method (B) suffered from the dissolution of polymer film in organic solvent, and the polyaniline no longer formed an evenly distributed thin film on the electrode surface, which greatly affect the conductivity of the polymer film. Method (C) was not successful mainly because the activating agents reacted with phosphate prior to carboxylates, which led to very low activation efficiency. With this knowledge, a two-

step process with an activation step in MES buffer will be used for further investigations.

4.4.3 Immobilized Enzyme Activity Assays

In order to investigate whether the enzymes that covalently bond to the polymer film have retained their biological catalytic properties, a free enzyme DCPIP/BCA activity assay and an immobilized DCPIP assay was performed. The free enzyme DCPIP/BCA assays were carried out as described in Chapter 2. For the immobilized DCPIP assay, a modified electrode with enzyme immobilization was immersed in the reaction mixture for 4 minutes, and absorbance change at 600 nm wavelength was recorded. Results are shown in Table 4.1. Significant absorbance changes were observed for ethanol and glyceraldehyde and glucose as substrate, showing that PQQ-dependent alcohol dehydrogenase, PQQ-dependent aldehyde dehydrogenase, and PQQ-dependent glucose dehydrogenase were successfully immobilized on the conducting polymer and retained their catalytic activity.

4.4.4 Electrochemical Measurements

Previous results have demonstrated that active PQQ-dependent enzymes have been successfully immobilized by covalently bonding to the polyaniline matrix structure. The next step is to demonstrate that immobilized PQQ-dependent enzymes can perform bioelectrocatalysis and investigate the electron transfer mechanism. First, in order to rule out the possibility of polymer catalyzing redox reactions of the substrate, control experiments were carried out where the polymerized Toray paper electrodes

without the carboxylate group activation process were tested with cyclic voltammetry with and without the addition of 10mM ethanol. Results showed no catalytic current appearing with ethanol addition, which indicated no catalytic property of polyaniline toward the ethanol substrate (Figure 4.9A). A fully modified electrode with enzyme loading was tested with cyclic voltammetry; an oxidation peak at 200 mV was observed, and this peak was not showing in the polymer electrodes without enzyme loading (Figure 4.9B, black line); and a catalytic current was observed when 10 mM ethanol was added (Figure 4.9B, red line). This result demonstrated the property of bioelectrocatalysis of the PQQ-dependent enzyme, but also raised a question of whether this 200 mV signal is from the PQQ-dependent enzyme (or more specifically, from the heme-c group) or from the conducting polymer. This is an important question to answer because it determines whether the electron transfer mechanism is MET or DET. Another experiment was carried out to answer this question: an activated polyaniline electrode was immobilized with bovine serum albumin (BSA), which is a commonly used protein that has been demonstrated not electrochemically active within the electrochemistry test window. The cyclic voltammetry result of the BSA electrode showed the same peak at 200 mV (Figure 4.9C), which indicates that this peak is from polyaniline and is not from PQQ-dependent enzymes. Cyclic voltammetry was also performed with the activated polyaniline polymer electrode without enzyme loading (Figure 4.9D); a peak at 200 mV was observed, and this result revealed the fact that the activation step shifted the peak to lower potential, and the electrochemical signal observed from the fully modified electrode is from the polyaniline, which indicated that the electron transfer is mediated by polyaniline polymer (MET).

Electrodes with different polymerization cycles were tested in order to optimize the electropolymerization process. Five-cycle, 15-cycle, and 30-cycle polymerization electrodes were prepared and activated (Figure 4.10), then immersed in the same batch of enzyme solution for overnight before electrochemical measurements were performed. All electrodes showed electrocatalytic responses, and the calibration curves showed that they all match the Michaelis–Menten mechanism, indicating enzymatic electrocatalysis (Figure 4.11). Electrodes with the 5-cycle polymerization amperometry test showed that the electrode has a maximum current response I_{max} of 0.232 ± 0.031 μA with a K_m value of 0.136 ± 0.015 mM. Electrodes with 15-cycle polymerization yielded a maximum current response I_{max} of 0.981 ± 0.121 μA and a K_m value of 0.180 ± 0.019 mM. With 30-cycle polymerization, the electrode amperometry results showed a I_{max} of 0.251 ± 0.074 μA and a K_m value of 0.080 ± 0.031 mM. By comparing the results above, it was shown that the 15-cycle polymerization has a 4.2-fold increase in maximum current response compared to 5-cycle polymerization and a 3.9-fold increase compared to 30-cycle polymerization. All three electrodes showed a similar K_m value, indicating similar enzyme-substrate affinities. The results showed that with polyaniline conducting polymer film covalently bonding with PQQ-dependent alcohol dehydrogenase (PQQ-ADH) in enzyme lysate, direct electron transfer can be achieved.

Amperometric measurements of polyaniline modified PQQ-dependent enzyme electrodes show that with 15-cycle electrochemical polymerization, the bioanode exhibits higher current density than 5-cycle and 30-cycle polymerized electrodes. Jean-Michel Savéant proposed that at redox polymer electrodes, the electrocatalysis rate is closely related to the polymer film thickness.[3] His strategy to determine the rate-limiting

elements in an electrochemical system is to express, as a set of characteristic currents, the maximum rates that would be observed if each individual dynamic element, in turn, defined the rate of the overall process entirely on its own. Those characteristic currents are caused by (1) Diffusion of substrate within the polymer film, (2) Diffusion of electrons in the film, and (3) Cross-reaction in the film.

In the situation where in the polymer film, the conversion of the substrate is fast, then the overall process is entirely controlled by the rate at which the substrate can arrive at the electrode surface by diffusion through the film. The concentration of substrate at the electrode surface is zero. Just inside the outer boundary of the film (ϕ^-), the concentration differs from that just outside the film (ϕ^+) because partitioning occurs. The concentrations are related via the partition coefficient, $\kappa = C_A(\phi^-)/C_A(\phi^+)$. The substrate diffusion current within the film, I_s, is expressed as $Is = nFAD_s \kappa C_A^*/ \phi$, where C_A^* is the substrate bulk concentration, Ds is the diffusion coefficient of the substrate in the film, A is the electrode surface area, and ϕ is the film thickness.

In the polyaniline structure the electrons are distributed through the polymeric structure. In the case where the electron hopping in the polyaniline film carries the whole weight of the process by which the substrate is converted, the electron diffusion current is expressed as $I_E = FAD_E C_p^*/ \phi$, where D_E is the apparent diffusion coefficient of electrons within the polymer film and C_p^* is the concentration of the electron mediator in the film.

In a system where the substrate partitions and permeates rapidly, suppose also that electrons diffuse rapidly through the structure. In this case, the maximum rate of charge delivery is defined by the maximum rate of cross-reaction. $I_k = nFA \phi k \kappa C_p^* C_A^*$.

According to Jean-Michel Savéant's theory, when the film thickness (ϕ) is small, the limiting current is the cross-reaction current, which increases with film thickness increase. As the redox polymer gets thicker, the characteristic current of permeation of substrate within the film and/or the charge propagation characteristic current start to become the limiting factor of substrate conversion rate as those two characteristic current decrease with film thickness increase. The limiting current with all of the processes contributing can be obtained by numerical solution of the differential equations governing the process.[4] Savéant also proposed that there is an optimal thickness for an electrochemical process that occurs in redoxpolymer.[3]

In order to study the effect of the polymer film thickness on bioelectrocatalysis rate, the polyaniline film thickness should be determined. Scanning Electron Microscopy (SEM) was performed on Toray paper electrodes modified with different cycle numbers. Results are shown in Figure 4.12. SEM results show that within the carbon fiber electrode, the formation of polyaniline is not evenly distributed throughout the carbon fiber structure, but rather forms clusters of polymer at certain areas. Results show that when a 5-cycle polymerization is performed, very limited amount of carbon fibers were coated with polymer, and when a 15-cycle polymerization is performed, uniformed coating for carbon fibers begins to occur. When the polymerization cycle is increased to 30, the results show that polymers start to form in the cavities of the carbon fiber electrodes, and clusters of polymer were accumulated. Therefore, in this case, the small bioelectrocatalysis rate with 5-cycle polymerization is due to incomplete coverage of polyaniline on carbon fibers, and the rate is increased with 15-cycle polymerization, but when increased to 30-cycle polymerization, the coverage of carbon fiber by

polyaniline is saturated, and excess formation of polyaniline is limiting the mass transfer of substrate within the carbon fiber structure, which leads to lower bioelectrocatalytic current.

In order to investigate the electrocatalysis property of PQQ-dependent aldehyde dehydrogenase (PQQ-AlDH) immobilized on polyaniline film, glyceraldehyde was used as the substrate in electrochemical measurements. Results are shown in Figure 4.13. Catalytic current was observed in the amperometry test; I_{max} of 0.843 ± 0.102 μA and a K_m value of 15.0 ± 1.9 mM were obtained. The results demonstrated the direct electron transfer from PQQ-AlDH to the electrode surface.

4.4.5 Comparison of Immobilization Techniques

In order to compare Toray electrode fabricated with mixture casting modified Nafion with the respective enzyme and fabricated with conducting polyaniline film, bioanodes were made with each technique with the same batch of PQQ-dependent enzymes lysate from *Gluconobacter*. TBAB-Nafion electrodes were prepared by drop-casting 100 μl of 1:1 (V:V) enzyme solution: TBAB-Nafion ethanol solution (10 mg/ml final protein concentration which is TBAB-Nafion protein capacity limit) to Toray paper electrode as discussed in Chapter 2. Electrodes were dried under fan for overnight before testing. Polyaniline modified Toray paper electrodes were prepared with the same methods described previously. Cyclic voltammetry was performed with TBAB-Nafion modified electrodes in 50 mM MES buffer with 10 mM ethanol, and results are shown in Figure 4.14A. An oxidation peak was observed at 350 mV versus Ag/AgCl. Amperometry measurement was performed on the TBAB-Nafion electrodes with an

applied potential of 360 mV; results and calibration curve are shown in Figure 4.14B and 4.14C. The calculated K_m value for TBAB Nafion electrode is 0.425 ± 0.092mM, and I_{max} is 0.099 ± 0.017 μA.

The same batch of enzyme mixture was used for polyaniline-modified bioanode fabrication, amperometry results are shown in Figure 4.15. The calculated K_m value is 0.178 ± 0.031 mM and I_{max} is 0.59 ± 0.09 μA, which is almost six times higher than TBAB-Nafion modified electrodes. This result suggested that the polyaniline conducting polymer immobilization method can yield a higher bioelectrocatalysis rate than TBAB-Nafion.

4.5 Conclusions

In this work, two aniline derivatives with different functional groups were copolymerized on the carbon fiber electrode surface for enzyme immobilization and charge transducing. The self-doped polymer was characterized and polymerization process was optimized. PQQ-dependent enzymes were successfully immobilized on the polymer film via covalent bonding through the activated carboxylic group site. DET was observed with PQQ-dependent alcohol and PQQ-dependent aldehyde dehydrogenases using ethanol and glyceraldehyde as substrates. Comparing this polyaniline conducting polymer with TBAB-Nafion polymer enzyme immobilization method showed a six-fold increase in current density.

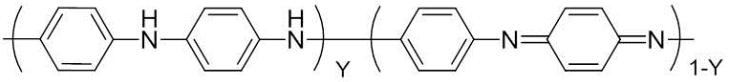

(A)

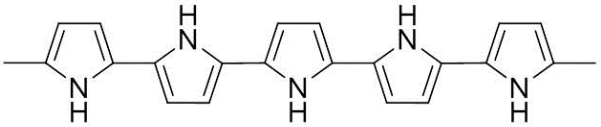

(B)

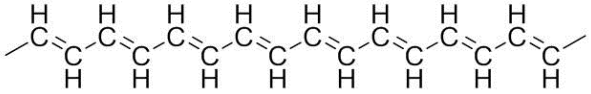

(C)

(D)

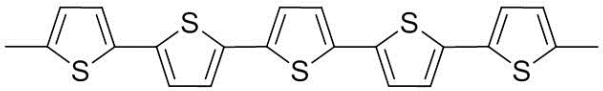

(E)

Figure 4.1. Chemical structures of commonly studied polyenes and polyaromatics conducting polymers. (A) Polyaniline. (B) Polypyrrole. (C) Polyacetylene. (D) Polyphenylene. (E) Polythiophene.

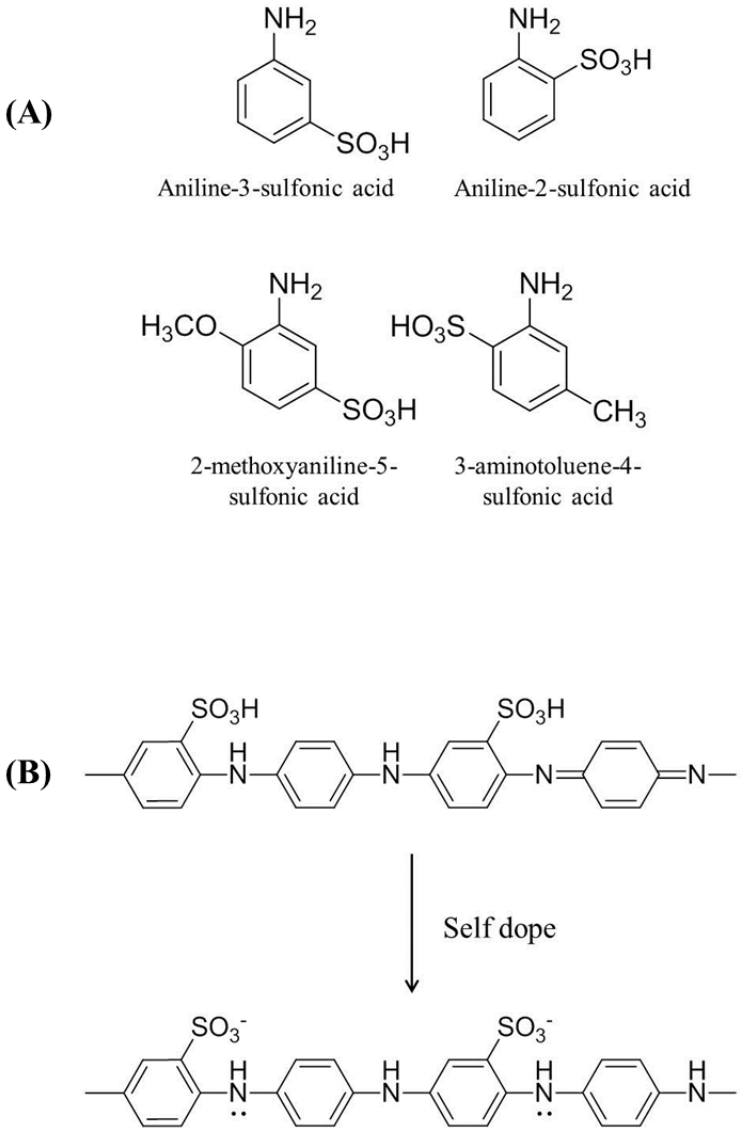

Figure 4.2. Self-doping process of sulfonated polyanilines. (A) Representative commercially available sulfonated anilines. (B) Sulfonated polyanilne self-doping process.

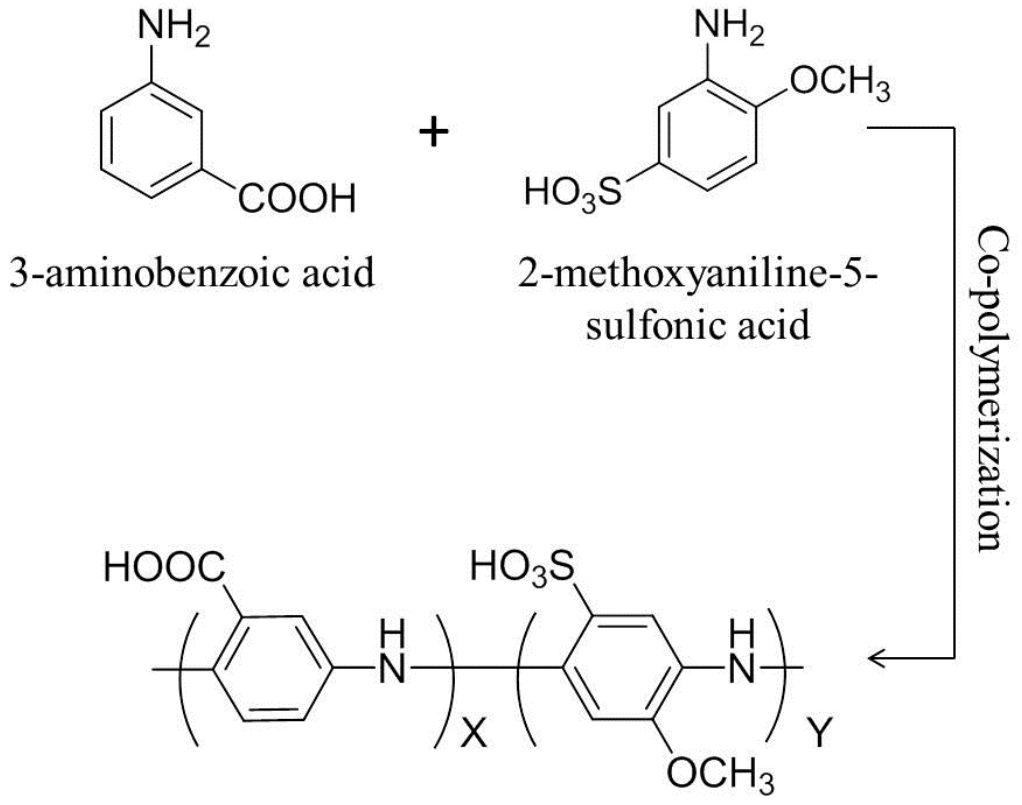

Figure 4.3. Schematic illustration of the copolymerization of 3-aminobenoic acid (ABA) and 2-methoxyaniline-5-sulfonic acid (MASA).

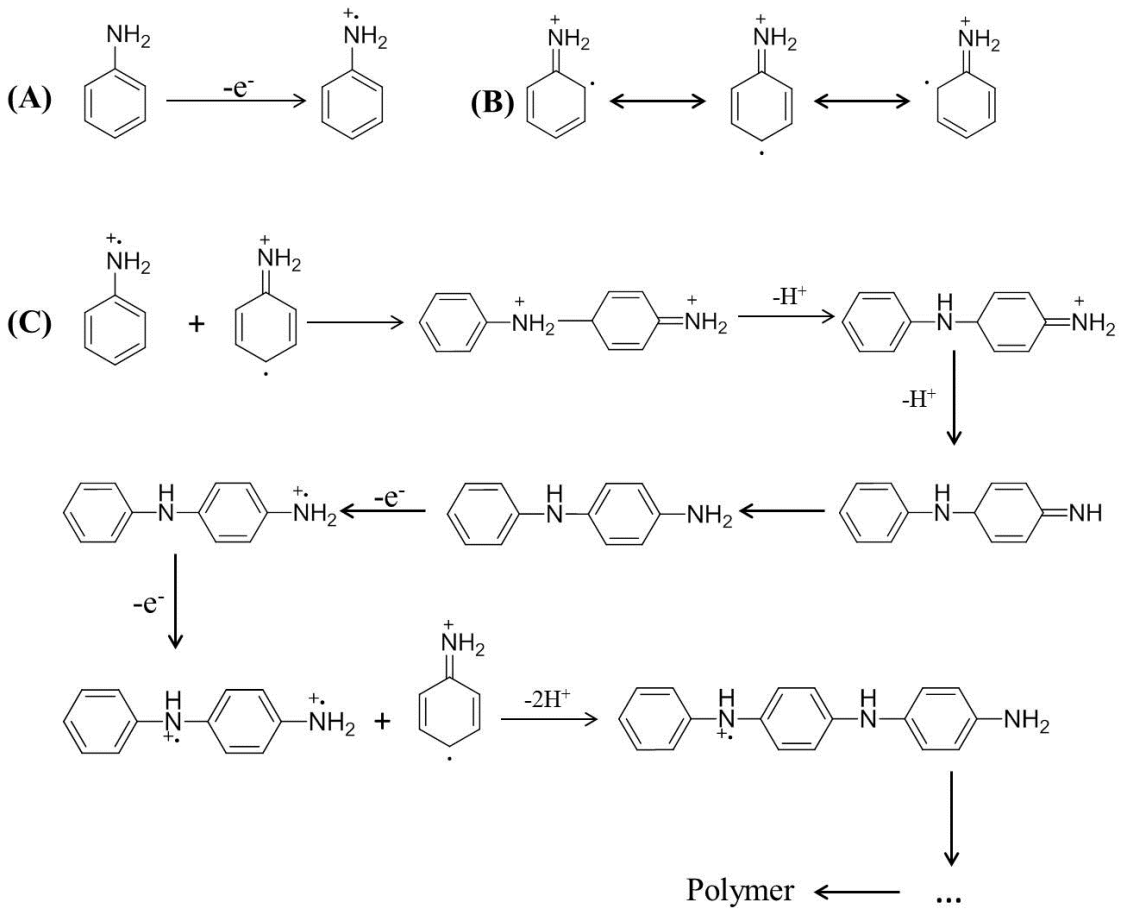

Figure 4.4. Aniline polymerization mechanism. (A) Oxidation of aniline monomer to form radical cation. (B) Three resonance structures of aniline radical cation. (C) Aniline polymerization pathway.

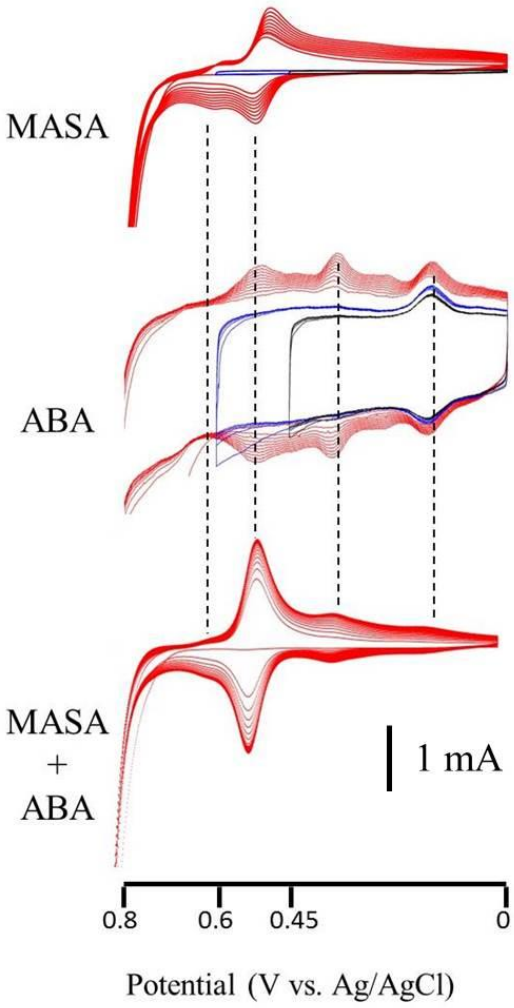

Figure 4.5 ABA and MASA electrochemical copolymerization study. Black lines represent 0.45V–0V scan window, blue lines represent 0.6V–0V scan window, red lines represent 0.8V–0V scan window. All measurements were performed in 1 M H_2SO_4 solution with 0.1 M KNO_3, 100 mV/s scan rate.

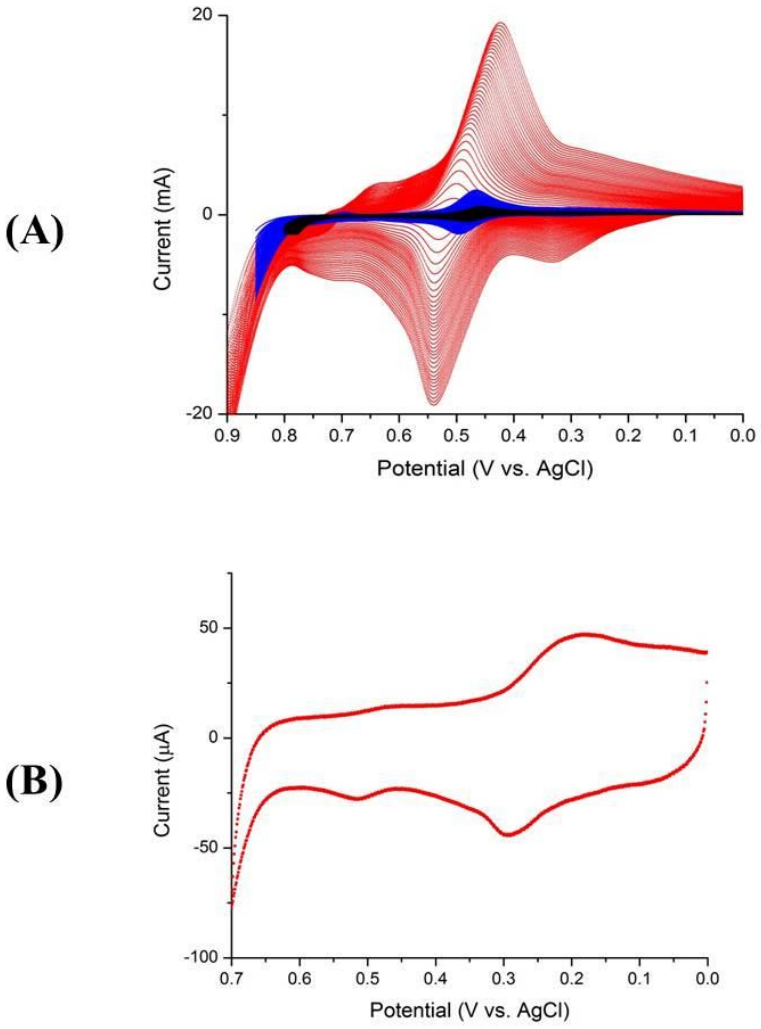

Figure 4.6 Electropolymerization optimization. (A) 30 cycle polymerizations with different scan window; black lines represent 0.8V–0V, blue lines represent 0.85V–0V, red lines represent 0.9V–0V (measurements were performed in 1 M H_2SO_4 solution with 0.1 M KNO_3, 100 mV/s scan rate). (B) Representative cyclic voltammogram of DI water rinsed polymerized Toray electrode in neutral pH buffer (50 mM MES buffer pH 6.5, 0.1 M KNO_3, 100 mV/s scan rate).

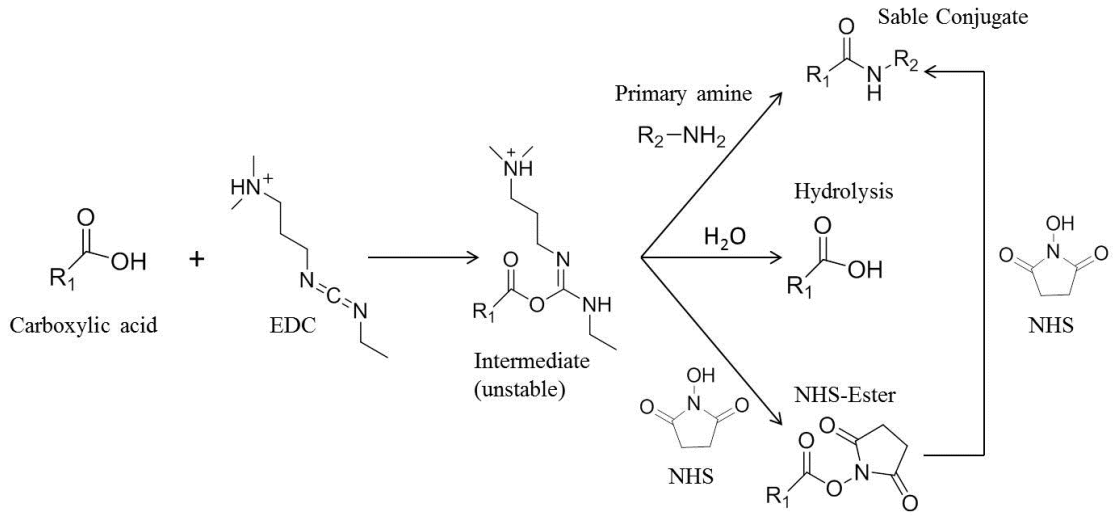

Figure 4.7 Carboxylic group activation with *N*-(3-Dimethylaminopropyl)-*N′*-ethylcarbodiimide (EDC) and *N*-hydroxysuccinimide (NHS).

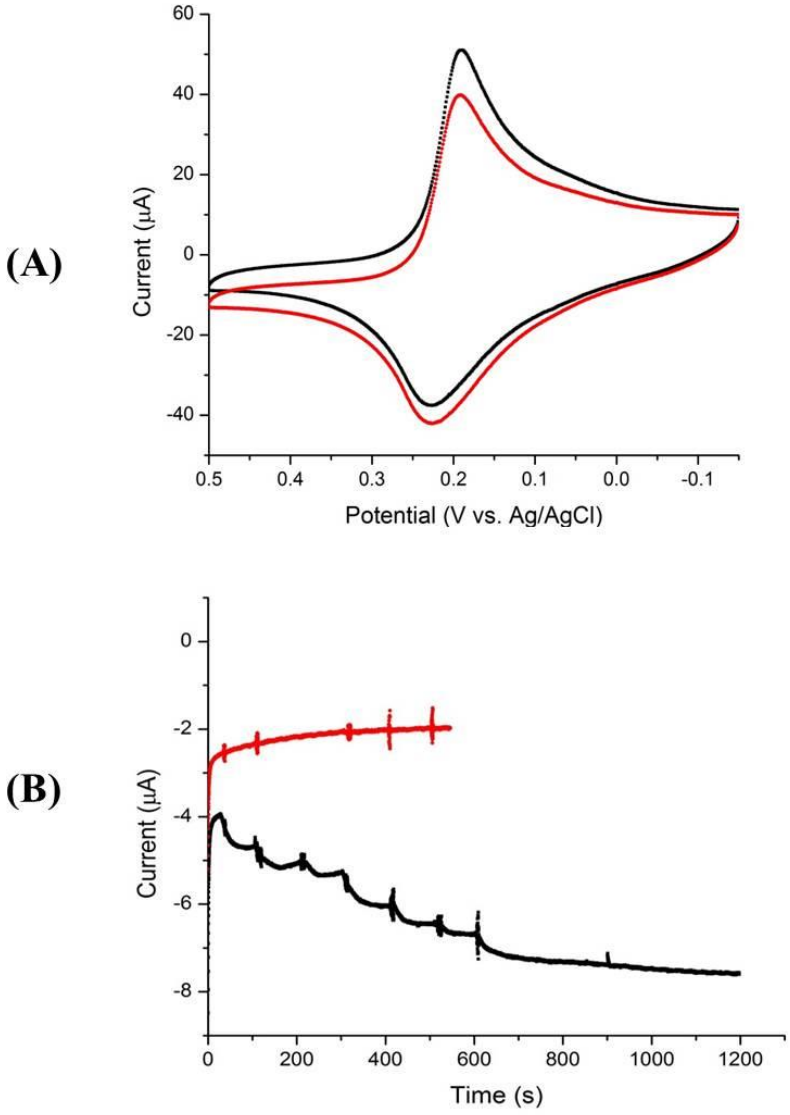

Figure 4.8. Electrochemical measurements of electrode activated in MES buffer (Method A). (A) Cyclic voltrammetry measurement results; black line represents blank, and red line represents 10 mM ethanol, scan rate 5 mV/s. (B) Amperometry measurement results. Blank (red): electrochemistry buffer was injected. Test electrode (black): 1 mM ethanol was injected at 30 s, 100 s, 200 s, 300 s, 400 s, and 500 s; 5 mM ethanol was injected at 600 s and 900 s. All measurements performed in 50 mM MES pH 6.5, 0.1 M KNO_3.

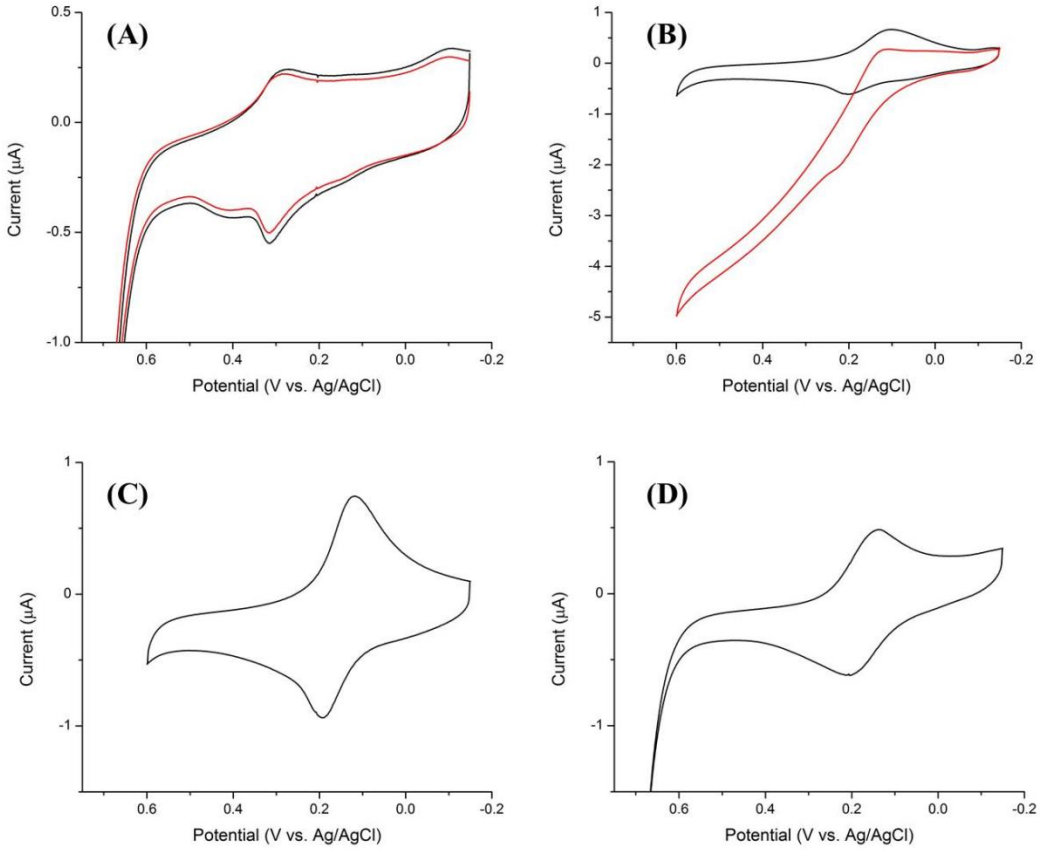

Figure 4.9 Cyclic voltammetry study results of polyaniline electrodes: (A) unactivated polymerized electrode in buffer solution (black) and in 10 mM ethanol solution (red). (B) Fully modified electrode in buffer solution (black) and in 10 mM ethanol solution. (C) Activated electrode with BSA immobilization in buffer solution. (D) Activated electrode without enzyme immobilization in buffer solution.

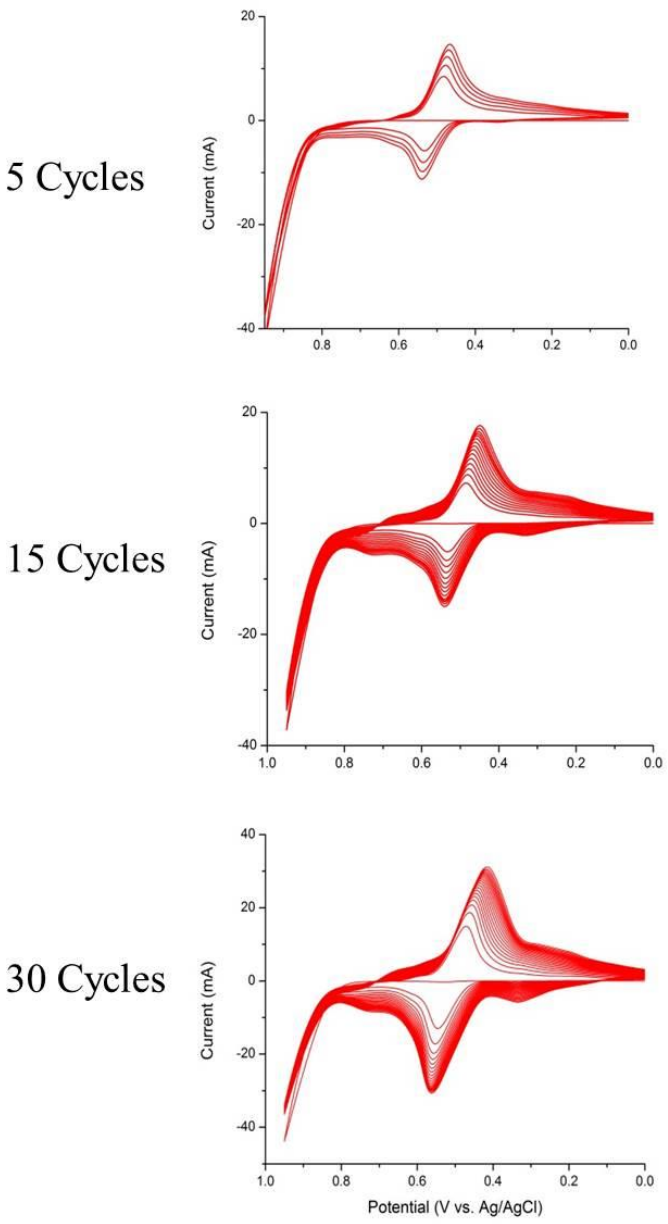

Figure 4.10. Cyclic voltammograms of 5-cycle, 15-cycle and 30-cycle electrochemical copolymerization. 0.02 M ABA, 0.08 M MASA in 1 M H_2SO_4, 0.1 M KNO_3, 100 mV/s scan rate.

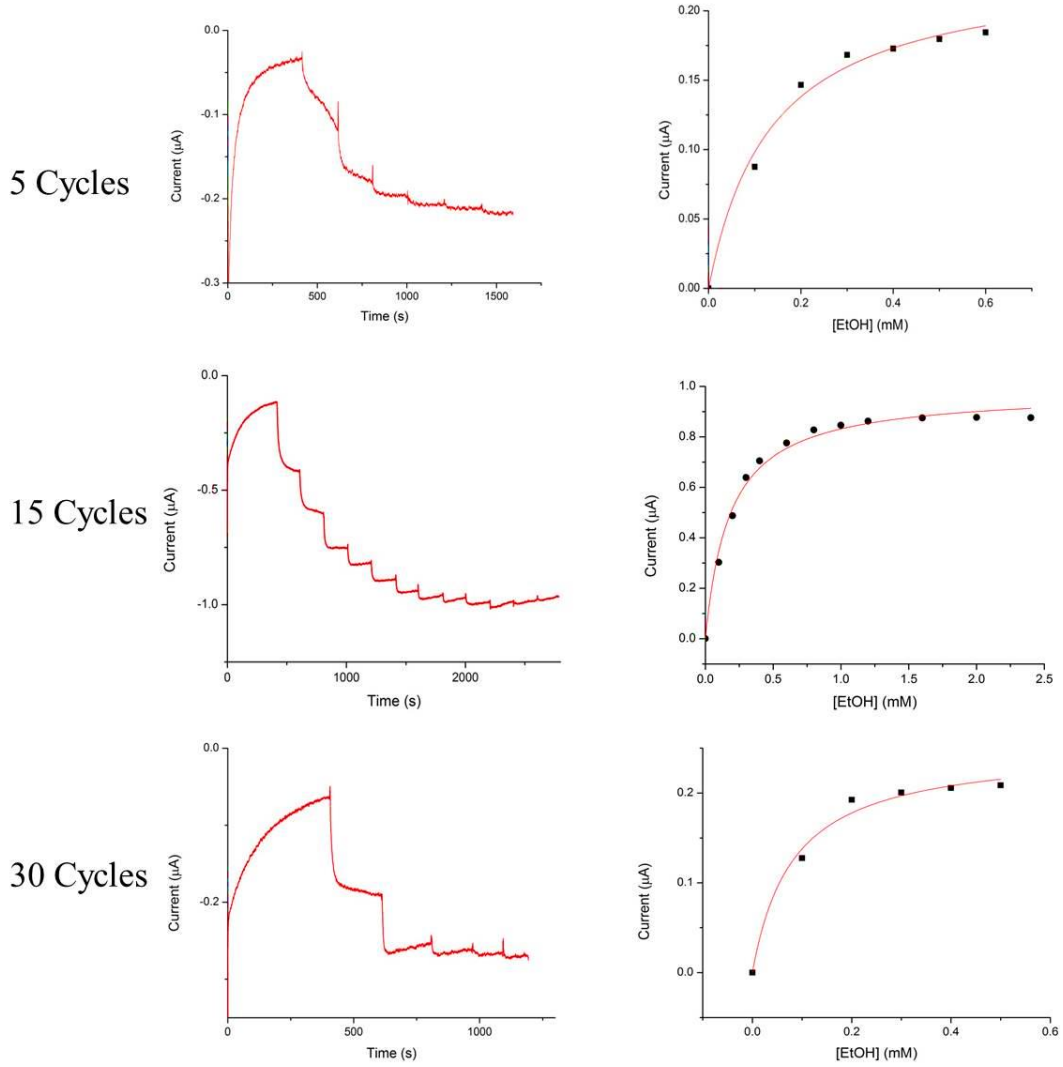

Figure 4.11. Amperometry measurements of electrodes with 5, 15, and 30 polymerization cycles. For 5-cycle polymerized electrode amperometry measurements. 100 uM ethanol injected at 400 s, 600 s, 800 s, 1000 s, 1200 s, and 1400 s time points, and calculated I_{max} = 0.232 ± 0.031 µA, K_m = 0.136 ± 0.015 mM. For 15-cycle polymerized electrode amperometry, 100 uM ethanol injected at 400 s, 600 s, 800 s, and 1000 s. 200 uM ethanol injected at 1200 s, 1400 s, 1600 s, and 1800 s. 400 uM injected at 2000 s, 2200 s, 2400 s, and 2600 s time points. Calculated I_{max} = 0.981 ± 0.121 µA and K_m = 0.180 ± 0.019 mM. For 30-cycle polymerized electrode amperometry, 100 uM injection at 400 s, 600 s, 700 s, 900 s, and 1100 s time points; I_{max} = 0.251 ± 0.074 µA, and K_m = 0.080 ± 0.031 mM.

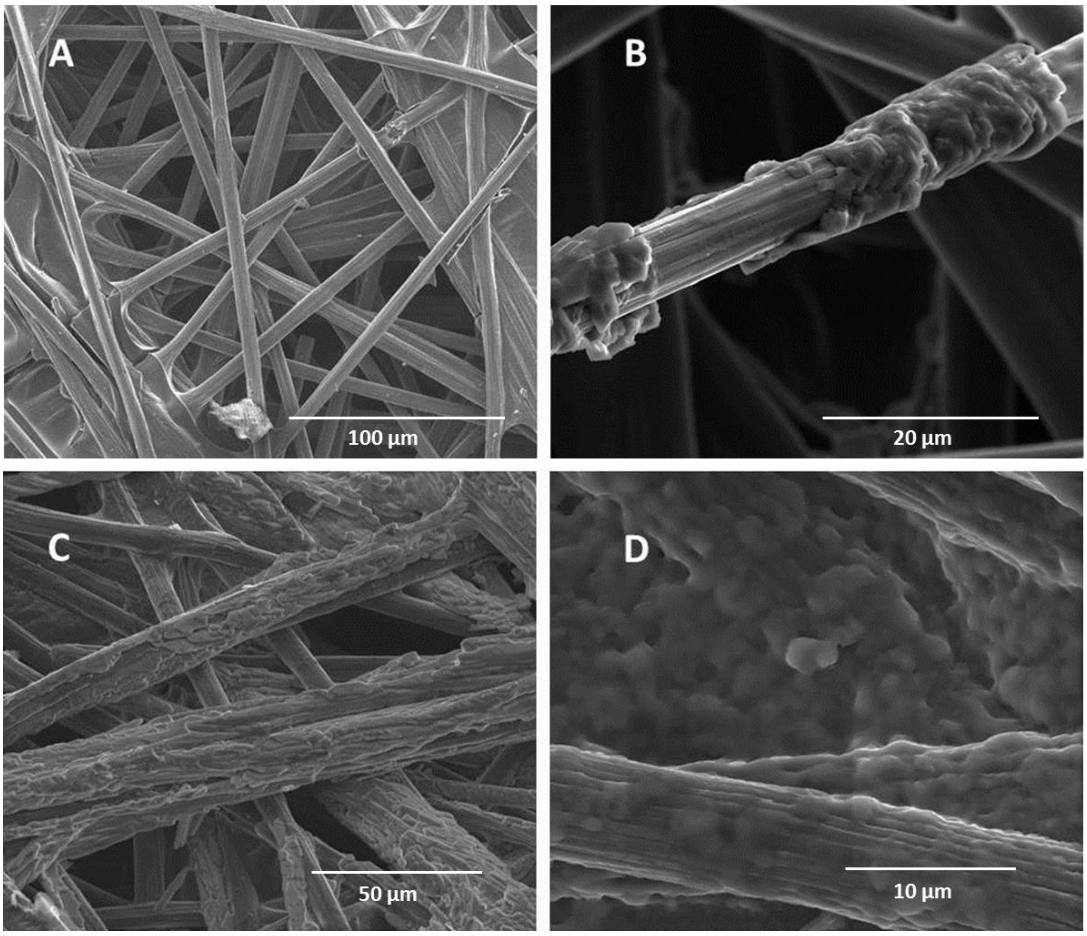

Figure 4.12 SEM images of (A) Bare Toray paper electrode. (B) 5-cycle polymerization. (C) 15-cycle polymerization. (D) 30-cycle polymerization.

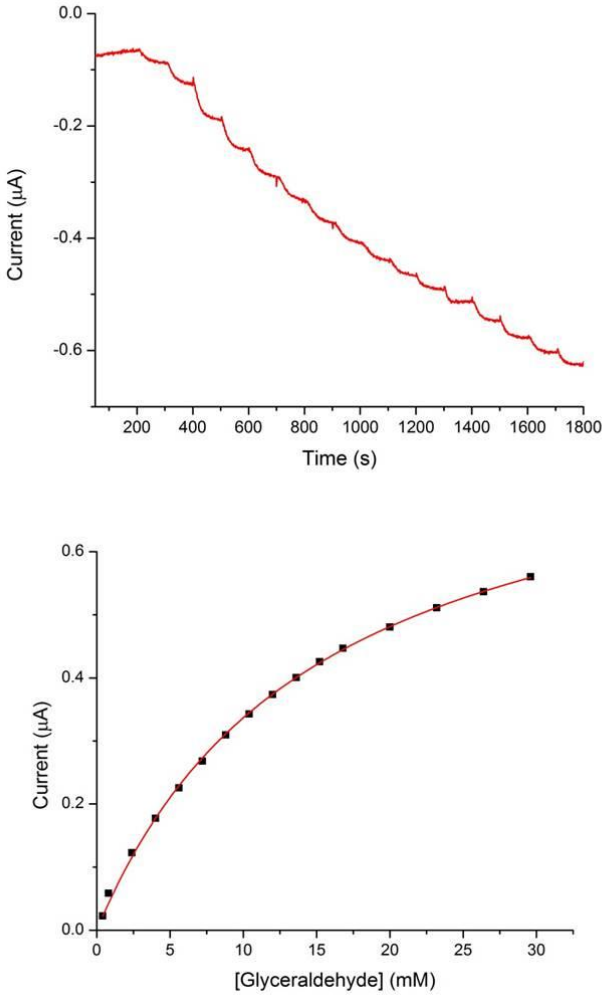

Figure 4.13 Amperometry measurement results of modified electrode with glyceraldehyde as substrate. 400 uM injection at 200 s, 800 uM injection at 300 s, 1.6 mM injections at 400 s, 500 s, 600 s,700 s, 800 s, 1000 s, 1100 s, 1200 s, 1300 s, and 3.2 mM injections at 1400 s, 1500 s, 1600 s, and 1700 s. Calculated V_{max} = 0.843 ± 0.102 μA, and K_m = 15.0 ± 1.9 mM.

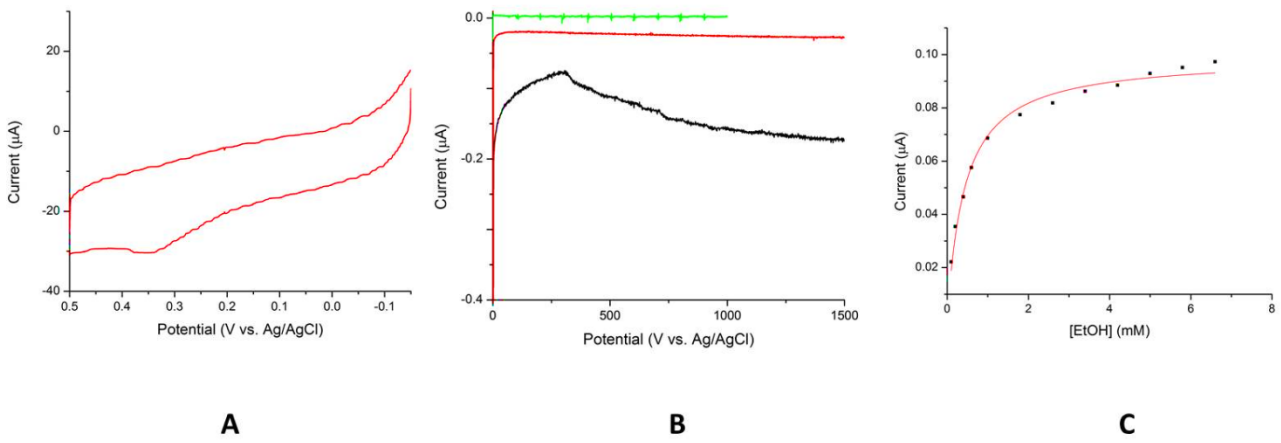

Figure 4.14 Electrochemistry study of TBAB Nafion immobilization technique. (A) Cyclic voltammogram of TBAB Nafion modified Toray electrode in 50 mM MES buffer pH 6.5, scan rate 100 mV/s. (B) Amperometry results, where the green line represents control experiment where TBAB-Nafion polymer without enzyme loading was tested with ethanol injections, the red line represents blank experiment where enzyme immobilized electrode was tested and MES buffer was injected, and the black line represents ethanol injection, where 0.1 mM ethanol was injected at 300 s and 400 s, 0.2 mM ethanol was injected at 500 s and 600 s, 0.4 mM ethanol was injected at 700 s, and 0.8 mM was injected at 800 s, 900 s, 1000 s, 1100 s, 1200 s, 1300 s, and 1400s. (C) Calibration curve of the TBAB-Nafion modified electrode.

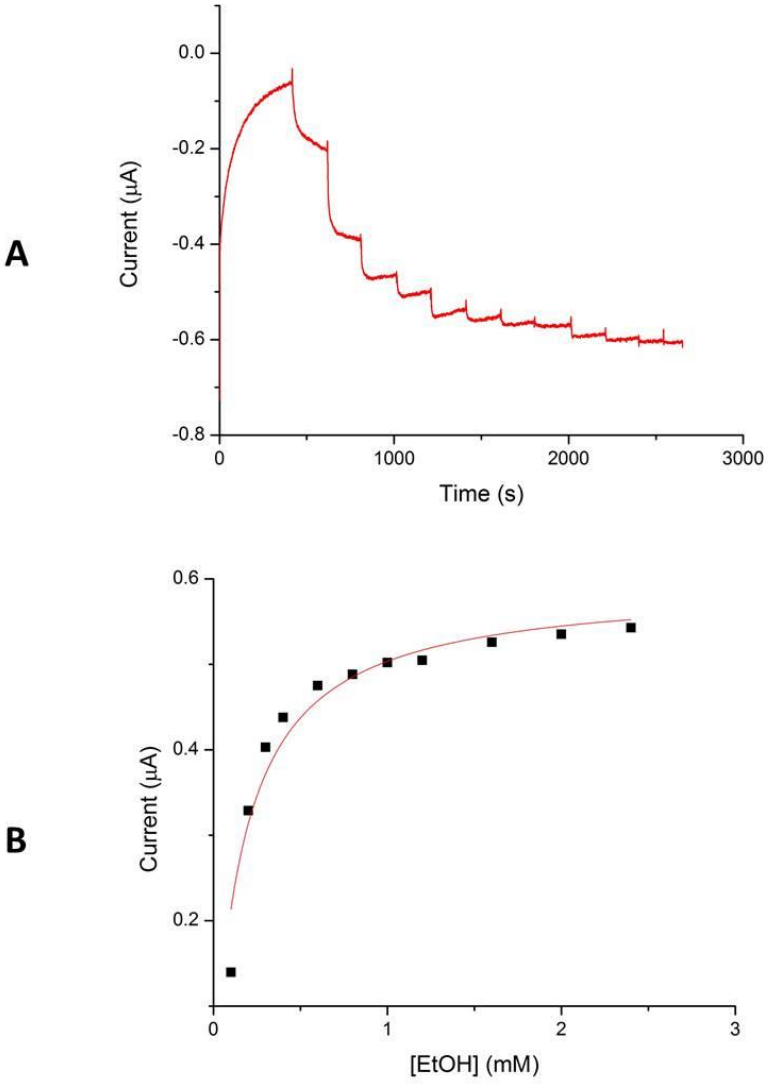

Figure 4.15 Amperometry results for polyaniline modified electrode. (A) 0.1 mM ethanol was injected at 400 s, 600 s, 800 s, and 1000 s; 0.2 mM ethanol was injected at 1200 s, 1400 s, 1600 s, and 1800 s; and 0.4 mM ethanol was injected at 2000 s, 2200 s, and 2400 s. (B) Calibration curve of polyaniline modified electrode.

Table 4.1 Immobilized assay results of modified electrodes with different substrate, Control is polymerized electrode without enzyme loading. EtOH was used as substrate in control.

Substrate	**A_0**	**A_{4min}**	**ΔA**
EtOH	0.399 ±0.07	0.070 ±0.012	0.329 ±0.014
Glucose	0.395 ±0.05	0.087 ±0.015	0.308 ±0.01
Glycerol	0.390 ±0.05	0.245 ±0.027	0.145 ±0.021
Acetaldehyde	0.394 ±0.04	0.194 ±0.018	0.200 ±0.014
Glyceraldehyde	0.401 ±0.07	0.043 ±0.007	0.358 ±0.016
Control	0.393 ±0.003	0.342 ±0.021	0.051 ±0.018

4.6 References

1. Dimitrakopoulos, C. D.; Mascaro, D. J. *IBM J. Res. Dev.* **2001,** *45*, 11–27.

2. Mikulski, C.; Russo, P.; Saran, M.; MacDiarmid, A.; Garito, A.; Heeger, A. *J. Am. Chem. Soc.* **1975,** *97*, 6358–6363.

3. Shirakawa, H.; Louis, E. J.; MacDiarmid, A. G.; Chiang, C. K.; Heeger, A. J. *J. Chem. Soc., Chem. Commun.* **1977,** 16, 578–580.

4. Brédas, J. L.; Chance, R. R. *Conjugated polymeric materials: Opportunities in electronics, optoelectronics, and molecular electronics*. Springer: 1990; Vol. 182.

5. Gurunathan, K.; Murugan, A. V.; Marimuthu, R.; Mulik, U.; Amalnerkar, D. *Mater. Chem. Phys.* **1999,** *61*, 173–191.

6. Hasik, M.; Turek, W.; Stochmal, E.; Lapkowski, M.; Pron, A. *J. Catal.* **1994,** *147*, 544–551.

7. McQuade, D. T.; Pullen, A. E.; Swager, T. M. *Chem. Rev.* **2000,** *100*, 2537–2574.

8. Roy, A.; Ganguly, A.; Bose, S.; Das, B. B.; Pal, C.; Jaisankar, P.; Majumder, H. *Mol. Pharmacol.* **2008,** *74*, 1292–1307.

9. Tallman, D. E.; Spinks, G.; Dominis, A.; Wallace, G. G. *J. Solid-State Electrochem.* **2002,** *6*, 73–84.

10. Birgerson, J.; Fahlman, M.; Bröms, P.; Salaneck, W. *Synth. Met.* **1996,** *80*, 125–130.

11. *Handbook of conducting polymers*. Skotheim, T. A.; Elsenbaumer, R. L.; Reynolds, J. R. CRC press: 1998.

12. Burroughes, J.; Bradley, D.; Brown, A.; Marks, R.; Mackay, K.; Friend, R.; Burns, P.; Holmes, A. *Nature* **1990,** *347*, 539–541.

13. Janietz, S.; Bradley, D.; Grell, M.; Giebeler, C.; Inbasekaran, M.; Woo, E. *Appl. Phys. Lett.* **1998,** *73*, 2453–2455.

14. Samuel, I.; Rumbles, G.; Collison, C. *Phys. Rev. B Condens. Matter.* **1995,** *52*, 11573–11579.

15. Chiang, C.-J.; Hsiau, L.-T.; Lee, W.-C. *Biotechnol. Tech.* **2004,** *11*, 121–125.

16. Huang, W.-S.; Humphrey, B. D.; MacDiarmid, A. G. *J. Chem. Soc., Faraday Trans. 1* **1986,** *82*, 2385–2400.

17. Macdiarmid, A. G.; Chiang, J.-C.; Halpern, M.; Huang, W.-S.; Mu, S.-L.; Nanaxakkara, L.; Wu, S. W.; Yaniger, S. I. *Mol. Cryst. Liq. Cryst.* **1985,** *121*, 173–180.

18. Jozefowicz, M.; Laversanne, R.; Javadi, H.; Epstein, A.; Pouget, J.; Tang, X.; MacDiarmid, A. *Phys. Rev. B* **1989,** *39*, 12958–12967.

19. Chiang, J.-C.; MacDiarmid, A. G. *Synth. Met.* **1986,** *13*, 193–205.

20. Letheby, H. *J. Chem. Soc.* **1862,** *15*, 161–163.

21. Cao, Y.; Andreatta, A.; Heeger, A. J.; Smith, P. *Polymer* **1989,** *30*, 2305–2311.

22. Ram, M.; Mehrotra, R.; Pandey, S.; Malhotra, B. *J. Phys.: Condens. Matter.***1994,** *6*, 8913–8918.

23. Rannou, P.; Nechtschein, M. *Synth. Met.* **1997,** *84*, 755–756.

24. Karyakin, A.; Strakhova, A.; Yatsimirsky, A. *J. Electroanal.Chem.* **1994,** *371*, 259–265.

25. Mu, S. *Synth Met.* **2004,** *143*, 259–268.

26. Wei, X.-L.; Wang, Y.; Long, S.; Bobeczko, C.; Epstein, A. *J. Am. Chem. Soc.* **1996,** *118*, 2545–2555.

27. Zhang, L.; Jiang, X.; Niu, L.; Dong, S. *Biosens. Bioelectron.* **2006,** *21*, 1107–1115.

28. Sheldon, R. A. *Adv. Synth. Catal.* **2007,** *349*, 1289–1307.

29. Cao, L.; Van Langen, L.; Sheldon, R. A. *Curr. Opin. Biotechnol.* **2003,** *14*, 387–294.

30. Kim, H.; Lee, I.; Kwon, Y.; Kim, B. C.; Ha, S.; Lee, J.-h.; Kim, J. *Biosens. Bioelectron.* **2011,** *26*, 3908–3913.

31. Schubart, I. W.; Göbel, G.; Lisdat, F. *Electrochim. Acta* **2012,** *82*, 224–232.

32. Gong, X.; Dai, L.; Mau, A. W.; Griesser, H. J. *J. Polym. Sci. A: Polym. Chem.* **1998,** *36*, 633–643.

33. Mu, S.; Kan, J. *J. Electrochim. Acta* **1996,** *41*, 1593–1599.

34. Rao, P. S.; Subrahmanya, S.; Sathyanarayana, D. *Synth. Met.* **2002,** *128*, 311–316.

35. Nicolas-Debarnot, D.; Poncin-Epaillard, F. *Anal. Chim. Acta* **2003,** *475*, 1–15.

36. Zhou, H.; Jiao, S.; Chen, J.; Wei, W.; Kuang, Y. *Thin Solid Films* **2004,** *450*, 233–239.

37. Genz, O.; Lohrengel, M.; Schultze, J. *Electrochim. Acta* **1994,** *39*, 179–185.

38. Rajendra Prasad, K.; Munichandraiah, N. *Synth. Met.***2001,** *123*, 459–468.

39. Kinyanjui, J. M.; Wijeratne, N. R.; Hanks, J.; Hatchett, D. W. *Electrochim. Acta* **2006,** *51*, 2825–2835.

40. Brusic, V.; Angelopoulos, M.; Graham, T., *J. Electrochem. Soc.* **1997,** *144*, 436–442.

41. Sazou, D.; Georgolios, C. *J. Electroanal. Chem.* **1997,** *429*, 81–93.

42. Tao, Y. T.; Pandian, K.; Lee, W. C. *Langmuir* **1998,** *14*, 6158–6166.

43. Prasad, K. R.; Munichandraiah, N. *J. Power Sources* **2002,** *112*, 443–451.

44. Liu, Z.; Guo, W.; Fu, D.; Chen, W. *Synth. Met.* **2006,** *156*, 414–416.

45. Carswell, A. D.; O'Rea, E. A.; Grady, B. P. *J. Am. Chem. Soc.* **2003,** *125*, 14793–14800.

46. Zhang, X.; Ogorevc, B.; Wang, J. *Anal. Chim. Acta* **2002,** *452*, 1–10.

47. Feng, W.; Bai, X.; Lian, Y.; Liang, J.; Wang, X.; Yoshino, K. *Carbon* **2003,** *41*, 1551–1557.

48. Taylor, R. L.; Conrad, H. *Biochemistry* **1972,** *11*, 1383–1388.

49. Staros, J. V.; Wright, R. W.; Swingle, D. M. *Anal. Biochem.* **1986,** *156*, 220–222.

50. Boels, K.; Glassmeier, G.; Herrmann, D.; Riedel, I. B.; Hampe, W.; Kojima, I.; Schwarz, J. R.; Schaller, H. C. *J. Cell Sci.* **2001,** *114*, 3599–3606.

CHAPTER 5

CONCLUSIONS AND FUTURE WORK

5.1 Conclusions

5.1.1 DET Enzyme Cascade for Complete Oxidation of Glucose

The natural metabolic pathway of glucose consists of glycolysis and the Kreb cycle processes in which 19 enzymes are involved.[1] Among these 19 enzymes, only 6 are oxidoreductases that can contribute to energy conversion. A low proportion of electrical energy producing enzymes in the cascade would negatively affect the power density if applied on bioanode.

A nonnatural, minimal oxidation pathway of glucose to carbon dioxide was designed with a six-enzyme cascade bioanode containing PQQ-dependent enzymes extracted from *Gluconobacter*, aldolase from *Sulfolobus solfataricus*, and oxalate oxidase from barley seeds. This bioanode enzyme cascade was demonstrated to be able to perform the 12-step oxidation of glucose, which contains 24-electron charge transfer per glucose molecule. Results show that for the bioanode with this six-enzyme cascade for complete oxidation, the power density increased by almost 50-fold compared to two-enzyme cascade (glucose dehydrogenase and 6-gluconate dehydrogenase), and the current density increased 34-fold. This result strongly suggests the importance of enzyme cascades for bioanode design from the perspective of power density and energy

density of the biofuel cell.

5.1.2 Impact of DET Enzyme Orientation on Catalysis Kinetics

DET enzymes catalyze the oxidation reactions of the fuels at the active site and release electrons. Electrons are then transferred to the redox active centers in DET enzymes and released to electrode surface from the closest redox active centers.[2] Therefore, the rate of direct bioelectrocatalysis for DET enzymes is closely related to the proximity and orientation of the enzymes toward the electrode surface, which determines the electron tunneling distances and the current density.

The role of DET enzyme orientations on electrochemical performance of a bioanode was investigated via an isotropic immobilization technique. PQQ-AlDH was deposited on flat gold electrode surface via a site specific immobilization method to form a monolayer of biocatalysts with a uniform orientation on a gold electrode. Six recombinant PQQ-AlDHs where the enzymes had been labeled with His-tags at the N- or C- terminus of each of the three subunits were employed. Results show that the orientation of PQQ-AlDHs can affect the direct biocatalysis rate greatly by varying the electron tunneling distances. The favorable orientation showed a current density that is 6.6-fold higher than the electrode with the orientation closest to the active site of the enzyme, while the unfavorable attachment to a nonelectroactive subunit showed no catalytic current.

The results explained why low power density was observed in the study of using DET enzyme cascade to completely oxidize glucose in a biofuel cell. With random orientation, only the enzymes with the “right” orientation toward the electrode, which

provide a redox active heme c group within the electron tunneling distance from the electrode surface, are actually contributing to the direct bioelectrocatalysis. Enzymes with other orientations are not able to promote the electron transfer from the enzyme to the electrode surface to generate bioelectrocatalytic current. The results of this study provided important information for future DET bioanode design to improve biofuel cell electrochemical performance.

5.1.3 Optimizing Enzyme Immobilization

There are generally two strategies to improve the direct electrochemical communication between DET enzymes and the electrode surface. One is to uniformly deposit DET enzymes with the favorable orientation toward the electrode surface. The other one is to use a very thin film linker to anchor enzymes onto electrode closely and decrease the average distance between the enzymes and the electrode surface. For the second strategy, conducting polymers are usually considered as the optimal choice of linking film due to the facts that they are chemically stable, fairly conductive and easy to prepare.[3]

In this study, a bifunctional polyaniline was utilized to immobilize DET enzymes. This electropolymerized conducting polymer film contains two important functional groups: sulfonic groups for a self-doping process to increase the conductivity of the film and carboxylic groups to be activated to covalently bound to enzymes. Electrochemical measurement results have shown that DET was observed with PQQ-dependent alcohol and PQQ-dependent aldehyde dehydrogeanses using ethanol and glyceraldehyde as substrates. Comparing this conducting polymer with TBAB-Nafion polymer enzyme

immobilization method showed a six-fold current density increase.

5.2 Future Work

5.2.1 Overall Goals

The overall goal of this study is to develop high energy density, high power density, and rugged bioanode for utilization in a complete enzymatic biofuel cell. This thesis focused on development and characterization of a specific aspect of the biofuel cell: utilization of direct electron transfer PQQ-dependent enzymes on bioanode of a glucose, ethanol, and glyceraldehyde biofuel cell. The concept of using a DET enzyme cascade to completely oxidize glucose to carbon dioxide will allow the fabrication of high energy density glucose biofuel cell. A thorough study of the role of DET enzyme orientations on direct bioelectrocatalysis provides important information for DET enzyme immobilization technique development in search for higher power output. The ability to work with numerous PQQ-dependent enzymes capable of direct electron transfer expands the power source options for biofuel cells and leads to more environmentally sound options to meet power demands.

5.2.2 High Surface Area Bioanodes

Nanostructure materials have played an important role in the study of traditional catalysis for over a decade and are beginning to gain interest for employment as high surface area support for biocatalysts. Attempts have been made to immobilize enzymes using different nanomaterials such as mesoporous media,[4] nanoparticles,[5] nanofibers,[6] and nanocomposites.[7] Adsorption of enzymes to large surface area nanomaterials can

lead to a great increase in enzyme lifetime and mass transfer, which will lead to high power output of the bioelectrochemical device. In bioelectrocatalysis, nanomaterials are typically used as a conductive bridge between the active site of the enzyme and the electrode surface. Carbon nanomaterial supports are employed in conjunction with PQQ-dependent enzymes to produce high surface area catalysts supports for bioanode fabrication. The structure of PQQ-ADH and PQQ-AlDH allows DET between the enzyme/carbon nanomaterial support and electrode without the use of additional charge carrying chemical mediators. DET between the enzymes and the electrode can be enhanced along with biocatalytic efficiency by employing different enzyme immobilization methods are different high surface area carbon substrates. Additional polymer layers are also incorporated to increase the ruggedness of the system.

In the study of the impact of DET enzyme orientations on direct electrocatalysis (Chapter 3), a favorable orientation of PQQ-AlDH was found, and fast electron transfer with this configuration was observed. With this knowledge, we can incorporate nanostructure supports to increase the surface area and aim to achieve high current direct electron transfer current density. Pyrene-nitrilotriacetic acid (NTA) is a promising candidate linker to bind His-tagged DET enzymes to nanocarbon material structure. The aromatic ring on pyrene can noncovalently bind (via ππ stacking) to the aromatic rings of the carbon nanotubes, and the NTA can chelate with metal ions such as Cu^{2+} and Ni^{2+} and further bind to the his-tags on recombinant DET enzymes and thus complete the site-specific immobilization. The immobilization strategy is shown in Figure 5.1.

5.2.3 Improving Glucose Bioanode Power Density

In this study, a six-enzyme minimal metabolic pathway cascade was designed. However, this high energy density bioanode showed low power output (6.74 ± 1.43 $\mu W/cm^2$) due to the inefficient enzyme immobilization method. This enzyme cascade design can be incorporated into a site-specific isotropic immobilization technique or conducting polymer technique to increase the direct bioelectrocatalysis rate and improve the overall performance of the bioanode.

5.3 End Remarks

This research has successfully demonstrated that the utilization of a well-designed enzyme cascade can overcome the bottleneck of enzymatic biofuel cell low-energy density. Factors that impact the direct bioelectrocatalysis were studied and analyzed. This is also the first record to compare the bioelectrocatalysis rate between different orientations of the PQQ-dependent direct electron transfer enzyme. Furthermore, a new DET-based bioelectrode was fabricated using conducting polymer as a linker to immobilize biocatalysts, and a large current density increase was observed compared to previous TBAB-Nafion immobilization techniques. This study has provided an important reference for future enzymatic bioelectronics design. Long term goals include investigating a variety of power application for this technology ranging from portable electronics to self-powered sensors.

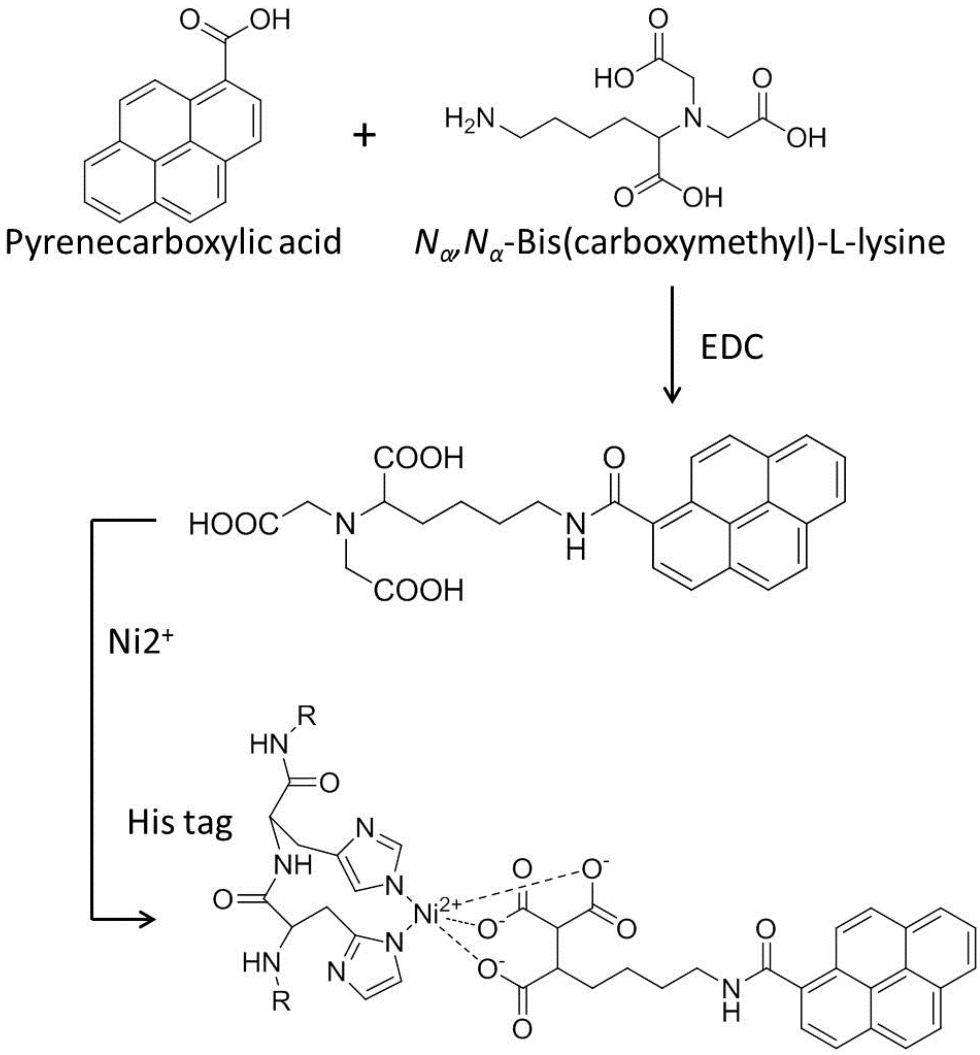

Figure 5.1 Pyrene-NTA synthesis and His-tag enzyme immobilization strategy.

5.4 References

1. Beilke, M. C. *Development and Characterization of Enzymatic Glycolysis Biomimics.* Saint Louis University, St. Louis, 2007.

2. Minteer, S. D.; Liaw, B. Y.; Cooney, M. J. *Curr. Opin. Biotechnol.* **2007,** 18, 228–234.

3. Kim, H.; Lee, I.; Kwon, Y.; Kim, B. C.; Ha, S.; Lee, J.-h.; Kim, J. *Biosens. Bioelectron.* **2011,** *26*, 3908–3913.

4. You, C.; Yan, X.; Kong, J.; Zhao, D.; Liu, B. *Talanta* **2011,** *83*, 1507–1514.

5. Tel-Vered, R.; Yehezkeli, O.; Willner, I. *Adv. Exp. Med. Biol.* **2012,** *733*, 1–16.

6. Marx, S.; Jose, M. V.; Andersen, J. D.; Russell, A. J. *Adv. Exp. Med. Biol.* **2012,** *733*, 47–52.

7. Tasviri, M.; Rafiee-Pour, H.-A.; Ghourchian, H.; Gholami, M. R. *Appl. Nanosci.* **2011,** *1*, 189–195.